4983

NAME OF AUTHOR... *Wayne Ralph Tinga* ....

TITLE OF THESIS... *Multiphase Dielectric Theory —* ...

...*Applied to Cellulose Mixtures* ......

....

UNIVERSITY... *of Alberta* ....

DEGREE FOR WHICH THESIS WAS PRESENTED... *Ph.D.* ....

YEAR THIS DEGREE GRANTED... *1969* ....

Permission is hereby granted to THE NATIONAL LIBRARY

OF CANADA to microfilm this thesis and to lend or sell copies

of the film.

The author reserves other publication rights, and

neither the thesis nor extensive extracts from it may be

printed or otherwise reproduced without the author's

written permission.

(Signed)... *Wayne Tinga* ......

PERMANENT ADDRESS:

...*728 W. 62 Ave* ...

...*Vancouver, B.C.* ......

....

DATED. *Oct. 3* 19*69*

THE UNIVERSITY OF ALBERTA

MULTIPHASE DIELECTRIC THEORY - APPLIED TO CELLULOSE MIXTURES

by

Ⓒ   WAYNE RALPH TINGA

A THESIS

SUBMITTED TO THE FACULTY OF GRADUATE STUDIES

IN PARTIAL FULFILMENT OF THE REQUIREMENTS FOR THE DEGREE

OF DOCTOR OF PHILOSOPHY

DEPARTMENT OF ELECTRICAL ENGINEERING

EDMONTON, ALBERTA

FALL 1969

UNIVERSITY OF ALBERTA

FACULTY OF GRADUATE STUDIES

The undersigned certify that they have read,
and recommend to the Faculty of Graduate Studies for
acceptance, a thesis entitled Multiphase Dielectric
Theory - Applied to Cellulose Mixtures submitted by
Wayne Ralph Tinga in partial fulfilment of the re-
quirements for the degree of Doctor of Philosophy.

. . . .
Supervisor

. . . .

. . . .

. . . .

. . . .
External Examiner

Date Aug. 29, 1969   . . . .

ABSTRACT

Experimental results for the complex dielectric constant of
the air-cellulose-water mixture as found in Douglas Fir and Western
Hemlock are given as a function of moisture content and temperature
at 2450 MHz with a maximum error of $\pm$ 6%. Theoretically the diel-
ectric constant of wood can be predicted to $\pm$ 10% by assuming a
Gaussian distribution of relaxation times. Experimental methods
are developed and explained in detail. Present dielectric mixture
relations are briefly reviewed and a more general case of multi-
phase mixtures with confocal ellipsoidal shell inclusions is ana-
lyzed. Values for the complex dielectric constant of bound water
as found in cellulose mixtures are estimated on a semi-empirical
basis and are found to vary with moisture content.

ACKNOWLEDGEMENT

TABLE OF CONTENTS

LIST OF FIGURES

LIST OF TABLES

A,B,C,D,k – constants used in the solution to the ellipsoidal shell problem

$\vec{A}$ – a vector

a,b,c – major axes of an ellipsoid

a',b',c' – major axes of the inner ellipsoid of an ellipsoidal shell

C_o – velocity of light in vacuum

$\vec{D}$ – dielectric displacement vector

$\vec{E}_i$ – electric field vector internal to an inclusion

$\vec{E}_{av}$ – average electric field vector in a mixture

f – frequency in Hz

M,MC – percentage moisture content based on oven-dry weight

Ma – moisture content above fibre saturation in wood

n_j – depolarization coefficient of an ellipsoid along the j-axis

n' – polarization coefficient of the inner ellipsoid of an ellipsoidal shell

$\vec{n}$ – normal unit vector

N – integer

Q – activation energy of polarization of a particle in calories per mole

q – activation energy of polarization of a particle in electron volts per mole

R – universal gas constant = 1.987 calories per mole per degree Kelvin

r – ratio of electric field strengths at two points on a standing wave pattern

S_o – surface of a mixture

S_i,S_h – surface of an inclusion and of the host material respectively

S_I – surface of all inclusions in a mixture

S – specific gravity of wood at a given moisture content

Sg – specific gravity of wood when green

T – temperature in °K or °C

T_i – ratio of the electric field in an inclusion to the average electric field in a mixture; $\bar{T}_i$ is a tensor of rank two

T_m – temperature at which the maximum dielectric loss occurs at a given frequency

$\vec{u}$ – unit vector

V,V' – product of the three major axes of the outer and inner ellipsoids respectively in an ellipsoidal shell

V_I, V_h – volume of all inclusions and the host material respectively

v_i – fractional volume filling factor

V_w, V_a – fractional volume of water and air in wood

x, x_o – $Ln(\tau/\bar{\tau})$ and $Ln(\tau_o/\bar{\tau})$ respectively

α – attenuation constant for waveguide propagation

α_ℓ – linear expansion coefficient of a dielectric

β – phase constant for waveguide propagation

γ – propagation constant of a dielectric filled waveguide

γ_o – propagation constant of an air filled waveguide

$\varepsilon = \varepsilon' - j\varepsilon''$ – complex dielectric constant

ε' – real part of dielectric constant

ε'' – imaginary part of dielectric constant

$\varepsilon_m, \varepsilon_h, \varepsilon_i$ – dielectric constant of mixture, host and included material respectively

ε^* – effective dielectric constant of material surrounding the inclusions

$\bar{\varepsilon}$ – the bar denotes a tensor dielectric constant of rank two

ε_o – value of the dielectric constant at a frequency low enough so that ε' achieves the highest value possible due to the assumed polarization mechanism

ε_∞ – value of the dielectric constant at a frequency high enough to make the dispersion of ε' due to the assumed polarization mechanism negligible

ζ, η, ξ – ellipsoidal coordinates

θ, ϕ – phase angles in radians or degrees

λ_o – free space wavelength

λ_c – cutoff wavelength

λ_g – guide wavelength in dielectric filled waveguide

List of Symbols (Cont.)

λ_{g_o} - guide wavelength in air filled waveguide

ρ_ω - density of absorbed water

τ - relaxation time in seconds of a particular polarization mechanism

τ_o - shortest relaxation time present in a material

$\phi, \psi,$ - arbitrary scalars

ϕ, ϕ', ϕ_o - potential functions in the ellipsoidal shell problem

ω - angular frequency in radians $\omega = 2\pi f$

$\vec{\nabla}$ - gradient operator

INTRODUCTION

Multiphase dielectric theory is important in many aspects of material research. One area where material research is extremely important is in the application of microwaves as a source of highly refined heat energy and in measurement techniques used in microwave processing of foods, chemicals, plastics, etc., and microwave moisture, thickness and fault-detection measurements. To do these jobs effectively, efficiently and economically, the microwave properties of the materials used must be known. This thesis extends the dielectric theory of multiphase mixtures with application to the wide class of cellulose-air-water mixtures as found for example in wood.

Given a dielectric mixture made up of different components each with its own dielectric characteristics, can the dielectric behavior of the mixture as a whole be predicted. To answer this problem, dielectric mixture theory was developed as far back as the late 19th century when Maxwell[29] (1891) tackled the problem of obtaining the electromagnetic characteristics of simple dielectric mixtures. Since then many scientists have modified, added to, and improved on the early theories.[64]

An exact solution of the problem is possible for only a few geometrically well-defined systems. For many naturally occuring dielectrics the geometries of the mixtures and the interaction between the inclusions can only be described statistically at best.

In the case of cellulose-air-water systems, as studied in this thesis, even a statistical description is extremely difficult to obtain and only a relatively crude mathematical model of the macroscopic mixture can be set down which nevertheless is shown to be a useful analytical tool.

Development of dielectric mixture theory has shown[13] that particle interactions and statistical variations in the mixture have only a second - or higher - order effect and that the particle geometry in the mixture is a far more important parameter[14]. As a result, existing averaging laws are used in this work but a more general inclusion geometry is assumed namely that of ellipsoidal shells which leads to a new mixture relation.

The problem of finding the internal to external electric field ratios for ellipsoidal shell inclusions is solved here for the first time. The final solution simplifies in special cases to that of ellipsoidal and spherical inclusions. Chapter 2 is devoted to the development of the new mixture relation. A brief history of mixture theories is presented and summarized in a tabular form which can be used as an easy reference chart.

Many mixed dielectrics exhibit a complex functional dependence on temperature and moisture content. This nonlinear functional behavior is evident when trying to measure the moisture content in materials using microwave, capacitance or resistance type moisture

meters.* The interaction of temperature and frequency dependence of the material properties makes it very difficult to calibrate these instruments. To analyze these functional variations, chapter 3 develops the theory of the temperature and frequency behavior of those dielectrics which exhibit a distribution of relaxation times. The theory gives an analytical description of the variation of dielectric constant with temperature frequency and moisture content and therefore is a useful tool in the analysis of those systems in which the dielectric properties are crucial in determining systems efficiency, stability and economics.

To test the theories presented it was necessary to make a large number of measurements on an actual complex dielectric mixture. Two wood species, Douglas Fir and Western Hemlock were chosen because of their economic importance on this continent and because wood is a good example of a much wider class of cellulose-air-water mixtures. Chapter 4 describes in detail the microwave measurement method chosen and an error analysis needed to obtain percentage errors is developed in Appendix A. Overall measurement errors are shown to lie between ± 5 and ± 10% eventhough the basic technique used is accurate to better than ± 2%.

Results of the measurements on Douglas Fir and Western Hemlock

---

* These meters are commonly used in the forest product industry and their reliability and accuracy has been much debated in the technical world.

are given in chapter 5 and Appendix B. It is shown that the temperature and frequency behavior of the dielectric properties of wood at varying moisture contents can adequately be described by the theory given in chapter 3. Agreement between the experimental and semi-theoretical behavior of wood is better than $\pm$ 10%.

Chapter 6 is devoted to the application of the new mixture relation, developed in chapter 2, to the wood mixture. Since the adsorbed water in wood is molecularly bound in varying degrees to the basic wood structure the dielectric properties of this adsorbed water differ considerably from the pure liquid water properties. Hence, the new mixture relation was used to semi-empirically obtain estimates of the dielectric properties of the bound water as a function of moisture content, data previously not available. The model assumed for the wood mixture below fiber saturation is one containing ellipsoidal, needle-like air cavities and thin shell-type water inclusions dispersed in a homogeneous cell-wall material. Calculations based on this model agree favorably with experimental data on Douglas Fir and Western Hemlock.

CHAPTER 2

DIELECTRIC MIXTURE THEORY

Introduction

Relating the dielectric constant of a mixture satisfactorily to the dielectric constant of its component has been a major problem in dielectric theory. The complete solution awaits mainly the development of an accurate theory of elementary particle interaction based on statistical mechanics which is by no means a trivial task. A brief review will be given here indicating the basic mixture problem and some of the contributions made in the literature towards its solution. A generalized approach will then be given to the problem of mixtures following the work of Taylor[9]. One of the more important parts of any mixture theory is to find the relationship between a particle's internal electric field and the average field present in the remainder of the mixed dielectric. A general solution to the electrostatic problem of an ellipsoidal shell will be given with a view to the solution of the macroscopic cellulose-air-water system to which the dielectric mixture theory will be applied.
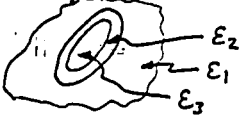
A chart of the important mixture relations is presented in Table 2.1. During the course of this research an excellent review of mixture relations was published by Van Beek[64], summarized in tabular form. However, Table 2.1 given here presents the major mixture relations from which all the others can be derived. It further covers the work of Taylor[9] and Franck[61] both of whom have made significant contributions by stating the mixture problem and solution in more general terms.

Table 2.1 – Summary of most important macroscopic mixture relations

Inclusion shape	Mixture Formula	Conditions and References
Ellipsoids 2-phase	$\varepsilon_m - \varepsilon_h = \{v_i/(1-v_i)\}(\varepsilon_i - \varepsilon_m)S'_{\varepsilon^*}$ * $\varepsilon^* = \varepsilon_h$	All interaction effects assumed negligible; Maxwell[29], Fricke.
Arbitrary 2-phase	$(\varepsilon_m-\varepsilon_h)/(\varepsilon_m+u)=v_i(\varepsilon_i-\varepsilon_h)/(\varepsilon_i+u)$ $u=\varepsilon_i(S'_{\varepsilon^*}-\varepsilon_h)/(1-S'_{\varepsilon^*})$; $\varepsilon^*=\varepsilon_h$	Semi-empirical; Wiener[14].
Arbitrary 2-phase	$(\varepsilon_m-\varepsilon_h)/(\varepsilon_i-\varepsilon_h)=\varepsilon'=[(1-k)v_i]/(1-kv_i)$ k is an empirical factor	Empirical; Pearce[63].
Spheres 2-phase	$\varepsilon_m-\varepsilon_h=3v_i\varepsilon_h/\{[(\varepsilon_p+2\varepsilon_h)/(\varepsilon_p-\varepsilon_h)]+v_i\}$	Interactions allowed for by ; Lewin[14].
Needles	$1-v_i=\{(\varepsilon_i-\varepsilon_m)/(\varepsilon_i-\varepsilon_h)\}\cdot\{(\varepsilon_i+5\varepsilon_h)/(\varepsilon_i+5\varepsilon_m)\}^{2/5}$	Interactions partially accounted for in the derivation; Bruggeman-Niesel[14].
Discs	$1-v_i=\{(\varepsilon_i-\varepsilon_m)/(\varepsilon_i-\varepsilon_h)\}\cdot(2\varepsilon_i+\varepsilon_h)/(2\varepsilon_i+\varepsilon_m)$	
Spheres 2-phase	$1-v_i=\{(\varepsilon_i-\varepsilon_m)/(\varepsilon_i-\varepsilon_h)\}\cdot\{\varepsilon_h/\varepsilon_m\}^{\frac{1}{3}}$	
Arbitrary multiphase	$Ln\,\varepsilon_m=v_h\,Ln\,\varepsilon_h+\sum_{i=1}^{N}v_i\,Ln\,\varepsilon_i$	Empirical; Lichtenecker[14,21].
Spheres 2-phase	$\{(\varepsilon_m-\varepsilon_h)/3\varepsilon_m\}=v_i(\varepsilon_i-\varepsilon_h)/(\varepsilon_i+2\varepsilon_m)$	Short range statistical variations neglected; Böttcher[30].
Ellipsoids multi-phase	$\varepsilon_m-\varepsilon_h=\sum_{i=1}^{N}v_i(\varepsilon_i-\varepsilon_h)S'_{\varepsilon^*}$ $\varepsilon^*=\varepsilon_m$	Short range statistical variations neglected; Polder and Van Santen[10].
Ellipsoids 2-phase	$\varepsilon_m-\varepsilon_h=v_i(\varepsilon_i-\varepsilon_h)S'_{\varepsilon^*}$ $\varepsilon_{h\text{ or }}\varepsilon_i<\varepsilon^*<\varepsilon_m$	ε^* contains interaction effects; DeLoor[14].
	* $S'_{\varepsilon^*}=\sum_{j=1}^{3}\dfrac{1}{1+n_j\left(\frac{\varepsilon_i}{\varepsilon^*}-1\right)}$	

Table 2.1 - continued

Inclusion shape	Mixture Formula	Conditions and References
Ellipsoids multi-phase anisotropic media	$\bar{E}_m - \bar{E}_h = \sum\limits_{i=1}^{N} V_i (\bar{E}_i - \bar{E}_h) \bar{\bar{T}}_i$ e.g., $\bar{\bar{T}}_i = \sum\limits_{j=1}^{3} \dfrac{1}{1 + n_j (\frac{\varepsilon_i}{\varepsilon_m} - 1)}$ $\bar{\bar{T}}_i$ is a dyadic relating the internal to the average electric field.	Interactions can be accounted for in $\bar{\bar{T}}_i$; solution is obtainable if statistical variations are neglected; Taylor[8,9].
Ellipsoidal shells multi-phase anisotropic mixtures	$\bar{E}_m - \bar{E}_h = \sum\limits_{i=1}^{N} V_i (\bar{E}_i - \bar{E}_h) \bar{\bar{T}}_i$ For Shells: $T_2 = \varepsilon_i \left[\varepsilon_2 + \dfrac{\varepsilon_3 - \varepsilon_2}{2} (n_j' + n_j \frac{V'}{V}) \right] \cdot$ $\cdot \left\{ \left[\varepsilon_2 + (\varepsilon_2 - \varepsilon_3)(n_j \frac{V'}{V} - n_j) \right]\left[\varepsilon_1 + n_j(\varepsilon_2 - \varepsilon_1) \right] + \right.$ $\left. - n_j \frac{V'}{V} (\varepsilon_2)(\varepsilon_2 - \varepsilon_1) \right\}^{-1}$ $V' = a'b'c'$; inner ellipsoid axes : a', b', c' $V = abc$; outer ellipsoid axes : a, b, c	Interaction effects can be approximately calculated through $\bar{\bar{T}}_i$; $\bar{\bar{T}}_i$ is solved for shells; Tinga (author).

Neglecting all particle interactions, Maxwell[29] treated the problem of anisotropic ellipsoidal inclusions in an isotropic medium for magnetic materials. For dielectric mixtures similar equations are obtained[9]. Rayleigh[14, 30]* showed that the Maxwell relation is a good first order approximation for cubically arranged spherical and cylindrical inclusions in a host material. A mixture equation developed by Wiener[14, 30] involves a form factor which, however, depends on the dielectric constants of the host material and the mixture in a complex way. Wiener did not account for particle interaction effects directly. Lewin[15], by applying scattering theory to a material loaded with regularly spaced spherical particles, allows for particle interaction by defining an effective dielectric constant as a complex function of the particle size and the dielectric constant of the included particles. He specifies the particle size to be much smaller than the propagating wavelength. Lewin's formula reduces to Rayleigh's formula for ordered spheres when the effective dielectric constant of the inclusions is assumed equal to the dielectric constant of the material in the inclusions. Bruggeman[14, 30] extended Wiener's theory and showed Wiener's "formzahl" (form number) to be a function of the dielectric constant of the host material and of the mixture. Bruggeman allowed for long-range particle interactions by the use of a limit procedure. Niesel[14] arrived at Bruggeman's results by using an integration process. Pearce[63] modified Bruggeman's equations by introducing an empirical factor, k, which

---

* Both De Loor[14] and Böttcher[30] have given critical reviews of the literature in mixed dielectrics.

is only dependent on the type of mixture used. Another empirical formula was given by Lichtenecker[14, 39] which has no obvious correlation to the other theoretical formula discussed above.

Onsager[60] was the first to propose that only a part of the internal field in a dielectric mixture is effective in directing a dipole. In effect, Onsager modified the average value of the internal field by a reaction field which accounts for long-range interaction effects and hence obtained a more accurate formula for a dipolar dielectric mixture. Böttcher[30] used Onsager's reaction field theory to derive a mixture formula for spherical particles in a continuous dielectric. Polder and Van Santen[10] generalized this approach for ellipsoidal shaped inclusions of more than one material and showed that Onsager's assumptions about the reaction field were equivalent to the hypothesis that "the mean value of the field in the interior of the particle, of dielectric constant ϵ_i surrounded by a medium of dielectric constant ϵ_m in which a homogeneous field $\vec{E}_{av}$ is maintained at a large distance from the particle, is a good approximation for the actual mean field in this special particle".

A further modification to the mixture relations of Polder and Van Santen was given by De Loor[14] who assigned an effective dielectric constant of ϵ^* to the immediate surroundings of an included particle. Even though no quantitative solution is given for the value of ϵ^*, De Loor clearly shows that the mixture dielectric constant must always lie within the range $\epsilon_{i,h} < \epsilon^* < \epsilon_m^*$. The latter condition thus leads to limiting values of the dielectric constant of a mixture.

---

* This limit condition was verified by De Loor[14] by plotting the results of all the other mixture relations for different materials. Hasted and Shah[62] applied this criterion to various types of brick and obtained favourable results. The lower limit is always given by the lowest dielectric constant.

Generalized mixture equations can be derived by the use of vector calculus and Maxwell's equations. Taylor[8, 9] developed the generalized equations for lossy anisotropic dielectric mixtures using the "average field approximation" of Polder and Van Santen. His development which is very concise and formal is based on the work of Korneenko[1] who uses Gauss' theorem to develop an averaging formula for the parameters in inhomogeneous media. Taylor further uses the contribution by Frank[61] who gives the penetration of a static homogeneous field in an anisotropic host material into an ellipsoidal inclusion consisting of another aniso-tropic medium. On the development of adequate theories relating particle interaction phenomena in closed form, use of Taylor's mixture formulas modified to allow short-range interaction effects should give a realistic approach and solution to the general problem of dielectric mixtures. Both Kirkwood[11] and Brown[13] developed statistical methods to solve the particle interaction problems. Brown shows that Maxwell's formula is a second order approximation in which statistical properties of particle geometry have been neglected. Bruggeman and Böttcher's formula try to account for interaction phenomena and agreement to the third order with Brown's treatment requires assigning values to one of Brown's statistical parameters which for Bruggeman's formula is twice as large as for Böttcher's formula. To decide which of these two is the best approximation a detailed calculation of the statistical particle distributions must be made. Taylor's approach uses basic assumptions about the mixture identical with those of Böttcher and Polder and Van Santen and develops the general mixture relations for dyadic permittivities for inclusions with an ellip-soidal surface.

This chapter will develop Taylor's equations[9] in modified form, using De Loor's designation of an effective permeability ε^* of the particle surroundings[14]. The electrostatic problem of finding the ratio of internal field to the average field at a large distance from the particle will be solved for various practical particle geometries. The resultant equations will be tested against experimental data for the cellulose-air-water mixture as found in wood species.

DERIVATION OF AVERAGING LAW

It is most important in mixture theory to find the relationship between the electric field internal to an inclusion and the electric field in the surrounding medium. To do this, use is made of Gauss' Divergence Theorem which relates volume characteristics of vector quantities to their values at the surface bounding the volume. Application of the Divergence Theorem to an individual inclusion in a host medium and satisfying the boundary conditions at the surfaces between the two, yields equations relating the mean value of the dielectric constant in the inclusion to the average value of the dielectric constant in the surrounding medium.

A typical mixture is schematically represented in figure 2.1.
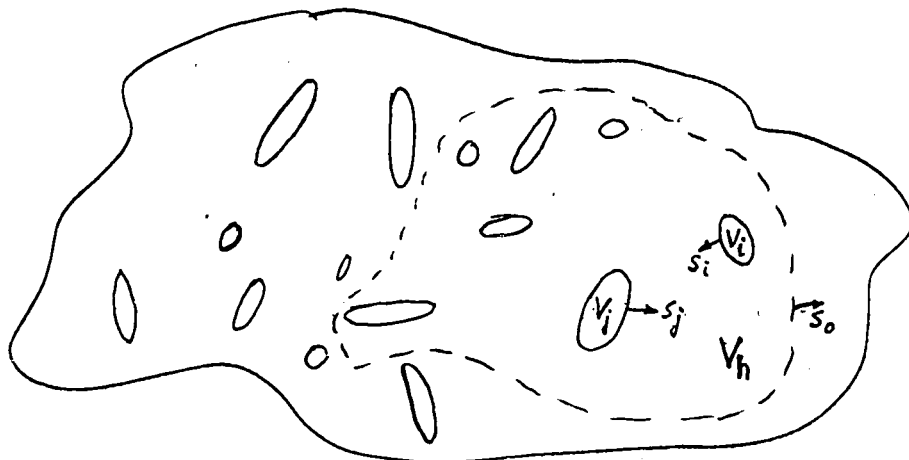
Fig. 2.1 - Multiphase Mixture.

An arbitrary volume V_h is selected whose surface lies inside the medium. Within this volume V_h, of surface S_h, consider a statistically large number of inclusions with the volumes V_i and surfaces S_i, ($i=1, 2, \ldots N$) where the subscript i, refers to a particular inclusion. Let the total volume and surface be denoted respectively, by

$$V=V_h+\sum_{i=1}^{N} V_i = V_h+V_I \tag{2.1}$$

and

$$S_h=S_o+ \sum_{i=1}^{N} S_i = S_o+S_I \tag{2.2}$$

For any vector $\vec{A}$ which has continuous first partial derivatives in V and on its surface S, the divergence theorem states

$$\int_V \nabla\cdot\vec{A}dV = \int_S \vec{n}\cdot\vec{A}dS \tag{2.3}$$

where $\vec{n}$ is a unit vector normal to the surface S drawn outward from V.

Consider now two arbitrary scalars ϕ and ψ.

Setting

$$\vec{A} = \phi\nabla\psi \tag{2.4}$$

and taking the divergence of equation 2.4 gives

$$\nabla\cdot(\phi\nabla\psi) = \nabla\phi\cdot\nabla\psi + \phi\nabla^2\psi \tag{2.5}$$

Application of the divergence theorem, equation (2.3), over the volume V_h and use of equation (2.5) yields the result

$$\int_{V_h} \nabla\cdot(\phi\nabla\Psi)dv=\int_{S_o} \phi\frac{\partial\psi}{\partial n}ds - \sum_{i=1}^{N}\int_{S_i} \phi\frac{\partial\psi}{\partial n}ds \tag{2.6}$$

The negative sign appears because the normals to the surfaces S_i are

directed into V_h.

The following quantities are now defined,

$$\nabla \psi = -\bar{\varepsilon} \cdot \vec{E} \qquad (2.7)$$

where $\bar{\varepsilon}$ is a dyadic permittivity and

$$\nabla \phi = \vec{u} \qquad (2.8)$$

a unit vector.

In a source free homogeneous anisotropic medium Maxwell's equations yield

$$\nabla \cdot \bar{\varepsilon} \cdot \vec{E} = 0 \qquad (2.9)$$

Equation (2.6) is now rewritten by the use of equations (2.7), (2.8), and

(2.9) as

$$\int_{V_h} \vec{u} \cdot \bar{\varepsilon}_h \cdot \vec{E}_h dv = \int_{S_o} \phi \bar{\varepsilon}_h \cdot \vec{E}_{h_n} ds - \sum_{i=1}^{N} \int_{S_i} \phi \bar{\varepsilon}_h \cdot \vec{E}_{h_n} ds \qquad (2.10)$$

At the boundaries between the host material and the inclusions the boundary

conditions are

$$\bar{\varepsilon}_i \cdot \vec{E}_{i_n} = \bar{\varepsilon}_h \cdot \vec{E}_{h_n} \qquad (2.11)$$

These boundary conditions hold for the general case of a source free material

with a complex dyadic permittivity. Applying equation (2.11) to the last

term in equation (2.10) one obtains

$$\sum_{i=1}^{N} \int_{S_i} \phi \bar{\varepsilon}_h \cdot \vec{E}_{h_n} ds = \sum_{i=1}^{N} \int_{S_i} \phi \ \bar{\varepsilon}_i \cdot \vec{E}_{i_n} ds \qquad (2.12)$$

Reapplying the divergence theorem over the volume V_i in the same manner as

before, equation (2.12) becomes

$$\sum_{i=1}^{N} \int_{S_i} \phi \bar{\varepsilon}_i \cdot \vec{E}_{i_n} ds = \sum_{i=1}^{N} \int_{V_i} \vec{u} \cdot \bar{\varepsilon}_i \cdot \vec{E}_i dv \qquad (2.13)$$

Furthermore, the basic assumption is made that the medium as a whole can be characterized by an equivalent, average, anisotropic dielectric constant, $\bar{\varepsilon}$, with a corresponding average uniform field, $\vec{E}_{av}$ maintained at a large distance from the inclusion. This is the Polder and Van Santen hypothesis which accounts for long-range interactions, but neglects short-range statistical variations in the particle geometry. For low value concentrations of inclusions ($\sum_{i=1}^{N} V_i < 1$) this is indeed a good approximation. Hence, by definition, the following equation holds

$$\vec{E}_{av} = \frac{1}{V}\left(\int_{V_h} \vec{E}_h dv + \sum_{i=1}^{N}\int_{V_i} \vec{E}_i dv\right) \tag{2.14}$$

The first term of the R H S of equation (2.10) can now, by the use of the boundary conditions, be written in a manner similar to equation (2.13) as

$$\int_{S_0} \phi \bar{\varepsilon}_h \cdot \vec{E}_{h_n} ds = \int_{S_0} \phi \bar{\varepsilon} \cdot \vec{E}_{av_n} ds = \int_V \vec{u} \cdot \bar{\varepsilon} \cdot \vec{E} dv = V\vec{u} \cdot \bar{\varepsilon} \cdot \vec{E}_{av} \tag{2.15}$$

Substituting for the R H S of equation (2.10) from equation (2.15) and (2.13) respectively and noting the direction of $\vec{u}$ is arbitrary, yields

$$V\bar{\varepsilon} \cdot \vec{E}_{av} = \int_{V_h} \bar{\varepsilon}_h \cdot \vec{E}_h dv + \sum_{i=1}^{N}\int_{V_i} \bar{\varepsilon}_i \cdot \vec{E}_i dv \tag{2.16}$$

Exact calculations of the fields in equations (2.14) and (2.16) is very difficult in general because of the many complicated interaction phenomena occuring within any one medium. However, the analysis can be carried further if it is assumed that each inclusion can be treated as an individual particle imbedded in an anisotropic but homogeneous material of permittivity $\bar{\varepsilon}$ and a field $\vec{E}_{av}$*. It is further assumed that all inclusions are of a shape which allows a homogeneous field to exist within the

---

* This is Polder and Van Santen's hypothesis and is valid at least for $\sum_{i=1}^{N} V_i \ll 1$

inclusion when the field in the surrounding host is also homogeneous. The latter statement allows use of all ellipsoidal inclusions and thin confocal ellipsoidal shells[61].

It follows, then, that the field within each inclusion is constant[*] under these assumptions[2, 3, 4, 61]. Stated generally

$$\vec{E}_i = \bar{T}_i \vec{E}_{av} \tag{2.17}$$

The quantity $\bar{T}_i$ is a tensor of rank 2 which in principle can be determined for each particle geometry satisfying the previous conditions.

Let the average values of $\vec{E}_h$ and $\vec{E}_i$ be defined by

$$<\vec{E}_h> = \frac{1}{V_h} \int_{V_h} \vec{E}_h \, dv \tag{2.18}$$

$$<\vec{E}_i> = \frac{1}{V_i} \int_{V_i} \vec{E}_i \, dv \tag{2.19}$$

Thus equation (2.14) can now be written as

$$V\vec{E}_{av} = V_h <\vec{E}_h> + \sum_{i=1}^{N} V_i <\vec{E}_i> \tag{2.20}$$

and similarly, for any homogeneous medium, equation (2.16) becomes

$$V\bar{\epsilon}\vec{E}_{av} = V_h \bar{\epsilon}_h \cdot <\vec{E}_h> + \sum_{i=1}^{N} V_i \bar{\epsilon}_i \cdot <\vec{E}_i> \tag{2.21}$$

Elimination of $<\vec{E}_h>$ between equations (2.20) and (2.21) and use of equation (2.17) finally yields

$$\bar{\epsilon} - \bar{\epsilon}_h = \frac{1}{V} \sum_{i=1}^{N} (\bar{\epsilon}_i - \bar{\epsilon}_h) V_i \bar{T}_i \tag{2.22}$$

---

[*] The condition of a constant internal field is a direct result of the finite solution to Laplace's equation in ellipsoidal coordinates.

Thus equation (2.22) expresses the dielectric constant, $\bar{\varepsilon}$, of the mixture in terms of the dielectric constants $\bar{\varepsilon}_i$ and $\bar{\varepsilon}_h$ of the inclusion and host material respectively. Each inclusion contributes to the mixture in proportion to its volume filling factor V_i/V and each contribution is weighted by the ratio of the internal inclusion field to the average field in the mixture as given by $\bar{T}_i$.

The dyadic $\bar{T}_i$ can be evaluated by methods of electrostatics as developed in the next section.

INTERNAL FIELD EVALUATION FOR DIFFERENT SHAPED INCLUSIONS

Inclusions in many mixtures are small compared to a wavelength even at microwave frequencies. Hence the electromagnetic solution to the internal field is quasi-stationary which expressed mathematically is

$$\omega \ll \frac{c_o}{\ell} \qquad\qquad (2.23)$$

Where c_o is the velocity of light ℓ is the characteristic linear dimension of the inclusions.

Internal fields in inclusions can be solved in closed form if the inclusions are ellipsoidal. The electrostatic problem of an ellipsoid in a homogeneous field has been treated by different authors[2, 3, 4, 61]. However, an even more general shaped inclusion would be in the form of an ellipsoidal shell. In practice, such a shape is found for example in the structure of wood. It is the solution to the latter problem which will be derived in this section. Solutions for inclusion shapes such as spheres, spheroids, needles and discs are all contained in the solution of the more general shell problem.

A schematic representation of a homogeneous ellipsoidal shell in a homogeneous medium is given in figure 2.2.
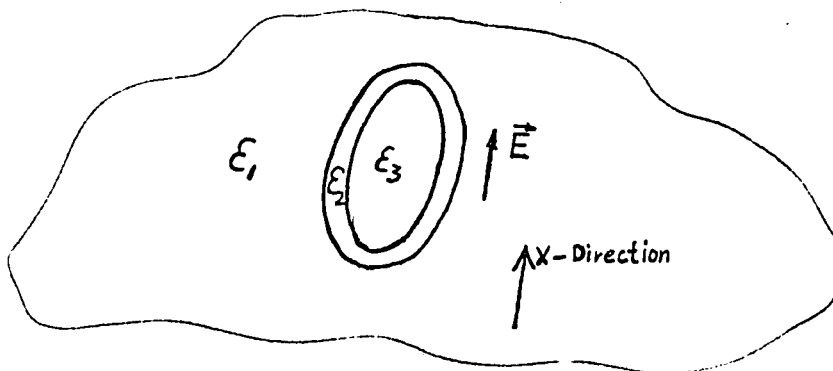
Fig. 2.2 - Homogeneous ellipsoidal shell in homogeneous medium.

In a source free medium the relation between the dielectric displacement, $\vec{D}$, and the electric field, $\vec{E}$, is given by

$$\text{div}\vec{D} = \text{div}\bar{\varepsilon}\cdot\vec{E} = 0 \tag{2.24}$$

By introducing the electric field potential

$$\vec{E} = -\text{grad }\phi$$

Maxwell's first equation

$$\text{curl}\vec{E}=0$$

is immediately satisfied and hence equation (2.24) becomes

$$\text{div}(\bar{\varepsilon}\cdot\text{grad}\phi) = 0 \tag{2.25}$$

For homogeneous media $\bar{\varepsilon}$ is a tensor of rank two whereby equation (2.25) reduces to Laplace's equation

$$\nabla^2\phi = 0 \tag{2.26}$$

In ellipsoidal co-ordinates Laplace's equation becomes[2]

$$\nabla^2\phi = \frac{4}{(\xi-\eta)(\zeta-\xi)(\eta-\zeta)} \cdot$$
$$\left[(\eta-\zeta)R_\xi\frac{\partial}{\partial\xi}(R_\xi\frac{\partial\phi}{\partial\xi})+(\zeta-\xi)R_\eta\frac{\partial}{\partial\eta}(R_\eta\frac{\partial\phi}{\partial\eta})+(\xi-\eta)R_\zeta\frac{\partial}{\partial\zeta}(R_\zeta\frac{\partial\phi}{\partial\zeta})\right]=0 \tag{2.27}$$

where

$$R_u = \sqrt{(u+a^2)(u+b^2)(u+c^2)}$$

A uniform electric field $\vec{E}$ is applied to the material lying along one of the ellipsoidal axis[*]. Hence the potential due to $\vec{E}$ is[**]

$$\phi_o = -Ex = -E\sqrt{(\xi+a^2)(\eta+a^2)(\zeta+a^2)/(b^2-a^2)(c^2-a^2)} \tag{2.28}$$

---

[*] Superposition can be used to obtain the case where $\vec{E}$ lies in an arbitrary direction.

[**] From here on it is assumed that all three regions are isotropic but the mixture itself may be anisotropic. In principle, the following procedure applies equally well for anisotropic media when the formalism of tensor analysis is employed.

Outside the shell the potential is modified due to the presence of the shell and the enclosed ellipsoid, whence

$$\phi_1 = \phi_0 + \phi'$$

where it is assumed

(2.29)

$$\phi' = \phi_0 F(\xi)$$

Therefore

(2.30)

$$\phi_1 = \phi_0 \{1 + F(\xi)\}$$

ϕ' was chosen to make the functional dependence of ϕ_1 on η and ζ the same as for ϕ_0 in order that the boundary conditions can be satisfied at the outer shell surface $\xi = 0$, for arbitrary η and ζ.

Substituting equation (2.29) into equation (2.27) gives a second order differential equation

(2.31)

$$\frac{d^2F}{d\xi^2} + \frac{dF}{d\xi} \frac{d}{d\xi} \log R_\xi (\xi + a^2) = 0$$

Two solutions, easily verified by substitution, can be found for equation (2.31), namely[2, 3]

(2.32)

$$F = constant$$

and

(2.33)

$$F = A \int_\xi^\infty \frac{d\xi}{(\xi + a^2) R_\xi}$$

The upper limit in equation (2.33) is determined by the condition that the perturbation effect due to the ellipsoidal shell and inclusion must go to zero at infinity.

In region 2 the potential must have the same dependence on η and ζ as in

region 1, hence

$$\phi_2 = C\phi_0 + \phi''$$

where

$$\phi'' = \phi_0 F'(\xi)$$

or

$$\phi_2 = \phi_0 \{C + F'(\xi)\} \tag{2.34}$$

with $F'(\xi)$, a solution to equation (2.32), given by

$$F'(\xi) = B \int_{\xi}^{\infty} \frac{d\xi}{(\xi + a^2) R_{\xi}} \tag{2.35}$$

In region 3, however, the behavior of the field due to the potential form given by equation (2.30) and (2.34) becomes irregular at the center of the ellipsoid. As $\xi \to -c^2$ the integral function F or F' behaves as $\sqrt{\xi + c^2}$ but the potential gradient behaves as $1/\sqrt{\xi + c^2}$ and hence at $\xi = -c^2$ the field becomes infinite.

The only remaining solution which satisfies equation (2.32) and the boundary conditions on the inner surface of the shell, for arbitrary η and ζ is given by equation (2.32). Therefore the potential in region 3 is written as

$$\tag{2.36}$$

$$\phi_3 = D\phi_0$$

A comparison of equations (2.28) and (2.36) indicates that for a uniform applied field $\bar{E}$ the field interior to the inner ellipsoid is also uniform. However, the field within the shell is nonuniform due to the added dependence on ξ, see equation (2.34).

Continuity of the potential across boundary 1-2 requires

$$\phi_1 \Big|_{\xi=0} = \phi_2 \Big|_{\xi=0} \tag{2.37}$$

Hence, by equations (2.30) and (2.34) and a comparison of (2.33) and (2.35) one obtains

$$1 + F(0) = C + F'(0) \tag{2.38}$$

Similarly at boundary 2-3 it is necessary that

$$\phi_2 \Big|_{\xi=-k^2} = \phi_3 \Big|_{\xi=-k^2} \tag{2.39}$$

The surface $\xi=-k^2$ is the inner surface of the shell. Just as the axes of the outer ellipsoid are given by a, b, and c, so the axes of the inner ellipsoid are designated as a', b', and c' which are defined as

$$\begin{aligned}
a'^2 &= a^2 - k^2 \\
b'^2 &= b^2 - k^2 \\
c'^2 &= c^2 - k^2
\end{aligned} \tag{2.40}$$

Thus equation (2.39) yields

$$C + F'(-k^2) = D \tag{2.41}$$

Furthermore, the normal derivatives must be continuous, hence, at boundary 1-2

$$\varepsilon_1 \left(\frac{\partial \phi_1}{h_1 \partial \xi} \right) \Big|_{\xi=0} = \varepsilon_2 \left(\frac{\partial \phi_2}{h_1 \partial \xi} \right) \Big|_{\xi=0} \tag{2.42}$$

where[*]

---

[*] In generalized coordinates the element of length is given by $du = h_1 dx$.

$$h_1 = \sqrt{(\xi-\eta)(\xi-\zeta)}/2R_\xi \qquad (2.43)$$

Substitution for ϕ_1 and ϕ_2 results in

$$\varepsilon_1 \left[1+F(0)\right]\frac{\partial\phi_0}{\partial\xi}\Big|_{\xi=0} + \left(\phi_0\frac{\partial F}{\partial\xi}\right)\Big|_{\xi=0} =$$

$$= \varepsilon_2 \left[C+F'(0)\right]\frac{\partial\phi_0}{\partial\xi}\Big|_{\xi=0} + \left(\phi_0\frac{\partial F'}{\partial\xi}\right)\Big|_{\xi=0} \qquad (2.44)$$

which by the use of equations (2.28) and (2.33) reduces to [*]

$$(2.45)$$

$$\varepsilon_1[1+F(0)] - \frac{2A}{abc} = \varepsilon_2[C+F'(0)] - \frac{2B}{abc}$$

At boundary 2-3

$$\varepsilon_2\left(\frac{1}{h_1}\frac{\partial\phi_2}{\partial\xi}\right)\Big|_{\xi=-k^2} = \varepsilon_3\left(\frac{1}{h_1}\frac{\partial\phi_3}{\partial\xi}\right)\Big|_{\xi=-k^2} \qquad (2.46)$$

which similarly reduces to

$$\varepsilon_2[C + F'(-k^2) - \frac{2B}{abc}] = \varepsilon_3 D \qquad (2.47)$$

Equations (2.38), (2.41), (2.45), and (2.47) can now be solved for the constants A, B, C and D with the aid of equations (2.33), and (2.35).

The ratio of the electric field internal to the region 3 to that of the field in region 1 can be expressed as

$$\frac{E_3}{E_1} = \frac{D\phi_0}{\phi_1} = \frac{D}{1+F(\xi)} \qquad (2.48)$$

---

[*] The term, $\frac{\partial F}{\partial\xi}$, gives rise to the negative signs in equation (2.45).

At distances large compared to the inclusion size[*], $F(\xi) \to 0$ whereby

$$\frac{E_3}{E_1} = \frac{E_3}{E_{av}} = D \tag{2.49}$$

Depolarization coefficients for an ellipsoid are defined as

$$n^x = \frac{abc}{2} \int_0^\infty \frac{d\xi}{(\xi+a^2)R_\xi} \tag{2.50}$$

with n^y and n^z defined similarly by replacing ξ and a^2 by η, b^2 and ζ, c^2 respectively. From equation (2.33) and (2.50)

$$F(0) = \frac{2n^x A}{abc} \tag{2.51}$$

For the inner ellipsoid the depolarization coefficients can be redefined as

$$n'^x = \frac{a'b'c'}{2} \int_{-k^2}^\infty \frac{d\xi}{(\xi+a^2)R_\xi} \tag{2.52}$$

hence

$$F(-k^2) = \frac{2n'^x A}{a'b'c'} \tag{2.53}$$

Use of equations (2.53) and (2.51) in (2.38), (2.41), (2.45), and (2.47) yields

$$C = 1 + \frac{2n^x}{V}(A-B) \tag{2.54}$$

$$C = D - \frac{2Bn'^x}{V'} \tag{2.55}$$

---

[*] By equation (2.48) it is possible to compute a correction factor to the internal to external field ratio. For low volume filling factors, however, this correction is negligible.

$$\varepsilon_2 C = \varepsilon_1 + \frac{2(n^x-1)}{V}(\varepsilon_1 A - \varepsilon_2 B) \qquad (2.56)$$

$$\varepsilon_2 C = \varepsilon_3 D - 2B \frac{(n'^x-1)}{V'} \varepsilon_2 \qquad (2.57)$$

where $V=abc$ and $V'=a'b'c'$

Eliminating C between equations (2.55) and (2.57) yields

$$D(\varepsilon_2 - \varepsilon_3) = 2B\frac{\varepsilon_2}{V'} \qquad (2.58)$$

From equations (2.54) and (2.56)

$$2A\{n^x(\varepsilon_1 - \varepsilon_2) + \varepsilon_1\} = 2B\frac{\varepsilon_2}{V} + \varepsilon_1 - \varepsilon_2 \qquad (2.59)$$

Substituting for B from equation (2.58) into (2.55) and combining the result with equation (2.54) gives

$$D\{\varepsilon_2 - n'^x(\varepsilon_2 - \varepsilon_3)\} = \varepsilon_2 + \frac{2n^x\varepsilon_2}{V}(A - B) \qquad (2.60)$$

Substituting for A from equation (2.59), for B from equation (2.58) and rearranging the result finally gives

$$D = \frac{E_3^x}{E_{av}^x} = \varepsilon_2\varepsilon_1\{[\varepsilon_2 + (\varepsilon_2 - \varepsilon_3)(n^x\frac{V'}{V} - n'^x)] \cdot$$
$$[\varepsilon_1 + n^x(\varepsilon_2 - \varepsilon_1)] - n^x\frac{V'}{V}\varepsilon_2(\varepsilon_2 - \varepsilon_3)\}^{-1} \qquad (2.61)$$

Therefore, the solution to equation (2.49) is given by the value of D in equation (2.61) which thus yields the ratio of the field in the inner ellipsoid to the average field in the surrounding material.

Similarly by equations (2.30) and (2.34) the ratio of the field in the shell to the average field in the material is given by

$$(E_2^x \,/\, E_{av}^x) = C + F'(\xi) \qquad ; \quad -k^2 < \xi < 0 \qquad\qquad (2.62)$$

Hence, the electric field in the shell is not uniform because of the dependence on ξ. For thin shells one can average over the thickness of the shell to obtain a mean value of the electric field in the shell. To do this the value of the integral function $F(\xi)$ at the shell boundaries can be found in terms of the depolarization coefficients. Thus the sum of $F'(\xi)$ at the two shell boundaries is given by

$$F'(\xi)\Big|_{-k^2}^{0} = B \int_{-k^2}^{\infty} \frac{d\xi}{(\xi+a^2)R_\xi} + B \int_{0}^{\infty} \frac{d\xi}{(\xi+a^2)R_\xi} = \frac{2B}{V}(n'^x \frac{V}{V'} + n^x) \qquad (2.63)$$

If a linear variation of E_2 across the shell is assumed, the average field in medium 2 is obtained by using half the value of equation (2.63) in equation (2.62) which yields

$$\frac{E_2^x}{E_{av}^x} \simeq C + \frac{B}{V}\left(n'^x\left(\frac{V}{V'}\right) + n^x\right) \qquad\qquad (2.64)$$

Solving for C and B from equations (2.55) and (2.58) and using (2.61) to eliminate D yields

$$\frac{E_2^x}{E_{av}^x} = \varepsilon_1[\varepsilon_2 + (\frac{\varepsilon_3 - \varepsilon_2}{2})(n'^x - n^x \frac{V'}{V})] \cdot$$

$$\{[\varepsilon_2 + (\varepsilon_2 - \varepsilon_3)(n^x \frac{V'}{V} - n'^x)][\varepsilon_1 + n^x(\varepsilon_2 - \varepsilon_1)] - n^x \frac{V'}{V}\varepsilon_2(\varepsilon_2 - \varepsilon_3)\}^{-1} \qquad (2.65)$$

Hence, equations (2.61) and (2.65) give the relationship between the fields in regions 3 and 1 and regions 2 and 1 respectively. The latter equation is a good approximation for thin shells only.

Setting $\varepsilon_3 = \varepsilon_2$ in equation (2.61) gives the well known solution for the internal field in ellipsoidal inclusions of dielectric constant ε_2 dispersed in a homogeneous isotropic medium of dielectric constant ε_1

$$\frac{E_{int}^x}{E_{av}^x} = \varepsilon_1[\varepsilon_1 + n^x(\varepsilon_2 - \varepsilon_1)]^{-1} \qquad\qquad (2.66)$$

Similarly, for a spherical shell of internal and external radii b and a and dielectric constant ϵ_3 and ϵ_2 respectively in a host material of dielectric constant ϵ_1, equation (2.61) becomes[*]

$$\frac{E_3^x}{E_{av}^x} = 9\epsilon_2\epsilon_1[(\epsilon_2+2\epsilon_1)(2\epsilon_2+\epsilon_3) - 2(\frac{b}{a})^3(\epsilon_2-\epsilon_3)\epsilon_2-\epsilon_1)]^{-1} \quad (2.67)$$

Equivalent relations can be written for the y and z directions of the electric field by replacing superscripts x by y or z.

However, the electric field in the vicinity of an inclusion is not exactly equal to that of the average field in the mixture. This is due to the spatial variation of the field in the neighborhood of a particle, see for example, equation (2.48). In order to account for this variation one can introduce an artificial dielectric constant, ϵ^* as suggested by DeLoor[14], to replace the dielectric constant of the material surrounding the inclusions. Alternatively, the correct field variation can be calculated by evaluating the expression $1+F(\xi)$.

Unfortunately, both procedures require a detailed knowledge about the statistical variation in particle location. In the case of solids, relatively little is known about their statistical properties and hence the solution to the problem of finding the exact depolarizing fields in dielectric mixtures can only be estimated by empirical methods. Nevertheless bounding values can be determined for the effective dielectric constant ϵ^* which, as

---

[*] Landau and Lifshitz solved this problem (see reference 2, p.45) and gave the solution for the sperial case $\epsilon_1=\epsilon_2=1$ (vacuo) and $\epsilon_2^*=\epsilon$.

De Loor showed for non-dissipative media, always falls between the value of the host and mixture dielectric constants.

In actual mixtures one often finds a thin shell of included material, such as absorption layers, inside a host medium in which case $\varepsilon_1 = \varepsilon_3$. Making the substitution $\varepsilon_1 = \varepsilon_3 = \varepsilon^*$ in equation (2.65) and substituting the results for T_i in equation (2.22) finally yields

$$\varepsilon^j - \varepsilon_h = v_2(\varepsilon_2 - \varepsilon_h)\varepsilon^*[\varepsilon_2 + \frac{\varepsilon^* - \varepsilon_2}{2}(n_j' - n_j\frac{V'}{V})] \cdot$$

$$\{[\varepsilon_2 + (\varepsilon_2 - \varepsilon^*)(n_j\frac{V'}{V} - n_j')][\varepsilon^* + n_j(\varepsilon_2 - \varepsilon^*)] - n_j\frac{V'}{jV}\varepsilon_2(\varepsilon_2 - \varepsilon^*)\}^{-1} \qquad (2.68)$$

where v_2 is the normalized filling factor and the subscript j refers to the jth coordinate axis.

Equation (2.68) relates the mixture dielectric constant, ε^j, to the dielectric constant of the host material, ε_h, with thin ellipsoidal inclusions of dielectric constant ε_2 and volume filling factor v_2. Limiting values for the mixture dielectric constant are obtained by solving equation (2.68) with $\varepsilon^* = \varepsilon_h$ and $\varepsilon^* = \varepsilon$. If spherical and ellipsoidal inclusions also exist within the mixture then other terms will appear in the equation as a direct result of the substitution for the various values of $\bar{T}_i$ in equation (2.22).

Since the boundary conditions to the above problem were stated without any restriction on the dielectric constants, the solutions are valid for lossless or lossy materials. The only restriction is that the assumption about the uniformity of fields be applicable. In order to calculate the low and high frequency dielectric constants of a mixture, the appropriate dielectric constants for the included and host materials are used in the equations. Generally, the equations developed here will be valid for any frequency and

temperature if the corresponding values of the individual dielectric constants are used.

Practical Significance of Thin Shell Inclusions

It can readily be shown that for the case of a spherical thin shell with $b \approx a$, $\varepsilon_3 = \varepsilon_1$, and $\varepsilon_2 >> \varepsilon_1$ that the field internal to the shell is approximately 2/3 times the average field in the mixture. Ellipsoidal shells would tend to enhance this internal field even further in the direction of the major axis. This internal field for a shell inclusion is about twice as large as the internal field found for spherical inclusions under the same assumptions. Increasing the internal field causes an increase in the dielectric constant of the mixture. This is significant since present mixture theories applied to materials assumed to have spherical or ellipsoidal inclusions yield values for the dielectric constant which are lower than the experimental values.[*]

It is suggested by the author that the neglect of thin shell inclusions, when they exist, will be an important contributing factor to such discrepancies. In any case, it becomes apparent that the geometry of the inclusions is an extremely important factor in dielectric mixture calculations.

VALIDITY OF THE MIXTURE RELATION

In the derivation of the general mixture relation the following assumptions were made: 1. The mixture can be described by an average dielectric constant, $\bar{\varepsilon}$, and an average electric field, $\vec{E}_{av}$. 2. Inclusions

---

[*] Hasted and Shah[62] found that the limiting values of mixture dielectric constants given by De Loor (14) fall below the experimental values found for brick. It is very likely that in brick thin shells of water are formed along the inside walls of air cavities and around particles making it necessary to use the internal field predicted by equation (2.65) rather than equation (2.66) commonly used.

are treated individually as being present in a material with the properties

just stated under (1). Hence, particle interaction effects are neglected

insofar as the value of the calculated internal field accounts only for

the individual reaction* fields of each inclusion and $\bar{\varepsilon}$ is an average

dielectric constant of the remaining mixture. 3. Quasistationary

arguments must be applicable to the mixed system.

Assumption (1) is a classification of the problem and its solution

rather than a restriction on the theory. It does, however, require the

validity of assumption (3) because, for inclusions comparable in size to

a wavelength, the field cannot be uniform any more and hence the mixture

cannot fairly be described by an average field distribution. It has been

shown that inhomogeneity of the local field in the neighborhood of a

small particle makes no primary contribution to the average field (see

Kirkwood[11]). Hence small irregularities in the shape of the particles

can be neglected.

Validity of assumption (2) requires that the square of the normalized

volume filling factor $\sum_{i=1}^{N} V_i/V$, is small compared to unity. For large

filling factors, deviation from the theoretical behavior is to be

expected** even though the interaction phenomena is often a second or

third order effect.[21] This author is of the opinion that a large number

----

*   When a particle is placed inside a cavity, the same size as the
     particle, in a dielectric medium, there is a contribution to the
     total average field in the medium due to the polarization of the
     particle. This added term to the total field is often called the
     'reaction field' (10, 11, 12, 14). In the previous section the
     reaction field was given by the potential function ϕ_1.

**   By virtue of equation (2.30) the electric field next to an inclusion
     is not uniform anymore but its spatial dependence is calculable.

of the errors associated with the various mixture theories are due to the fact that mixtures to which the relations are applied do not meet the basic assumptions of the theory <u>aside</u> from particle interaction phenomena. A distribution of a large number of particle shapes in a mixture can contribute major errors if the theoretical relation simply assumes particles of one specific geometry. The present generalized treatment of the problem should yield more accurate estimates of practical mixtures, eventhough the computational difficulty is increased. The latter objection is largely negated by the increased availability of direct access computer terminals. All the calculations in this thesis were done by using APL[24] programs on an IBM 360/67 computer. The theory of this chapter is applied to the cellulose-air-water system in chapter 6 and the results compared to experimental data on such a mixture.

TEMPERATURE AND FREQUENCY DEPENDENCE OF DIELECTRICS

INTRODUCTION

Knowledge about the temperature and frequency behavior of dielectric materials is essential for designing systems in which dielectrics play an important role. For example, in microwave power applicators the dielectric properties of the treated material determine the heating rate, drying rate, stability, maximum attainable temperature, energy distribution and electromagnetic coupling efficiency.

This chapter, divided into two sections, will give the fundamental equations relating the dynamic properties of dielectrics to some basic material constants. Experimental verification of a few of the results is given here with the more extensive experimentally obtained data analyzed in chapter 5.

In the first section the treatment covers a generalized formulation of the temperature dependence of wide dispersion, low loss dielectrics. The second section gives a detailed analysis of the temperature and frequency dependence for materials exhibiting a Gaussian distribution of relaxation times. Solutions of the integral equations are obtained by the use of numerical techniques on a digital computer.

A. TEMPERATURE BEHAVIOR OF WIDE-DISPERSION DIELECTRICS

The work of Gevers and Du Pré [38] (1945) represents a major contribution to the understanding of the temperature dependence of materials

which they classified as "technical solids" (low loss tangents). Their analysis shows that in the case of dielectrics having either a small thermal expansion coefficient, or a low value of the dielectric constant, the ratio, A, between the temperature coefficient of the dielectric constant and the loss tangent is approximately independent of the nature of the dielectric in the frequency range of 1000 Hz to 10 MHz and at temperatures between -50 and 150°C. They show A to have a value lying between .04 and .06.

Underlying their analysis is the basic assumption that relaxation phenomena in dielectrics can be described in a manner similar to a chemical rate process and that a distribution of relaxation times exists in the material. Gevers' [39] work includes a comprehensive review of the literature. His results have been used extensively by other authors. [41, 44, 66]

Garton [41] has suggested that a more generalized approach should be taken to the derivation of Gevers' and Du Pré's law. This general law, relating the ratio of dielectric temperature coefficient and loss tangent is derived for the first time in this thesis. Experimental data will show the new law to be more accurate and satisfactory in practice.

DERIVATION OF A GENERAL LAW FOR WIDE DISPERSION DIELECTRICS

Any dielectric polarization mechanism which is linear with regard to the applied field can be represented by [40, 43, 66]

$$\mathcal{E}' = \mathcal{E}_\infty + \left(\mathcal{E}_0 - \mathcal{E}_\infty\right)\int_{\tau_0}^{\infty} \frac{f(\tau)\, d\tau}{1 + \omega^2 \tau^2} \tag{3.1}$$

$$\mathcal{E}'' = \left(\mathcal{E}_0 - \mathcal{E}_\infty\right)\int_{\tau_0}^{\infty} \frac{f(\tau)\, d\tau}{1 + \omega^2 \tau^2} \tag{3.2}$$

where τ is the relaxation time of a particular polarization mechanism, ω is the radial frequency, $f(\tau)$ is a distribution function of relaxation times, ε_∞ is the value of the dielectric constant at a frequency high enough to make the dispersion of ε' due to the assumed polarization mechanism negligible, ε_0 is the value of ε' at a frequency much smaller than the frequency at which maximum loss occurs, and τ_0 is the shortest time constant present in the substance.[*]

It is desirable to find a distribution function $f(\tau)$ such that the frequency variation of the loss tangent is nearly constant over a wide range of frequencies since many solid dielectrics exhibit such a behavior. By inserting a few trial functions into equation (3.2) it is found that a form of $f(\tau)$ which leads to a constant value of ε'' over a wide frequency range is given by

$$f(\tau) = 1/\tau \tag{3.3}$$

Substitution of equation (3.3) into equation (3.2) and using the change of variable $\omega\tau = \tan\theta$ under the condition that

$$0 < \omega\tau_0 \ll 1 \tag{3.4}$$

whence

$$\tan^{-1}\left(\omega\tau_0\right) \simeq \omega\tau_0$$

gives

$$\varepsilon' = \varepsilon_\infty - \left(\varepsilon_0 - \varepsilon_\infty\right) \ln \omega\tau_0 \tag{3.5}$$

and

$$\varepsilon'' = \pi\left(\varepsilon_0 - \varepsilon_\infty\right)/2 \tag{3.6}$$

---

[*] τ_0 is the time required for molecules to turn from one equilibrium position to another multiplied by a probability factor which is related to the temperature dependence of the energy barrier separating two equilibrium positions. (39, 66) (see also section B of this chapter.)

From equation (3.6) it follows that

$$\varepsilon_0 - \varepsilon_\infty = 2\varepsilon''/\pi = 2\varepsilon'\tan\delta/\pi \qquad (3.7)$$

which when combined with equation (3.5) yields

$$\varepsilon' = \varepsilon_\infty - \left[2\varepsilon'\tan\delta \, Ln(\omega\tau_0)/\pi\right] \qquad (3.8)$$

It is usually assumed that the high-frequency dielectric constant, ε_∞, is independent of temperature. That this assumption is in fact correct is shown by Van Vleck [18] in his quantum mechanical treatment of the dielectric constant.* Furthermore, τ_0, the shortest time constant present, is assumed to be independent of temperature as well and can be regarded as a constant of the material.**

Differentiating equation (3.8) w.r.t. the temperature, T, yields

$$\frac{d\varepsilon'}{dT} = -(2/\pi)Ln(\omega\tau_0)\left[\frac{d\varepsilon'}{dT}(\tan\delta) + \varepsilon'\frac{d\tan\delta}{dT}\right] \qquad (3.9)$$

or

$$\frac{1}{\varepsilon'\tan\delta}\frac{d\varepsilon'}{dT} = \frac{\frac{2}{\pi}Ln(1/\omega\tau_0)\frac{d}{dT}Ln\tan\delta}{1 - \frac{2}{\pi}\tan\delta \, Ln(1/\omega\tau_0)} \qquad (3.10)$$

When either the linear coefficient of thermal expansion, or the dielectric constant of the material is very large the temperature expansion term, $d\varepsilon_\infty/dT$, may be appreciable but can readily be calculated*** and included

---

* There is a temperature dependence of the high frequency dielectric constant only insofar as the density of the material changes with varying temperatures.
** Experimental evidence to justify this assumption is given later in this chapter.
*** Based on Clausius-Mossotti's Law, Gevers and DuPré[38] derived the following expression for the temperature dependence of ε_∞:

$$\frac{1}{\varepsilon'}\frac{d\varepsilon_\infty}{dT} = -\alpha_\ell\left(1 + \varepsilon_\infty - 2/\varepsilon_\infty\right)$$

where α_ℓ is the linear expansion coefficient of the dielectric.

in equation (3.10). The temperature dependence of the loss tangent for the class of materials treated here can be written as[*]

$$\tan \delta \propto T^n e^{-a/T} \tag{3.11}$$

Hence

$$\frac{d}{dT} \ln \tan \delta = \frac{1}{\tan \delta} \frac{d \tan \delta}{dT} = \frac{n}{T} + \frac{a}{T^2} \tag{3.12}$$

Thus, equation (3.10) can be rewritten as

$$A' = \frac{1}{\varepsilon' \tan \delta} \frac{d\varepsilon'}{dT} = \frac{\frac{2}{\pi} Ln(1/\omega\tau_0)\left(\frac{n}{T} + \frac{a}{T^2}\right)}{1 - \frac{2}{\pi} Ln(1/\omega\tau_0)\tan \delta} \tag{3.13}$$

The term in the denominator on the R.H.S. of equation (3.13) is only close to unity when

$$\frac{2}{\pi} Ln(1/\omega\tau_0) \tan \delta \ll 1 \tag{3.14}$$

In the special case when n=1, a=o and the condition (3.14) holds, the general law given by equation (3.13) reduces to Gevers' and Du Pré's result, namely,

$$A = \frac{1}{\varepsilon' \tan \delta} \frac{d\varepsilon'}{dT} = \frac{2}{\pi T} Ln(1/\omega\tau_0) \tag{3.15}$$

The relation in equation (3.15) is a good approximation only when the loss tangent depends linearly on temperature and obeys condition (3.14).

---

[*] Equation (3.11) is based on a theoretical treatment given by Garton[40] and relates favorably to experimental results on low loss materials.
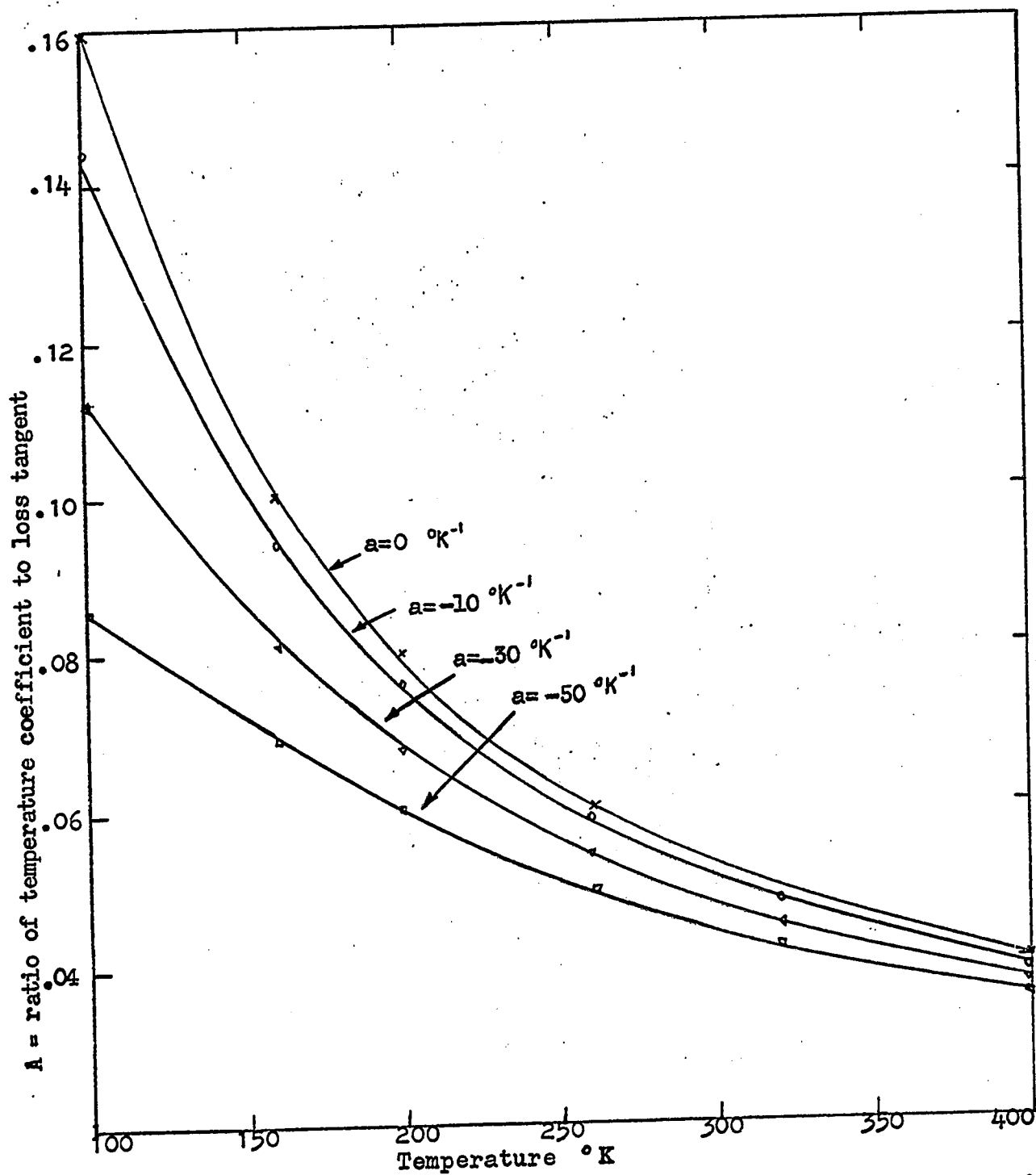
Fig. 3.1 - Graphical solution of equation (3.13) as a function of temperature with n=1 and a as the parameter. The case a=0 is equivalent to equation (3.15).

A plot of equation (3.13) and its special case, equation (3.15), for an arbitrary value of $Ln(1/\omega\tau_o)$ is given in figure 3.1 with n chosen as unity and a given as a parameter. The plot shows very distinctly the effect of the exponential factor, $e^{-a/T}$, in the loss tangent – temperature expression.

For the sake of simplicity the denominator of equation (3.13) was set to unity to obtain figure 3.1. The added effect of the denominator is an increased magnitude of the ordinate for nonzero a-values with the largest positive correction occurring at the highest temperatures.

Figures 3.2 through 3.4 give plots of A as a function of temperature for mycalex, porcelain, and ebonite respectively. The data were originally plotted by Gevers (see part V of Reference 39) and compared with a plot of equation (3.15) which gave rise to large deviations at the low temperature end. Here the general equation (3.13) and its special case, equation (3.15), are plotted and compared with actual experimental data, quoted from Gevers' work, indicating an improved correspondence between theory and experiment, especially at the lower temperatures. It is further evident that the generalization of the temperature behavior of the loss tangent still allows the value of A to remain fairly constant for the class of materials under discussion. Values of the exponent a were chosen to give a reasonable fit between the theoretical and experimental curves.

In part III of Gevers' paper[39] it is stated that the ratio of the temperature coefficient and loss tangent for a mixture having components with both positive and negative temperature coefficients cannot be a constant anymore. However, a plot of $(d\varepsilon'/dT)/\varepsilon' \tan \delta$ vs. temperature for
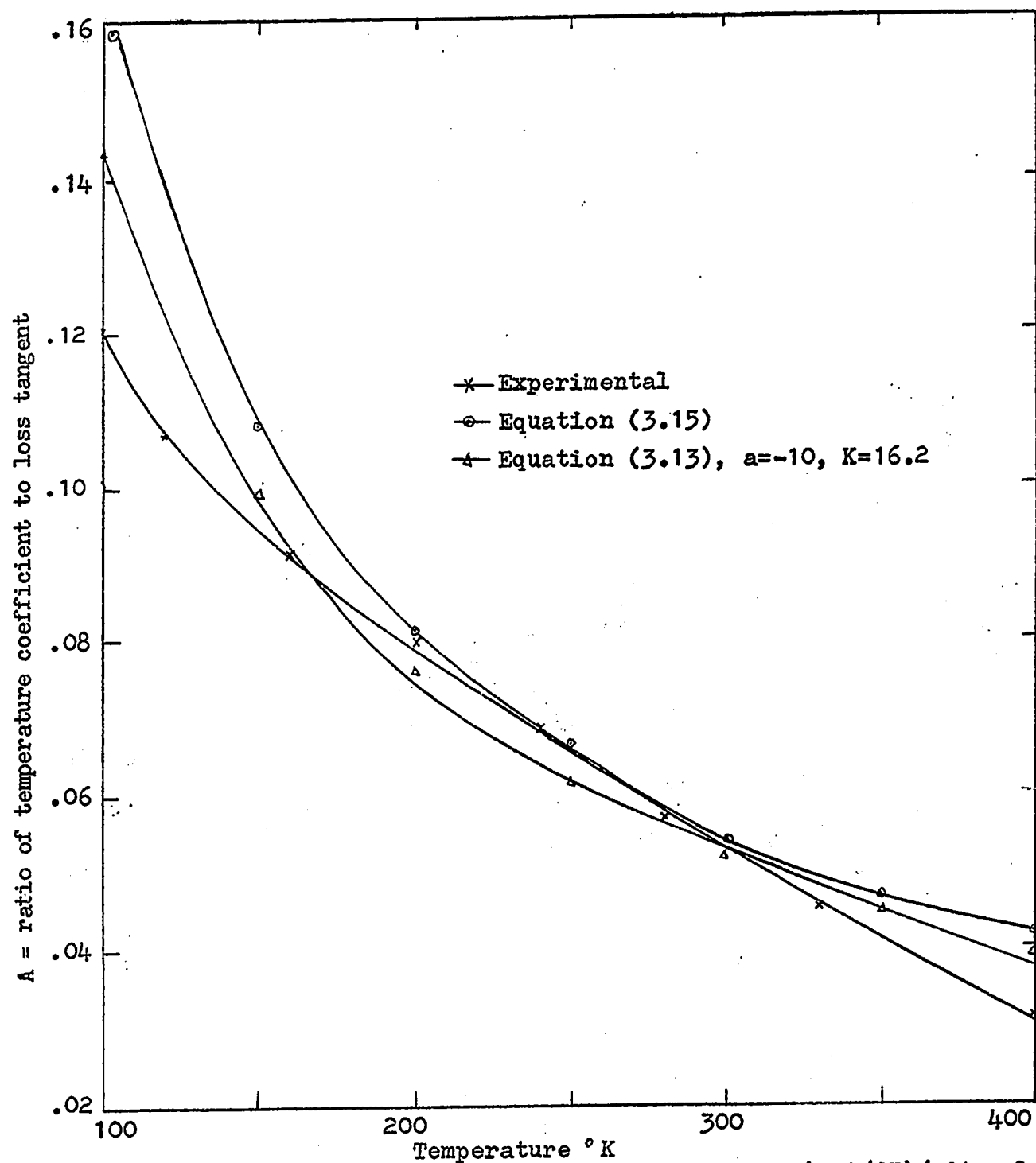
Fig. 3.2 — Theoretical and experimental plot of $(d\mathcal{E}'/dT)/\mathcal{E}'\tan\delta$ versus temperature for Mycalex.
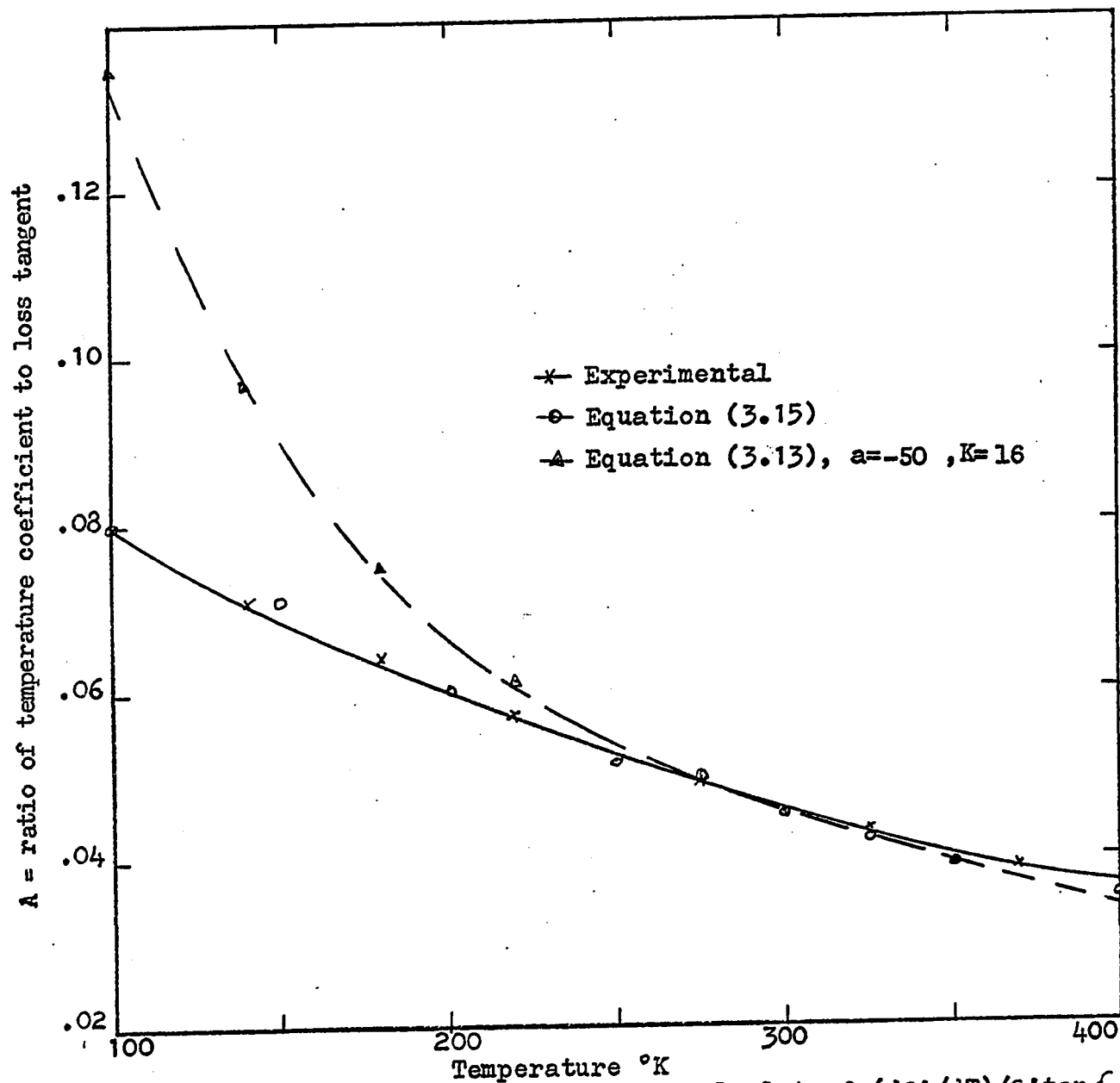
Fig. 3.3 - Theoretical and experimental plot of $(d\varepsilon'/dT)/\varepsilon'\tan\delta$ versus temperature for Porcelain.
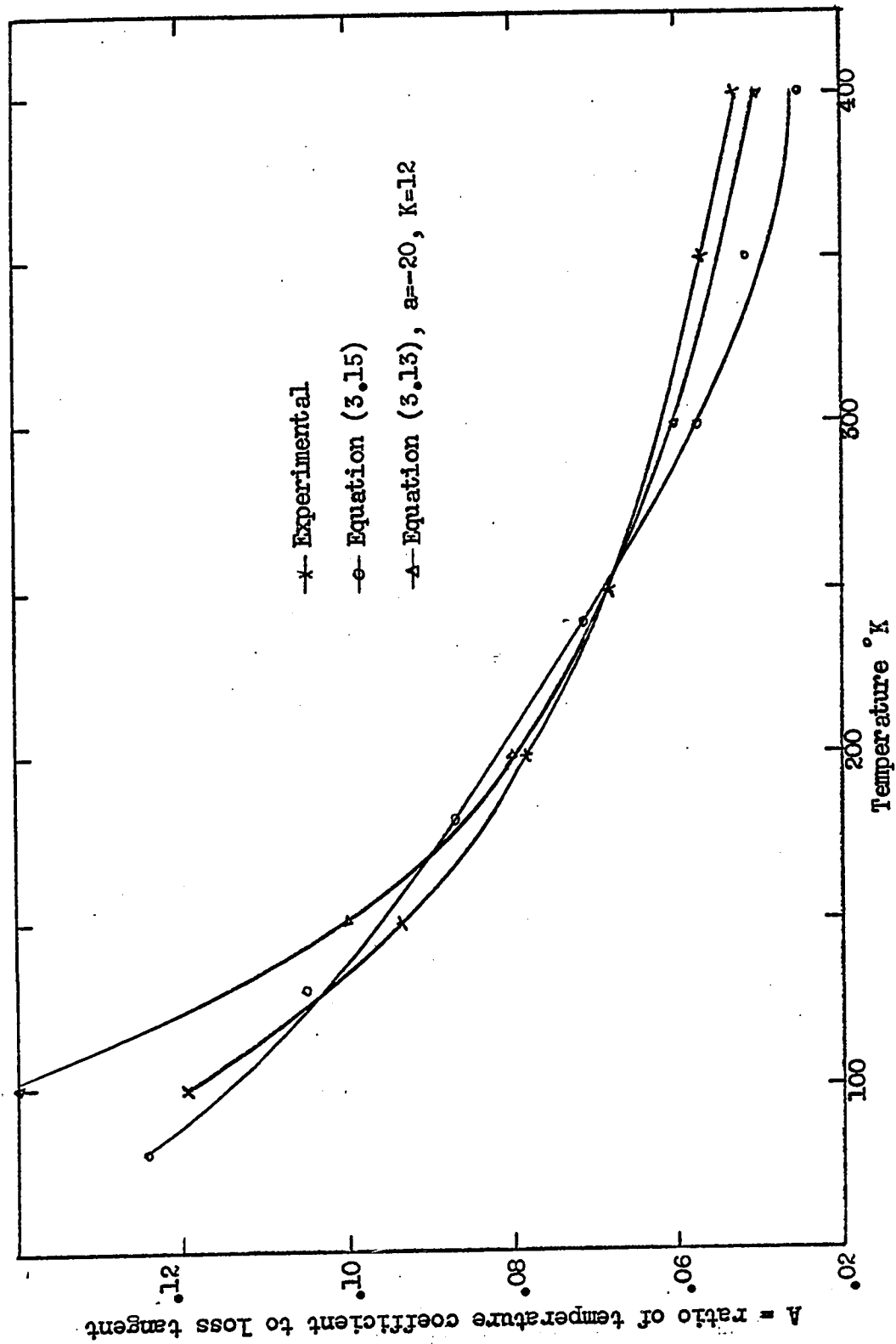
Fig. 3.4 — Theoretical and experimental plot of $(d\epsilon'/dT)/\epsilon'\tan\delta$ versus temperature for Ebonite.

Douglas Fir at a low percentage moisture content indicates values for A

falling within the range of .02 to .08, (see figure 3.5) over a narrow tempera-

ture range. Even though cellulose and water have temperature coefficients of

opposite sign, a cellulose-air-water mixture such as wood gives rise to a wide

distribution of relaxation times, flattening the loss vs. frequency curve,

and hence approximately obeying the basic assumption used to derive equation

(3.13).

It will be shown in chapter 5 that the distribution of relaxation times

exhibited by wood obeys a Gaussian distribution and not a $1/\tau$ distribution as

assumed here. For this reason the temperature variation of A as a function

of T calculated for Douglas Fir by means of equation (3.13) is not as great

as the experimental temperature variation which is evident from figure 3.5.

It is concluded that the ratio of the temperature coefficient of the

dielectric constant to its loss tangent is reasonably constant for a wide

range of dielectric materials which have an extremely wide dispersion range.

The frequencies at which this law holds are very much lower than the

frequency corresponding to the shortest relaxation time in the material.

B. GENERAL TEMPERATURE AND FREQUENCY DEPENDENCE OF DIELECTRICS

The analysis given in this section is based on fundamental equations

in dielectric theory. By assuming a particular distribution of relaxation

times these equations are developed to give the frequency and temperature

behavior of the material in terms of basic material constants. In chapter

5 the theory is applied to a very practical and naturally occurring
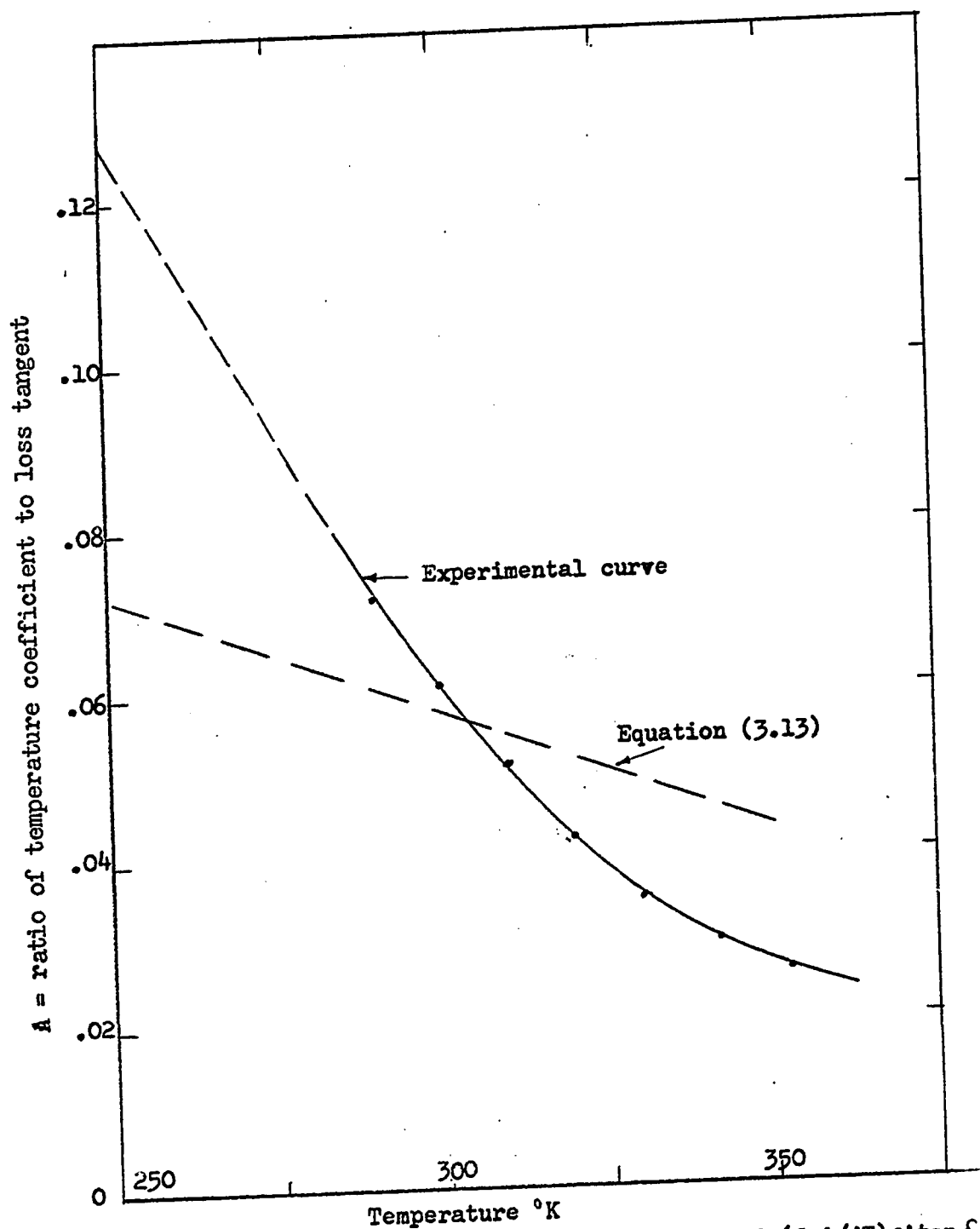
Fig. 3.5 - Theoretical and experimental plot of $(d\varepsilon'/dT)\varepsilon' \tan\delta$ versus temperature for Douglas Fir at 1% moisture content.

dielectric mixture and the results compared with experimental data. It is assumed throughout the analysis that the dielectric dispersion is caused by orientation polarization. Since application of the theory is to be made at microwave frequencies, conduction effects are small and therefore ignored. Neglect of the atomic and electronic polarization mechanisms, giving rise to a resonance type of behavior at frequencies in the infrared range, does not effect the generality of the present analysis.

Discussions on relaxation times, activation energies, and their dependence on temperature can be found in the literature (References 19, 38, 39, 40, 44, 45, 47, 49 and 66). An effort is made to combine the work of various authors, in as far as it aids the analysis, to extend the results and to apply them to the cellulose-air-water system.

For dilute solutions of dipoles in liquids and solids the Debye equations predict the dielectric behavior very satisfactorily. However, these equations give rise to only a single relaxation time. In practice it is found that mixtures of materials contain more than one relaxation time. In fact, very wide distributions of relaxation times may exist.

Equations (3.1) and (3.2) of the previous section have been formulated to allow for such a distribution. In the following analysis it is assumed that the spread of relaxation times obeys a Gaussian distribution function. Such a distribution function allows relaxation times with values between zero and infinity and is mathematically stated as

$$f(\tau)d\tau = \frac{b}{\sqrt{\pi}} e^{-b^2 x^2} dx \qquad (3.16)$$

Experimentally, it is observed that the dielectric dispersion and loss is symmetric on a logarithmic frequency scale. Equation (3.16) will behave similarly by making the transformation

$$x = \ln(\tau/\bar{\tau}) \qquad (3.17)$$

in which τ is the relaxation time, $\bar{\tau}$ is the most probable relaxation time, and b is a probability density parameter. Equation (3.16) substituted into equation (3.2) results in

$$\varepsilon'' = \frac{b(\varepsilon_0 - \varepsilon_\infty)}{\sqrt{\pi}} \int_{x_0 = \text{Ln}(\tau_0/\bar{\tau})}^{\infty} \frac{e^{-b^2 x^2} \omega\tau}{1 + \omega^2\tau^2} \, dx \qquad (3.18)$$

The temperature dependence of ε'' is implicit in the temperature behavior of the relaxation time τ. Following closely the arguments set forth by Gevers[*] the polarization mechanism is explained in subsequent paragraphs.

Particles, such as dipoles and ions, give rise to dielectric losses and are subject to various force fields (Van der Waal's forces, Coulomb forces) due to their surroundings. Each individual particle thus has a certain potential energy w.r.t. its neighbors. Cellulose, the dielectric under study, consists of long molecular chains which when part of a solid, amorphous-crystalline structure like wood, has a great variety of orientations. Hence the assumption is made that a large spread of energy levels exists. A schematic presentation of such an energy system is given in figure 3.6.

When the material is in a state of equilibrium the particles oscillate, due to Brownian motion, in the potential energy wells. From figure 3.6 it follows that in order for a particle to jump to another energy level, say q_{i+1} it must receive a boost in energy equivalent to the

---

[*] Gevers[39] (part III). Garton[40] also treats this subject, but restricts his analysis to the specific case of materials with a low but constant loss tangent, whereas Gevers' arguments are more widely applicable and are substantiated by others (44, 45, 46, 66) who treat relaxation in a manner similar to a chemical rate process.
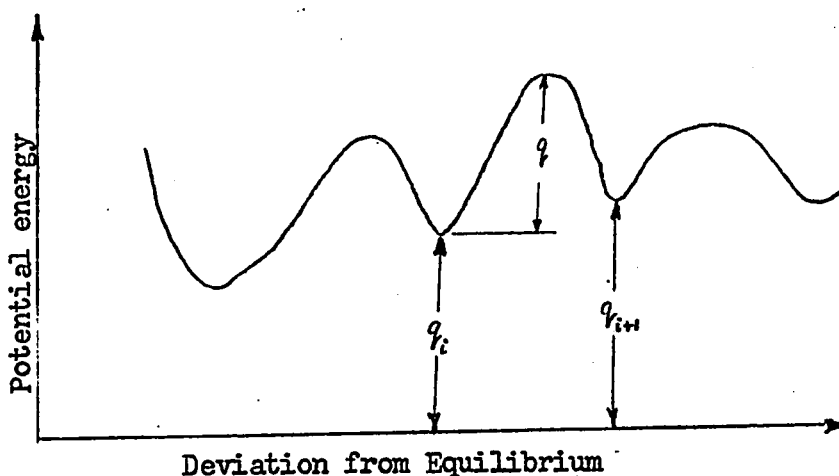
Fig. 3.6 – Schematic presentation of an energy position
diagram for a typical solid dielectric.

barrier height, q, which can occur through Brownian motion or by

collision with other particles arriving or present at that particular

energy level q_i, hence the name activation energy. The probability that

a particle acquires an extra energy q is proportional to $e^{-q/kT}$ where T

is the absolute temperature and k is Boltzman's constant. Thus, the

number of oscillations about the equilibrium position which a particle

has to carry out is proportional to $e^{q/kT}$ and therefore the mean time

during which a particle is in its equilibrium position is

$$\tau = \tau_0 \, e^{q/kT} \tag{3.19}$$

where τ_0 is the proportionality factor.[*]

---

[*] τ_0 consists of the product of two terms. One term represents the time
of oscillation between equilibrium positions and the second term is a
probability factor related to the population density in the higher and
lower energy states. τ_0 is usually found to be shorter than the time
required for a molecule to change equilibrium positions.

Hereafter it is assumed that equation (3.19) describes the temperature dependence of the relaxation time of the molecular polarization because when an electric field is applied to the material the dipoles rotate and the ions move in the direction of the applied field requiring for this process the activation energy q.

The proportionality factor τ_0 active in the process is assumed independent of the activation energy and the temperature. In general the activation energy will depend on temperature as is the case for cellulose mixtures[47]. If such a dependence is approximated linearly as

$$q_1 = q - aT \tag{3.20}$$

where a is a constant, then equation (3.19) can be rewritten as

$$\tau = \tau_0' e^{(q-aT)/kT} = \tau_0' e^{-a/k} e^{q/kT} \tag{3.21}$$

hence

$$\tau_0 = \tau_0' e^{-a/k} \tag{3.22}$$

Using Q as the activation energy in calories per mole of material, the expression (3.21) becomes

$$\tau = \tau_0 e^{Q/RT} \tag{3.23}$$

where R is the gas constant and is 1.987 cal/mole $-$ $^\circ$K.

From equation (3.17)

$$x = \ln \tau/\bar{\tau} \tag{3.17}$$

then

$$\tau = \bar{\tau} e^x \tag{3.24}$$

Equation (3.24) can now be substituted into equation (3.18) to give

$$\varepsilon'' = \frac{b(\varepsilon_0 - \varepsilon_\infty)}{\sqrt{\pi}} \int_{x_0}^{\infty} \frac{e^{-b^2 x^2} \omega \bar{\tau} e^x}{1 + (\omega \bar{\tau} e^x)^2} \, dx \tag{3.25}$$

where

$$\bar{\tau} = \tau_0 \, e^{Q/RT} \tag{3.26}$$

Hence equation (3.25) and (3.26) describe the functional relationship between dielectric loss, temperature, and frequency, under the assumption that polarization occurs because of molecular displacement and rotation subject to a Gaussian distribution of relaxation times.

In a completely analogous manner, the temperature and frequency dependence of the real part of the dielectric constant is derived. Use of equations (3.16) and (3.24) in equation (3.1) yields

$$\mathcal{E}' = \mathcal{E}_\infty + \frac{b(\mathcal{E}_0 - \mathcal{E}_\infty)}{\sqrt{\pi}} \int_{x_0}^{\infty} e^{-b^2 x^2} \frac{\omega \bar{\tau} e^x}{1 + (\omega \bar{\tau} e^x)^2} \, dx \tag{3.27}$$

To find the temperature at which the maximum loss occurs, equation (3.25) is differentiated w.r.t. temperature. Therefore, under the assumption that the integral is continuous,

$$\frac{d\mathcal{E}''}{dT} = \frac{b(\mathcal{E}_0 - \mathcal{E}_\infty)}{\sqrt{\pi}} \int_{x_0}^{\infty} e^{-b^2 x^2} \frac{d}{dT} \frac{\omega \bar{\tau} e^x}{1 + (\omega \bar{\tau} e^x)^2} \, dx \tag{3.28}$$

Carrying out the differentiation by the use of

$$\frac{d\mathcal{E}''}{dT} = \frac{\partial \mathcal{E}''}{\partial \tau} \frac{\partial \tau}{\partial T}$$

equation (3.28) becomes

$$\frac{d\mathcal{E}''}{dT} = -\frac{Qb(\mathcal{E}_0 - \mathcal{E}_\infty)}{RT^2 \sqrt{\pi}} \int_{x_0}^{\infty} e^{-b^2 x^2} \frac{\omega \bar{\tau} e^x [1 - (\omega \bar{\tau} e^x)^2]}{[1 + (\omega \bar{\tau} e^x)^2]^2} \, dx - f(x_0) \frac{dx_0}{dT} \tag{3.29}$$

where $f(x_0)$ is the term due to the lower limit. This term can be neglected if

$$\frac{d^2 \mathcal{E}''}{dT} (\Delta T_{max}) \geqslant f(x_0) \frac{dx_0}{dT}$$

where ΔT_{max} is the maximum uncertainty in the temperature at which the loss maximum occurs ($\approx 1°C$). It can be shown that the right hand side of the inequality is extremely small, namely, $< 10^{-10}$, over the frequency and temperature range of interest so that the inequality holds.

Similarly, differentiating equation (3.27) w.r.t. temperature gives

$$\frac{d\varepsilon'}{dT} = \frac{d\varepsilon_\infty}{dT} + \frac{Qb(\varepsilon_0-\varepsilon_\infty)}{RT^2\sqrt{\pi}} \int_{x_0}^{\infty} e^{-b^2x^2} \frac{(\omega\bar{\tau}e^x)^2}{[1+(\omega\bar{\tau}e^x)^2]^2} dx$$

$$+ \ term \approx 0 \tag{3.30}$$

In order to find the maximum loss temperature it is required that

$$\frac{d\varepsilon''}{dT} = 0 \qquad if\ \tau=\bar{\tau}\ \ and\ \ \omega = constant$$

since the point of maximum loss occurs at $\tau=\bar{\tau}$ by definition. The right hand side of equation (3.29) vanishes if and only if

$$\omega\bar{\tau}e^x = \omega\tau = 1 \tag{3.31}$$

Hence, at $\tau=\bar{\tau}$ equation (3.31) can be written as

$$\omega\bar{\tau} = \omega\tau_0 e^{Q/RT_m} = 1 \tag{3.32}$$

where T_m is the temperature at which the maximum loss occurs.

In order to evaluate some of the constants in equations (3.25) and (3.27), condition (3.32) is substituted in these equations so that

$$\varepsilon''(T_m) = \frac{b(\varepsilon_0-\varepsilon_\infty)}{\sqrt{\pi}} \int_{x_0}^{\infty} e^{-b^2x^2} \frac{e^x}{1+e^{2x}} dx \tag{3.33}$$

Let

$$g(x) = \int_{x_0}^{\infty} e^{-b^2x^2} \frac{e^x}{1+e^{2x}} dx \tag{3.34}$$

and therefore

$$(\varepsilon_0-\varepsilon_\infty)\frac{b}{\sqrt{\pi}} = \frac{\varepsilon''(T_m)}{g(x)} \tag{3.35}$$

Also,

$$\mathcal{E}'(T_m) = \mathcal{E}_\infty + \frac{(\mathcal{E}_o - \mathcal{E}_\infty)b}{\sqrt{\pi}} \int_{x_o}^{\infty} \frac{e^{-b^2 x^2}}{1 + e^{2x}} dx \tag{3.36}$$

Now let

$$f(x) = \int_{x_o}^{\infty} \frac{e^{-b^2 x^2}}{1 + e^{2x}} dx \tag{3.37}$$

Hence

$$\frac{\mathcal{E}_o - \mathcal{E}_\infty}{\sqrt{\pi}} b = \frac{\mathcal{E}'(T_m) - \mathcal{E}_\infty}{f(x)} \tag{3.38}$$

Substitution of equation (3.35) into equation (3.38) gives the value for

$\mathcal{E}_\infty$ as

$$\mathcal{E}_\infty = \mathcal{E}'(T_m) - \mathcal{E}''(T_m) \frac{f(x)}{g(x)} \tag{3.39}$$

Using equations (3.35), (3.38) and (3.39) in equations (3.25),
(3.27), (3.29) and (3.30) finally gives the complete macroscopic di-
electric properties of a material w.r.t. frequency and temperature in
terms of a few basic material constants. These constants, the shortest
relaxation time τ_o, the activation energy of polarization, Q, and the
most probable relaxation time $\overline{\tau}$ are related through equation (3.32).
The dispersion factor b in the assumed Gaussian distribution is deter-
mined by fitting the theoretical data to the experimental data.

EVALUATION OF THE BASIC CONSTANTS

Activation energy is the energy required to make a particle jump
from one equilibrium position to another. The value of this energy
barrier can be obtained from the slope of a plot of $\ln T\tau$ versus $1/T$ [47].
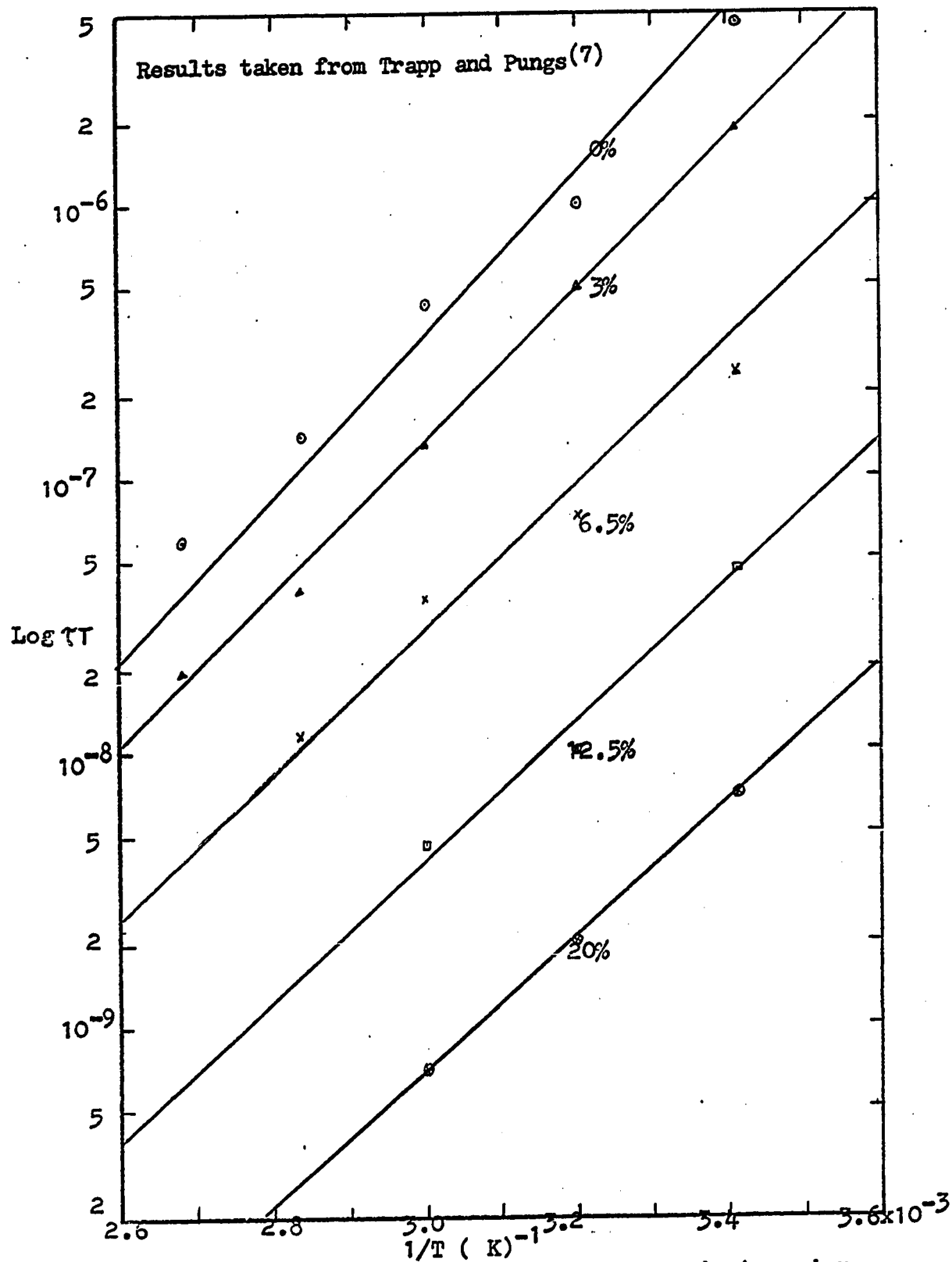
Fig. 3.7 — Log(τT) versus 1/T for Pinewood at various moisture contents.

For the case of pinewood the variation of τ vs T is given in the litera-ture[7]. The data are plotted with moisture content as a parameter in figure 3.7. The activation energy can be shown to obey the relation

$$Q = R\left[Ln\left(T_2\tau_2\right) - Ln\left(T_1\tau_1\right)\right]/\left[\left(1/T_1\right) - \left(1/T_2\right)\right]$$ (3.40)

However, the deviation of the points in figure 3.7 doesn't allow for a very accurate determination of Q vs. moisture content. Hence, an iterative numerical procedure was used to evaluate Q using equation (3.2) which can be written as

$$Q = RT\,Ln\left(\tau/\tau_0\right)$$ (3.41)

as pointed out in the previous section, the temperature dependence of the activation energy is accounted for in the value of τ_0. Thus, there should exist a value Q, for a specific τ_0 which is constant with tempera-ture. In order to find that value of Q an iterative procedure was used on equation (3.41) for a trial value of τ_0. Q was calculated for the different temperatures and the resulting deviation noted. By incrementing the value of τ_0, a complete set of deviations was obtained. The value of Q finally chosen corresponded to a value of τ_0 which gave a minimum variation of Q with temperature. The procedure was repeated for various moisture contents and the results plotted in figure 3.8.

The energy of activation required to rotate a water molecule absorbed on 0% moisture content wood is found to be about 13.4 to 14 Kcal/mole. According to measurements on pure ice and water[51] the activation energy for ice (3 bonded water molecules) is 13.5 Kcal/mole and for water the bond energy is 4.5 Kcal/mole. It is clear from figure 3.8 that the activation energy required for polarization of pinewood drops considerably with increasing moisture content. However, it is also
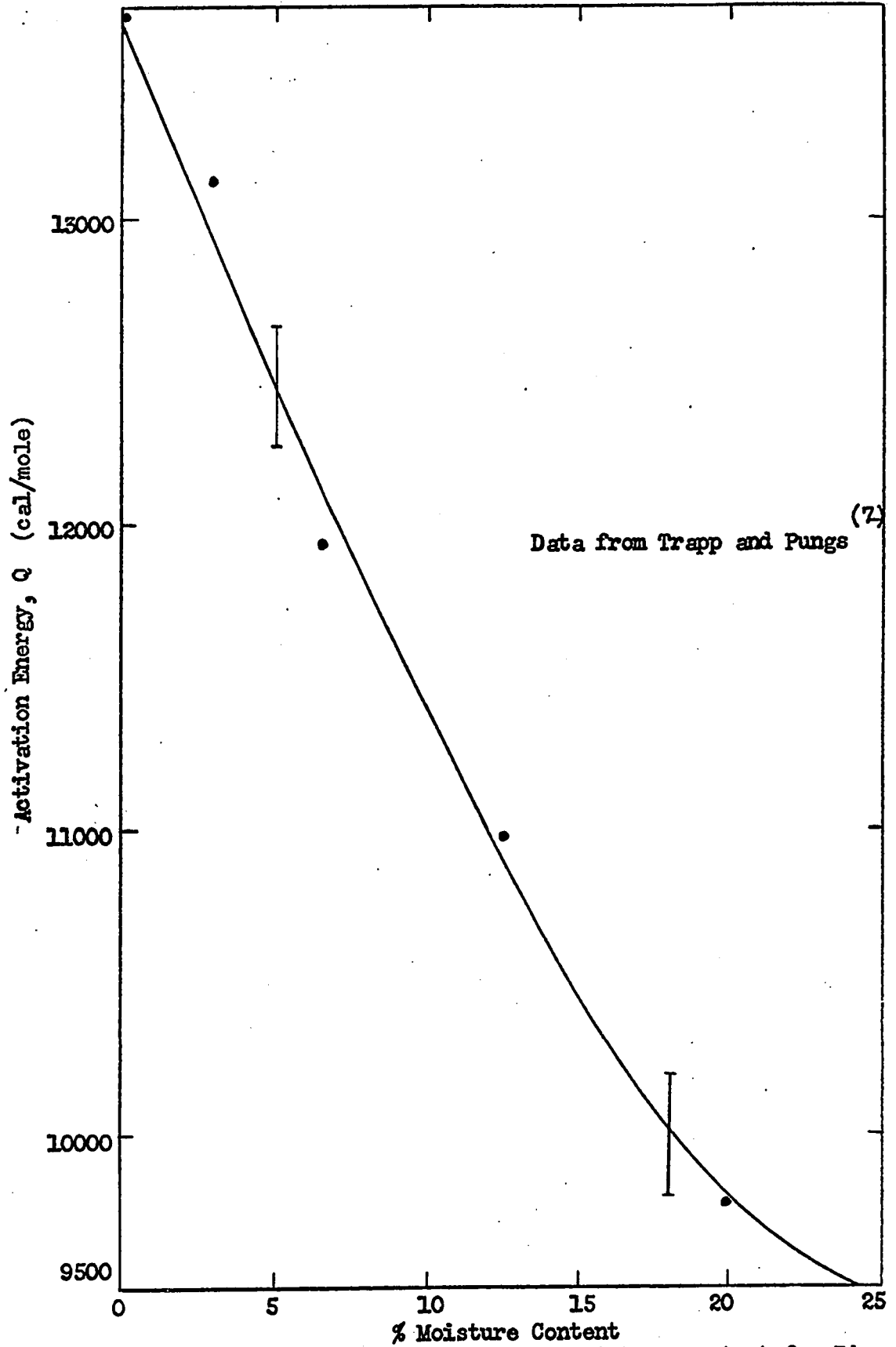
Fig. 3.8 - Activation energy versus moisture content for Pine.

of interest to note that close to fiber saturation ($\approx 30\%$M.C.) the
activation energy is still much larger than that required to break one
hydrogen bond.

The factor T_0 is usually smaller than the time required for a molecule
to go from one equilibrium position to another because of internal
excitation of the molecule. This constant further includes any tempera-
ture dependence of the activation energy as pointed out previously.

For purposes of analysis, T_0 will be assumed to be a constant with
regard to temperature and moisture content, which is a reasonable approx-
imation. Hence from the data available on pinewood a value of $T_0 = 10^{-18}$
is found. Experimental data on Douglas Fir and Western Hemlock (presented
in chapter 5) confirm the values of the constants found here from pinewood
data.

Unfortunately no closed form solution is known for equations (3.25),
(3.27), (3.28) and (3.29) and thus numerical integration had to be used
to solve the problem. Using I.B.M.'s direct access APL language the
problem was programmed and solved to a high degree of accuracy on an I.B.M.
360-67 digital computer. The density of distribution denoted by b was
obtained by iteratively fitting the theoretical curves to the experi-
mental curves to obtain a fit to within 10% accuracy. Hence theoretical
plots of dielectric constant vs. temperature and frequency were obtained
for semi-empirical values of the constants b, T_0, Q, and $\mathcal{E}_0$.

Generally the agreement between theoretical and experimental results
was very satisfactory.

CHAPTER 4

MEASUREMENT METHODS AND TECHNIQUES

INTRODUCTION

When looking for an appropriate technique for measuring the complex permittivity of a material, one discovers that it is not an easy task. At microwave frequencies alone, more than 30 different measuring methods exist[23, 31, 32, 34] and, depending on the particular material to be measured, one of the existing methods has to be chosen, after which the actual experimental technique is often modified to suit the particular need. Some important factors which will affect the choice are a) accuracy desired; b) simplicity of the measurement; c) simplicity of the calculations; d) geometry and make-up of the material to be tested; e) environmental requirements for the sample; f) the number of measurements to be made. The third factor, simplicity of calculations, is of decreasing importance with availability of third generation computer facilities.

In the present investigation it was necessary to vary the sample temperature over a considerable range, which was one of the reasons for choosing a short-circuit technique. Short-circuited mounts have only one open port and consequently the temperature distribution can be made more uniform than for a two port device. Moreover, the frequency of interest, namely 2450 MHz, and the structure of the material to be measured (wood), made the waveguide technique preferential. The fact that nearly 1500 measurements had to be made narrowed the choice of methods down even further to those techniques with the simplest experimental pro-
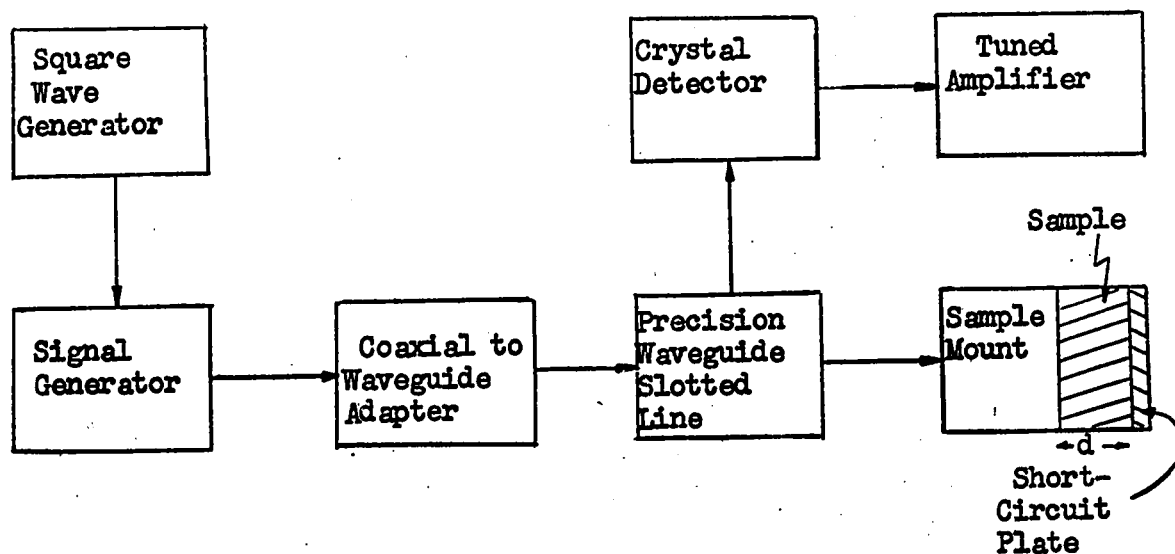
Fig. 4.1 - Von Hippel's Measurement Technique.
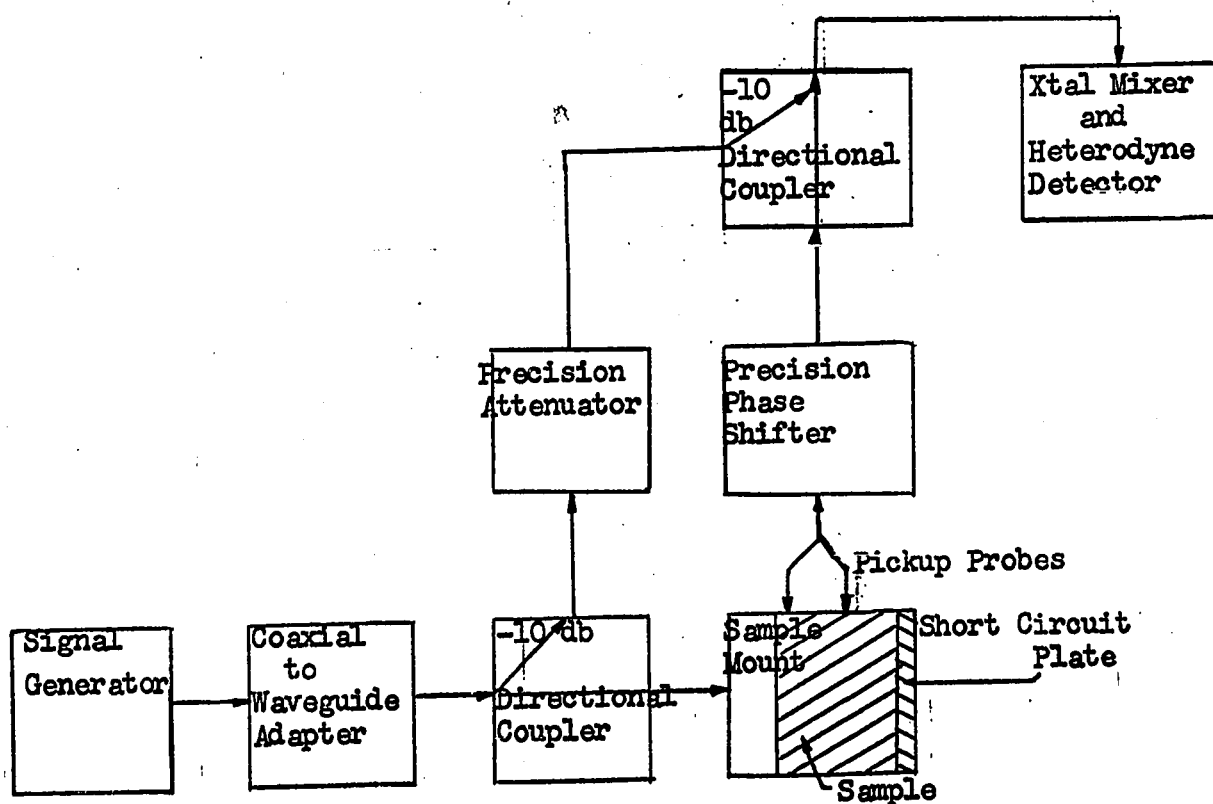
Fig. 4.2 - Buchanan's Bridge Technique.

cedures. Left were either Von Hippel's short-circuit technique[23], see

figure 4.1, or the bridge method developed by Buchanan see figure 4.2.

Because of the much simpler calculations and ease of measurement in the

latter method, it was the measuring technique chosen. Another important

advantage of the Buchanan technique is that front face reflections of

the sample do not affect the experimental accuracy as they do in Von

Hippel's method.

BASIC METHOD

Consider the sample mount shown in figure 4.3. The sample is backed

by a short-circuit plate and two ports in the broad wall of the waveguide

are designated by A and B. The distance from the short-circuit plate to

B is exactly twice the distance to A.

For propagation of the fundamental mode in a dielectric filled guide,
the constant, γ, is given by (31, 32).

$$\gamma = \alpha + j\beta = j(2\pi/\lambda_0)\sqrt{\varepsilon - p} \tag{4.1}$$

With ε, the complex permittivity, defined by

$$\varepsilon = \varepsilon' + j\varepsilon'' \quad and \quad p = (\lambda_0/\lambda_c)^2 \tag{4.2}$$

from which

$$\varepsilon' = p + (\lambda_0/2\pi)^2(\beta^2 - \alpha^2) \tag{4.3}$$

$$\varepsilon'' = 2(\lambda_0/2\pi)^2 \alpha\beta \tag{4.4}$$

where λ_0 is the free space wavelength, β and α are the phase and atten-

uation constants of the material and λ_c is the cut-off wavelength for the

waveguide. In order to find values for ε' and ε'', expressions for α

and β in terms of the experimental quantities need to be obtained.

Writing the expressions for the electric field strength in the material

at points A and B in figure 4.3, yields
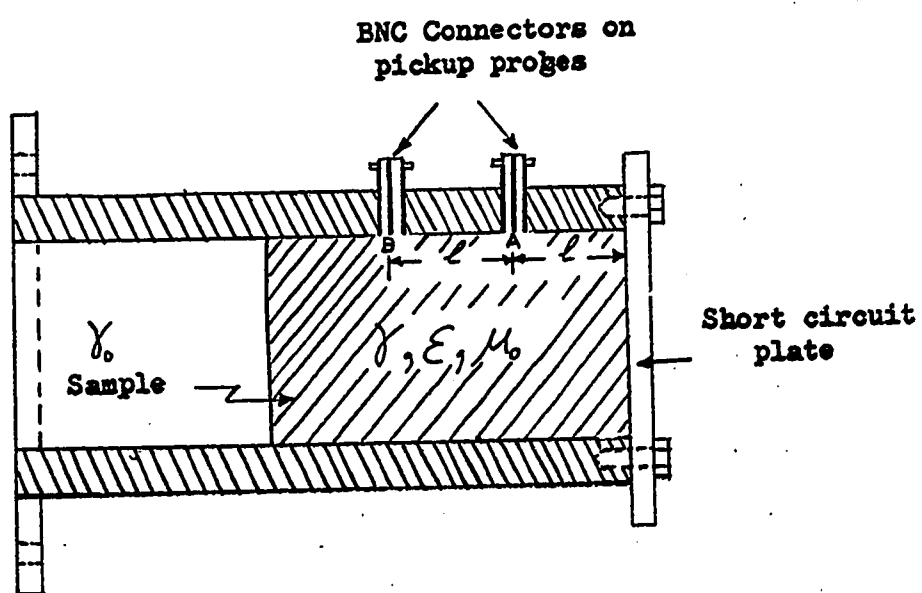
Fig. 4.3 - Sketch of a sample mount

$$E_A = E_o\left(e^{\gamma l} - e^{-\gamma l}\right) e^{j\omega t} \tag{4.5}$$

$$E_B = E_o\left(e^{2\gamma l} - e^{-2\gamma l}\right) e^{j\omega t} \tag{4.6}$$

The ratio of equation (4.6) to equation (4.5) gives

$$\frac{E_B}{E_A} = (\sinh 2\gamma l)/\sinh \gamma l = 2\cosh \gamma l \tag{4.7}$$

Experimentally one can measure E_B/E_A as a quantity having amplitude, r and phase, θ, hence, Equation (4.8).

$$\frac{E_B}{E_A} = 2\cosh \gamma l = r e^{j\theta} \tag{4.8}$$

Solving for γ results in

$$\gamma = \alpha + j\beta = \cosh^{-1}\left[(r/2)e^{j\theta}\right] \tag{4.9}$$

Expanding the inverse hyperbolic cosine function, equation (4.9) yields

$$\alpha + j\beta = Ln\left[re^{j\theta/2} + \sqrt{1 - (re^{j\theta/2})^2}\right] \tag{4.10}$$

Hence, equation (4.10) gives the value of α and β in terms of the measured amplitude and phase r and θ. Because equation (4.10) gives a multivalued solution, it is necessary to repeat the measurement for a different value of probe spacing. From figure 4.3 it is clear that a number of ports could be built in the sample mount to achieve the different probe spacings. However, since this doubles the number of measurements to be taken and adds experimental complexity, another scheme was devised. By attaching the sample to the short-circuit plunger, the distance between the short-circuit and the pick-up probe could be set to any desired value. To detect the position of the probe with respect to the short-circuit, the reference arm of the bridge network, see figure 4.2, was

shorted out by means of a short circuit switch. The short circuit

plunger with attached sample was then moved all the way in past the

pick-up probe. By watching the meter indication on the heterodyne

detector while slowly moving the plunger back out of the guide, the

actual short-circuit position, as well as the positions of the minima

and maxima of the standing waves, were easily determined.

Since the short circuit position is moved a distance l away from the

generator for the second measurement, the incident wave entering the

sample will have advanced its phase by an amount equal to

$$\phi = 360 \, l / \lambda_{g_0}$$

where λ_{g_0} is the guide wavelength in the empty guide. Therefore, the

total phase difference between the two probe positions on the sample is

the sum of the phase shifter reading plus the angle ϕ given above.

If the principal value of the phase angle in the solution of Equation

4.10 is desired, it implies that the length l should be less than or

equal to a 1/4 wavelength in the material, corresponding to the first

maxima in the standing wave pattern from the short-circuit side. The

second measurement is then taken at twice that distance or at the first

minima from the short-circuit side. Ambiguity in the measurement is

removed by the above procedure.

Highest accuracy in the measurement is obtained when the amplitude

ratio, r, is a minimum because the derivatives of Equation (4.10) taken

with respect to r and Θ are directly proportional to r. By means of the

above mentioned procedure, locating the minimum of the standing wave

pattern, corresponding to minimum r, was a simple matter. Therefore, use

of the moving short-circuit, to locate the 1/4 and 1/2 wavelength

positions in the sample, removes the multivalue uncertainty in the

solution of equation (4.10) and guarantees maximum accuracy.

EXPERIMENTAL APPARATUS

A block diagram of the experimental apparatus is given in figure 4.4. A signal from the microwave generator goes through a directional coupler where part of the signal is coupled to a reference arm. The reference arm of the network contains a precision rotary vane attenuator and a 20 db variable attenuator. The latter is used for setting the bridge up for maximum sensitivity. The signal in the main arm of the bridge goes to a sample mount backed by a moveable short-circuit. A probe in the sample mount, flush with the inside of the guide, picks up a signal of some amplitude and phase. The unknown signal then goes through a precision phase shifter, is mixed together with the reference and local oscillator signals and the output fed to the heterodyne detector. Both attenuator and phase-shifter are adjusted to obtain a deep null on the detector indicating a balanced condition.

To reduce the number of experimental runs, the signal arm of the bridge is split into three by means of a waveguide junction, each arm of which goes through a 10 db padding attenuation,for reducing mount interaction,to a sample mount backed by a moveable short-circuit. See Figure 4.4. Only one of the sample mounts is connected in the bridge network at any one time through the coaxial selector switch. Precision dial-type indicators were used to determine the short-circuit position to an accuracy of 0.001". Care was taken to ensure that both arms of the bridge were properly matched. This was facilitated by using a swept frequency reflectometer and thus the whole system was aligned for a
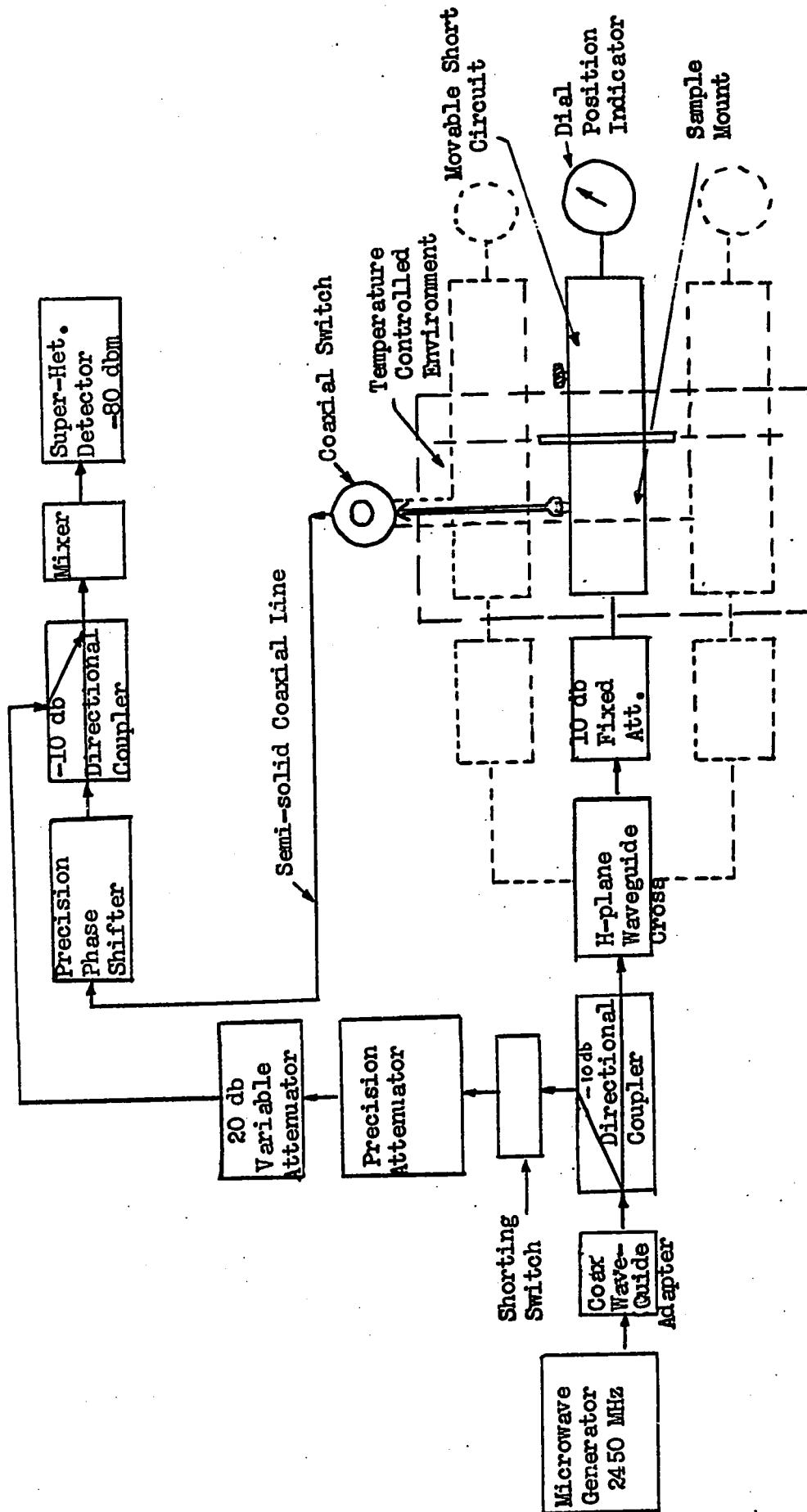
Fig. 4.4 – Experimental apparatus

standing wave ratio of less than 1.15. Some of the system components will be discussed in more detail in following sections.

PRECISION PHASE SHIFTER

Since no satisfactory phase shifter, coaxial or waveguide, could be obtained commercially for 2450 MHz, it was necessary to design a phase shifter particularly suited for this experiment. The specifications were: a minimum accuracy of $\pm 4^\circ$, a maximum variation in insertion loss of 0.05 db over a range of 0 to 360°, and a direct linear readout in degrees. Specifications were met by utilizing a movable short circuit plunger in a section of S-band waveguide, see figure 4.5. The short circuited guide was fed through the back of the short by means of a coaxial line and coupling loop which was empirically designed to achieve a good match at the design frequency. However, movement of the short circuit also caused the coaxial line to move and flex which resulted in excessive spurious phase shift even though Buchanan[33], found that spurious phase shift with his equipment was negligible. To eliminate this problem, a sliding, constant impedance, coaxial line was used with the sliding section attached to the short circuit plunger. If now the waveguide short circuit position is changed, the length of both the coaxial line and of the waveguide changes.

Mathematically, the phase shift, θ_g , due to the change in waveguide length is given by

$$\theta_g = 360 \left(X / \lambda_g \right) \tag{4.11}$$

where X is the distance travelled from some reference point, and λ_g is the guide wavelength. The phase shift, θ_c , due to the change in coaxial
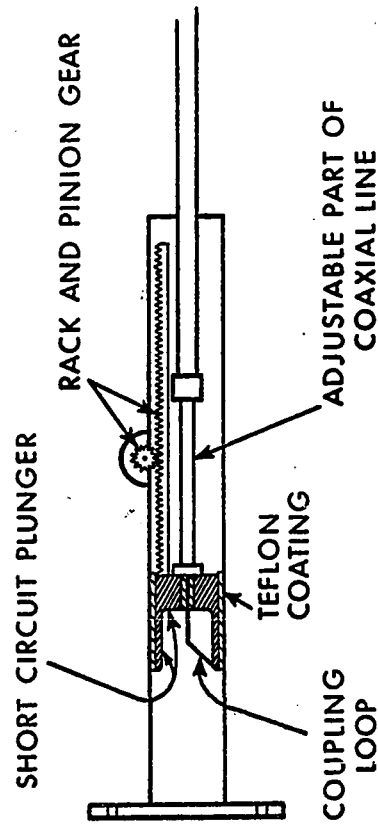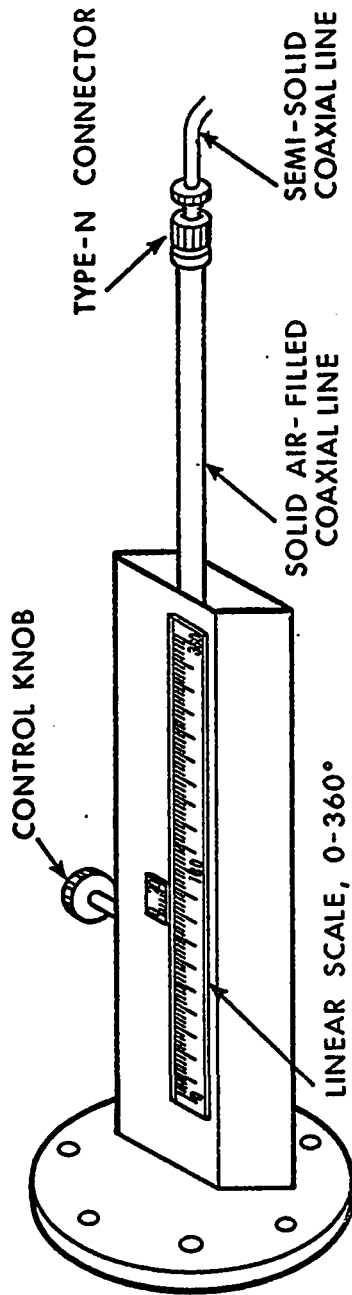
line length, is similarly given by

$$\theta_c = 360 \left(X/\lambda_0 \right)$$

(4.12)

where λ_0 is the free space wavelength. Since the travel is always in the same direction for both the coaxial line and for the waveguide, one can take the difference between equation (4.11) and equation (4.12) to obtain the overall phase shift,

$$\theta = 360 \cdot X \left[\left(1/\lambda_0 \right) - \left(1/\lambda_g \right) \right]$$

(4.13)

The wavelength in the waveguide and the coaxial line is fixed for any given measurement frequency and thus the total phase shift, θ, becomes directly proportional to the position of the short circuit plunger, X. The total length of travel can now be easily calculated by setting $\theta = 360°$ and substituting the value of λ_0 and λ_g at the required frequency in equation (4.13). At 2450 MHz in S-band guide, WG284, the required total travel is found to be 26.02 cm. A linearly engraved scale was made to give direct readout in degrees for the particular test frequency.

It is important to insure a good match between the coaxial line and the waveguide in order to keep the insertion loss variation to a minimum. Note also that the phase shifter only behaves in a linear fashion if the device sees a matched load at the waveguide end. This condition is quite easily obtained at a single frequency. After fabrication of the device, it was checked for linearity and accuracy by using a substitution technique. The phase shift of various, accurately known, lengths of standard guide were measured by setting the phase shifter to obtain a null at the output with and without the waveguide sections in the circuit. Results indicated a maximum error of ± 1.5 degrees. Maximum variation of insertion loss of

the phase shifter was measured and found to be 0.025 db. Therefore, this phase shifter design was subsequently used in the experiments.

TEMPERATURE CONTROL OF SAMPLE MOUNTS

To obtain information on the temperature behavior of the dielectric properties of wood, some means of controlling the temperature of the sample mounts was necessary. The low temperature limit was chosen to be -10°C so that the effect of freezing temperatures on the dielectric behavior could be studied. At the high temperature end the limiting factor was that of wood decomposition, hence the limit was specified as 100°C. In practice, the boiling action of water in the wood cells dictated a maximum attainable temperature, at constant moisture content, of about 95°C at 3000 ft. elevation. Temperature control was specified to be $\pm 1/2^\circ$C to give acceptable accuracy on the temperature behavior of the materials under test. A temperature control system was designed to meet the specifications and is described below. The block diagram of the apparatus is shown in Figure 4.6.

Block 1 is a 3/4 HP refrigeration unit used to provide cooling of the thermostatic fluid. It was capable of pulling the whole system down to -10°C when all components were well insulated. A solenoid in the refrigerant line controled the action of this equipment. The solenoid, in turn, was governed by a solid state control unit, which received its control signals from a Copper-Constantan thermocouple immersed in the thermostatic fluid. The refrigerant passed through a 50 ft. copper cooling coil, block 2, completely immersed in the thermostatic fluid, thus ensuring good thermal contact between the two media. Heat was supplied
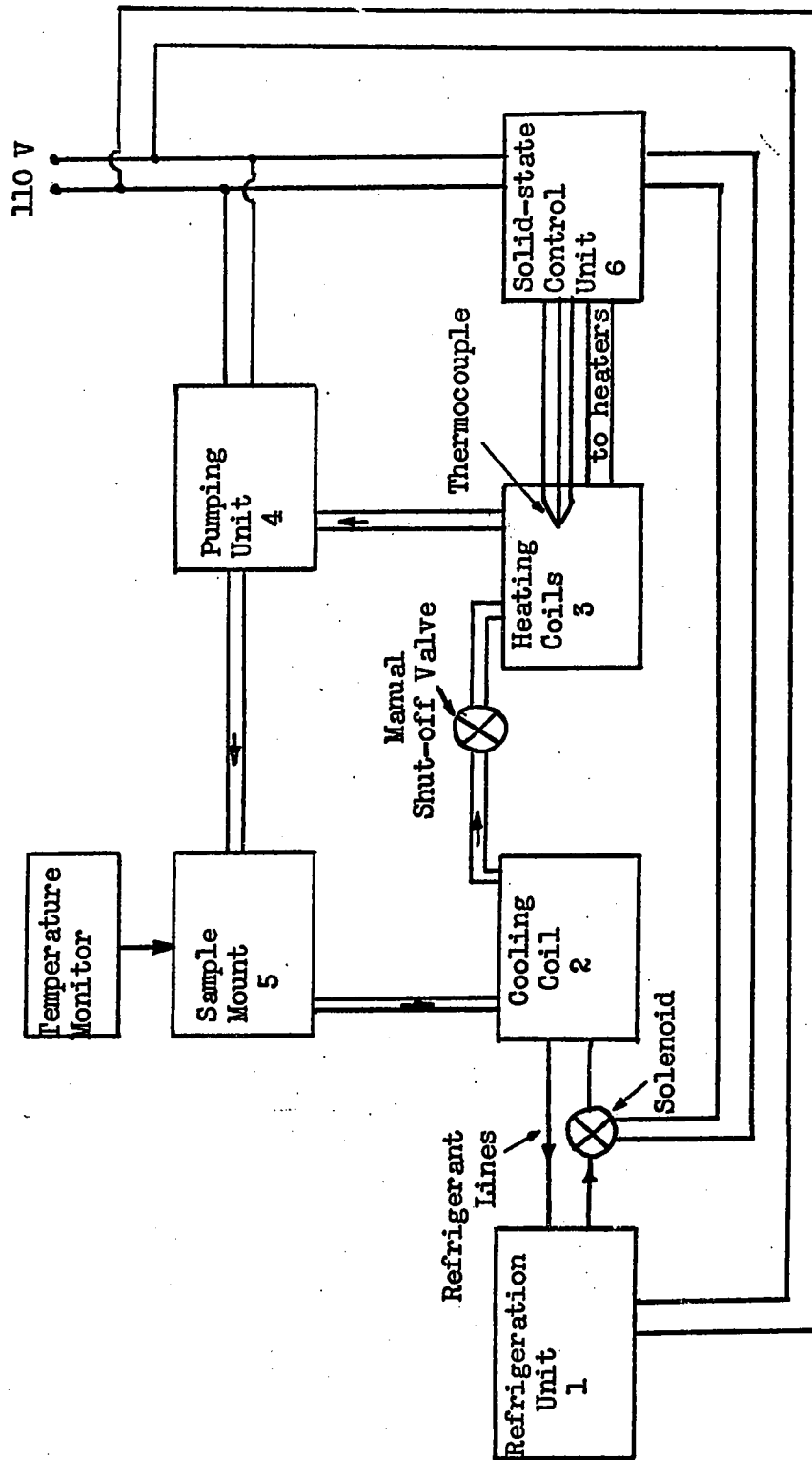
Fig. 4.6 — Temperature Control System

by two 750 watt immersion type heaters, block 3, which also were con-
trolled by the control unit in block 6. The sensing tip of the ther-
mocouple was immersed in the tank containing the heaters in close
proximity to the intake of the sample mounts. The tank was wrapped on
the outside with two 500 watt sections of heating tape which could be
turned on or off manually as required to maintain a given heat input to
the system. The voltage on these heating tapes could be controlled by
means of a variac to obtain some control over the total heat generated
by these units.

Ethylene glycol (antifreeze without additives) mixed with water was
used as the thermostatic fluid. It has good thermal properties, is
relatively inexpensive, and the mixture has a boiling point of about
$150^\circ C$. Oil was tried but, because of the high circulation rate required
to maintain accurate temperature control, it caused excessive foaming
and air trapping. The system was operated at atmospheric pressure and,
therefore, foaming took place very easily. Block 4 represents a 1 HP
pumping unit capable of pumping against a 40 ft. head of water at 4.5
gpm. This capacity was necessary in order to offset the losses and
accumulation of head in the hoses, valves, etc.

Three identical sample mounts, block 5, were fed simultaneously by
means of a set of manifolds, each of which had twelve ports. The
sample mounts consisted of 8" sections of waveguide with four separately
fed water jackets soldered to each side of the guide. The water jackets
were made up from a series of 1/4" copper tubes laid parallel to each
other and joined by manifolds at each end. In this way, uniform tempera-
ture distribution across the mount was obtained. Sample mount temperature
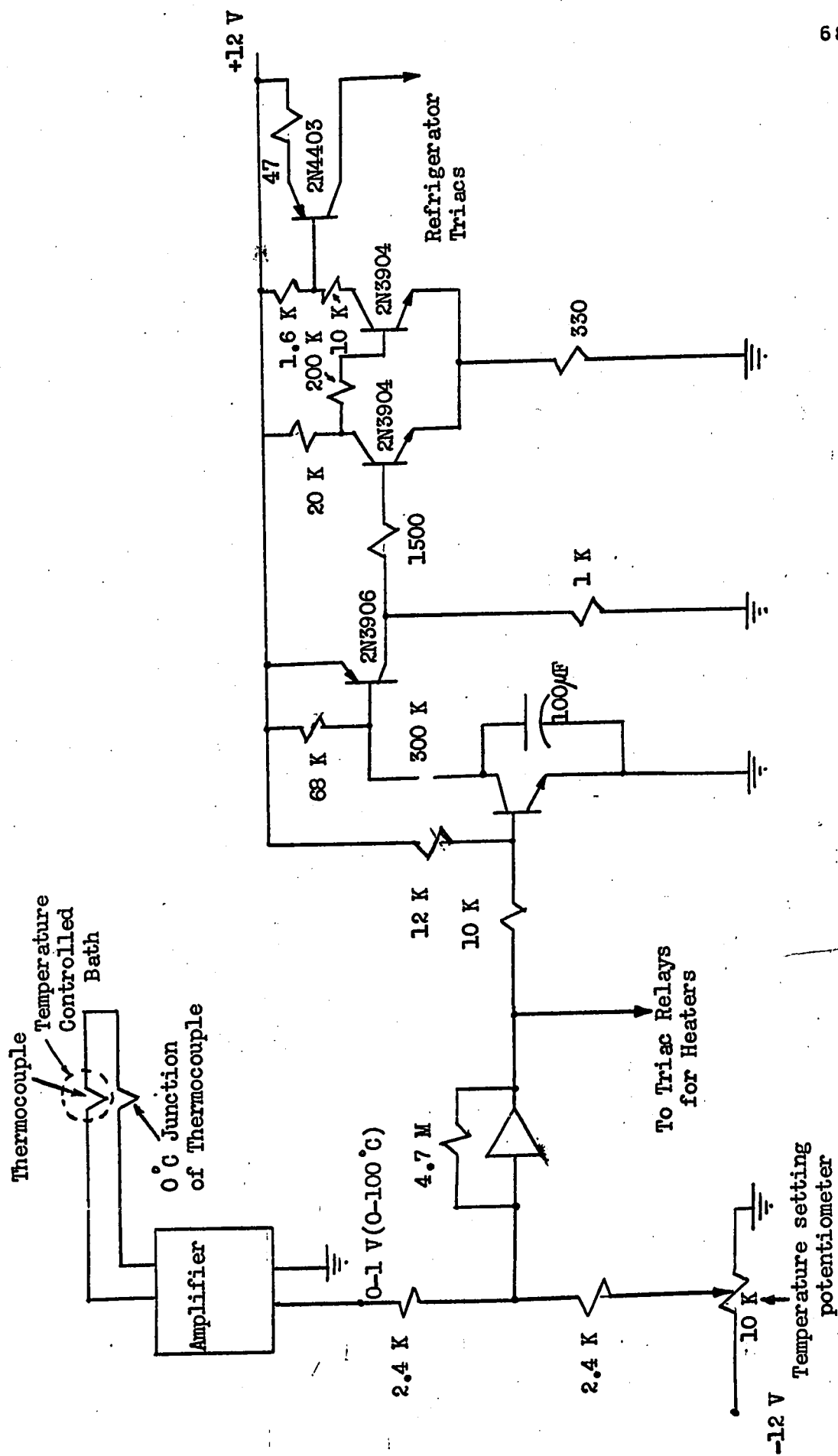
Fig. 4.7 — Control Circuit for Maintaining Constant Sample Mount Temperature

was continually monitored by means of a thermocouple junction soldered to the outside waveguide wall.

The solid state control unit in block 6 consisted of a series of operational amplifiers and Triacs, three-terminal solid state ac switches, which did the switching and controlling of the heating and cooling units. A detailed schematic of the electronics is given in Figure 4.7.

SAMPLE MOUNT DESCRIPTION

A sketch of the actual sample mount with a variable short circuit is shown in Figure 4.8. Mounted in the center of the broad wall and flush with the inside of the guide is a lengthened BNC connector which is used as the pick up probe. Its presence in the waveguide wall caused negligible disturbance to the fields in the guide. At the open end of the guide, a thin mica window was provided to minimize moisture loss from the sample mount, especially at the higher temperatures. The water jacket's construction is evident and was described previously.
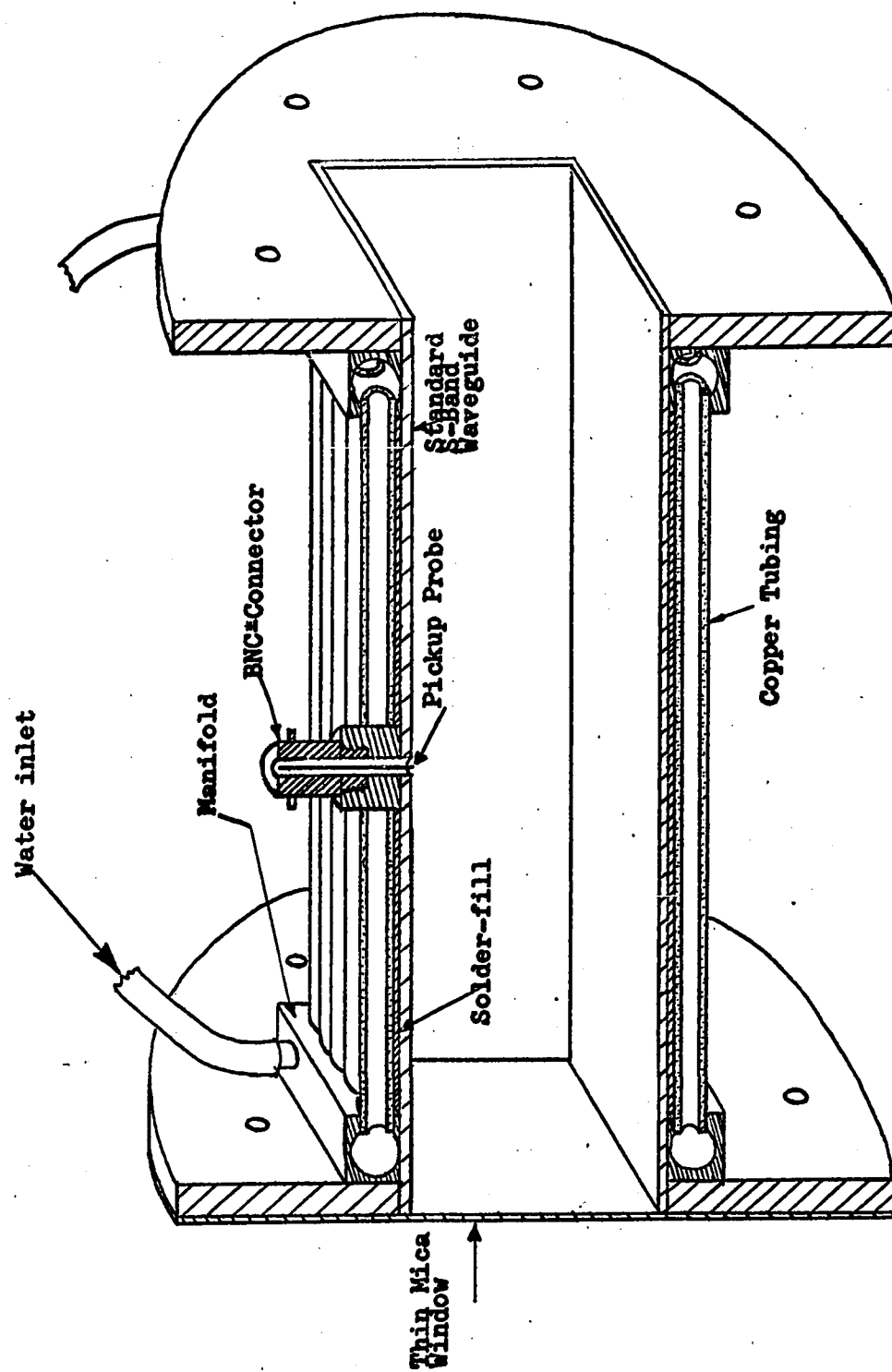
Fig. 4.8 – Sample Mount Sketch Showing Cooling Jacket and Probe.

To obtain a good variable short circuit, a resonant box-type short
was used which had its electrical short circuit position very close to
the physical front face position of the short. Design of this short is
described in reference (35) and can be obtained commercially as well[*].
To accurately position the short circuit, a large dial type position
indicator was attached to the back of the short making it possible to
read the short circuit position to 0.001" and had the added advantage
of easy readability.

CONDITIONING OF SAMPLES

Moisture content in wood is dependent upon temperature and humidity,
hence, to condition the wood specimens it is necessary to control these
two variables in some way. Furthermore it is important to note that in
order to get a uniform moisture content in a specimen a fairly long
conditioning period is necessary, since diffusion of the moisture between
a controlled atmosphere and the specimen's interior is a slow process.
To obtain the desired data for a plot of dielectric constant versus
moisture content it was decided to use specimens of the same wood species
conditioned at eight different equilibrium moisture contents, covering
the range of 0-25%.

Moreover, because of the anisotropic nature of wood, due to its
grain structure, it would be useful to measure the dielectric properties
for all three grain directions, namely, tangential, radial and longitudinal.

---

[*] De Mornay-Bonardi
1313 N. Lincoln Ave., Pasadena, California, U. S. A.

Because wood samples are non-uniform in structure and make-up, three samples, of the same density and matched as close as possible in grain structure, were to be measured under identical conditions and the results averaged. Thus it follows that to obtain a meaningful set of measurements for each species it would be necessary to have a total of 8 (no. of different moisture contents) times 3 (no. of grain directions) times 3 (no. of samples for averaging), or 72 samples made up. It was decided to double this number to allow for spoiled samples, initial test runs, and some added tests on the samples if desired.

Two species, Western Hemlock and Douglas Fir, were chosen for the measurement to compare the effect of the species on the dielectric properties. This brought the total number of samples to be prepared to 288.

In order to be able to condition all of these simultaneously at the required moisture contents it became necessary to build a set of cabinets with a controlled air atmosphere. Figure 4.9 shows a system layout for one of the conditioning cabinets. Seven of these units were placed side by side, each with its own control circuit for humidification. The de-humidifying part of the system feeds the seven cabinets in series with the option of manually controlling the dry air intake in each cabinet by means of a valve. All cabinets were operated at their own ambient temperature which was usually somewhat above the room temperature because of heat added to the cabinet by the steam injection process.

When the humidity in the cabinet dropped below its set point, the resistance of the sensor increased and caused the amplifier to put out a trigger signal causing the solid state relay (Triac) to close allowing the vaporizer to generate steam. The steam entering the cabinet was
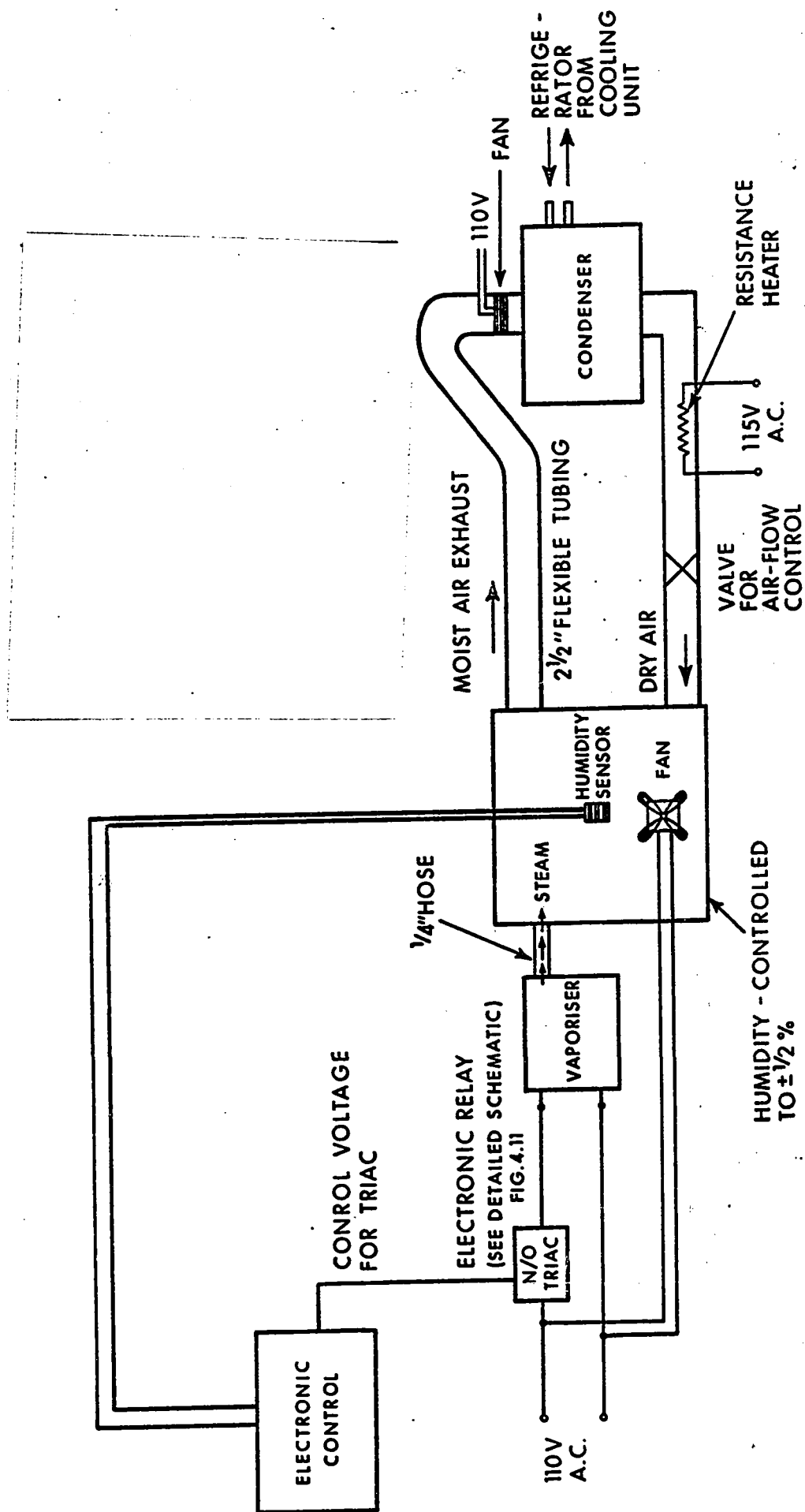
Fig. 4.9 - Humidity controlled cabinets - System layout
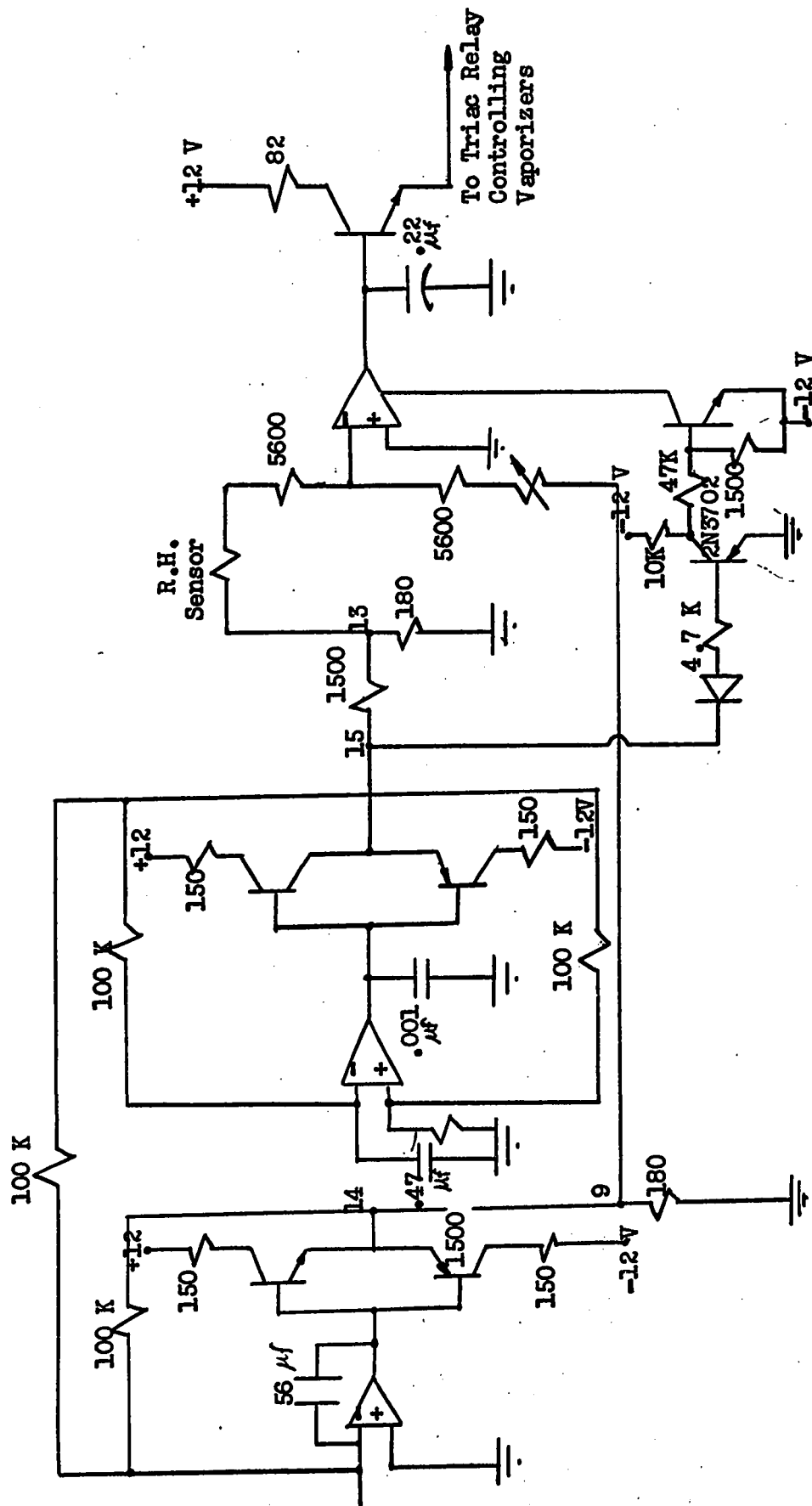
Fig. 4.10 - Control Circuit for Humidifying Cabinets

circulated by a small electric fan which ran continuously. As soon as
the sensor reached the required equilibrium value, the output of the
differential amplifier became zero and the relay opened, thus cutting
off the power to the vaporizer. The dehumidifier ran continuously, but
was necessary only for those cabinets which were set for humidities
close to or below that of the room humidity. The door seals on the
higher humidity cabinets were purposely made leaky so that overshoot
effects of the vaporizers were minimized. An on-offratio of 1/5 to
1/2 was necessary to achieve accurate humidity control, depending on the
effectiveness of the dehumidifier unit. The dehumidifier sucked moist
air from the cabinets over a set of cooling coils which were kept close
to $0°C$, whereby the moisture in the air condensed. The dried air was
passed over a small resistance heater raising the air temperature to
that of the cabinets.

The above scheme was found to be very effective in controlling
humidities between 10% and 90% R.H. to an accuracy of about $\pm\frac{1}{2}\%$. The
Honeywell[*] humidity sensors do tend to drift somewhat with age, but a
periodic change of the calibration resistors in the differential ampli-
fiers would bring the units back to their original operating points.
This procedure was found to be necessary about once every six weeks.
This time interval is normally sufficient to bring a reasonable sized
wood sample to its equilibrium moisture content.

Figure 4.11 shows a schematic of the solid state relay used for
control purposes. These units have proven highly satisfactory in a
continuous operating environment. Over a year of service these units

---

[*] Honeywell humidity sensors, series QL
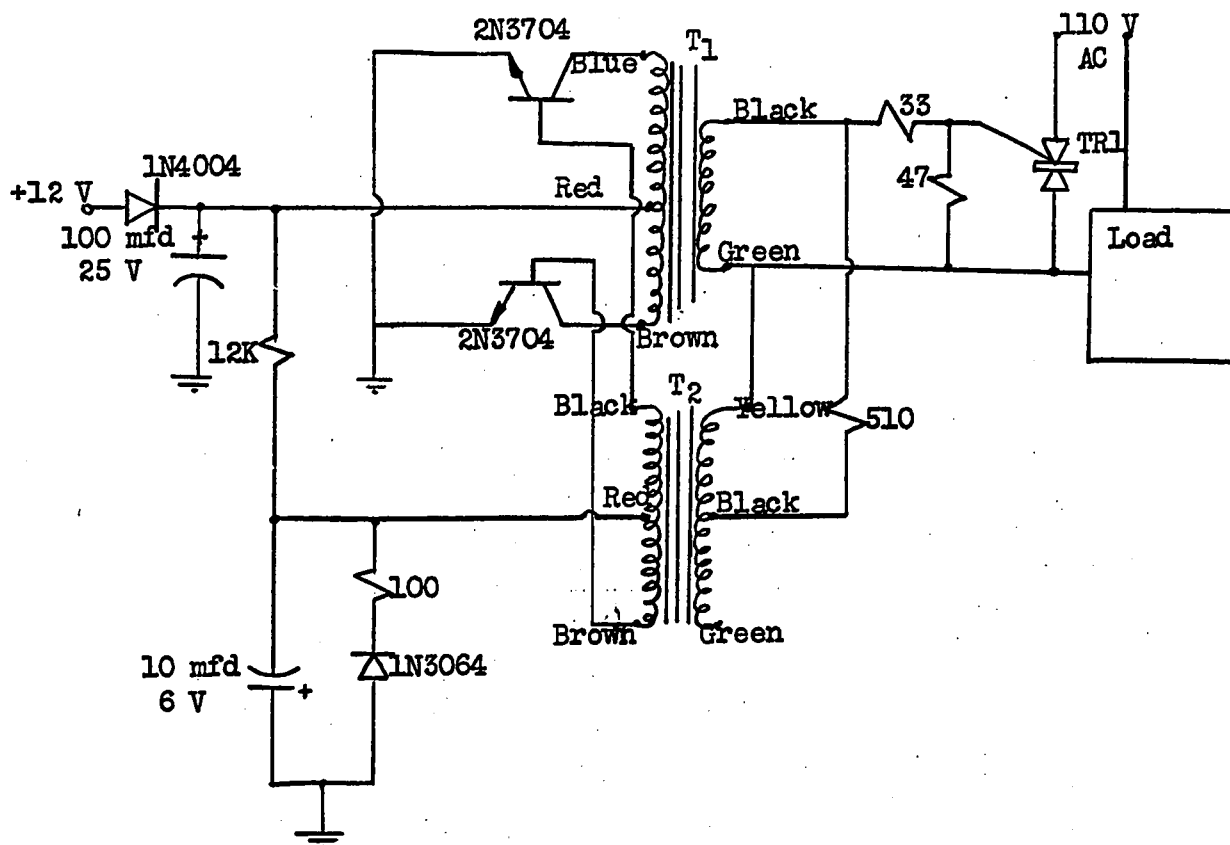
Notes

1. Inverter runs at about 3 KHz, square wave.

2. Trigger requirement: +12V at 20mA; minimum=8.5V DC, maximum=24V DC.

3. T1-Hammond Transformer, 144G
   T2-Hammond Transformer, 144I
   TR1-G.E. Triac, SC46B

Fig. 4.11 - Solid State Relay 7.5A, 117 V.AC. - Circuit Diagram

have cycled many millions of times and never failed. Mechanical relays were tried initially, but were found highly unreliable and caused many a system failure due to the arcing and burning of contacts. The solid state units, on the other hand, have proven reliable, relatively inexpensive, multi-purpose, as well as being noiseless.

SAMPLE FITTING

In order to fit the samples into the waveguide the raw samples had to be planed or milled down to slightly less than the internal waveguide dimensions. The raw samples which were about 30% oversize were planed down to size after they had been properly conditioned. Final dimensions of the samples were nominally 2.825" by 1.325" by 3". The blocks were then returned to the conditioning cabinets for final conditioning. This left a clearance of .015" between sample and waveguide walls to allow for movement of the samples in the guide over the complete temperature range. The actual clearance of each block in its mount was measured just prior to the test and corresponding corrections were applied in the final calculations of the dielectric properties.

Double sided adhesive transfer tape* was used to attach the samples to the short circuit plungers. A layer of tape was applied to the plunger and to the sample end face which had negligible effect on the measurement. By applying reasonable hand pressure the blocks were forced against the plunger face, resulting in a satisfactory bond.

---

* Scotch Brand Adhesive Transfer Tape, No. 465
Minnesota Mining and Manufacturing of Canada Ltd.
London, Ontario

MEASUREMENT PROCEDURE

A description of a typical measurement using the bridge technique, see figure 4.4, is given. A sample was weighed immediately after it was removed from its conditioning cabinet, its weight recorded after which adhesive tape was applied to one end of the block and to the front face of the short circuit plunger. The clearance between the sample and the broad waveguide walls was measured and recorded. The sample was pressed against the short circuit plunger and the whole assembly fitted onto the sample mount and the sample pushed up tight against the mica window to minimize air circulation around the block. After setting the temperature control to the desired value the whole system was allowed to reach an equilibrium temperature. Allowing 30 minutes per $10^{o}C$ change in temperature was found sufficient for stabilization. To determine the time interval required to obtain equilibrium, the bridge was balanced corresponding to a null at the detector. When no further change in the null condition of the bridge occured the system was assumed at equilibrium.

By means of a thermocouple soldered to the waveguide wall the mount temperature was continually monitored. Because of heat losses, the sample temperature was usually somewhat different from the mount temperature. A curve of sample vs. mount temperature was obtained, see figure 4.12, by inserting a thin thermocouple through the waveguide wall into the center of the sample after equilibrium was reached. This procedure was repeated for various temperatures in the range and for a few different samples. The resultant curve was a straight line. Sample temperature and mount temperature were, of course, equal at room temperature. The

$T_s = 2.2 + .903T_m$

Mount Temperature, T_m, °C

Sample Temperature, T_s, °C
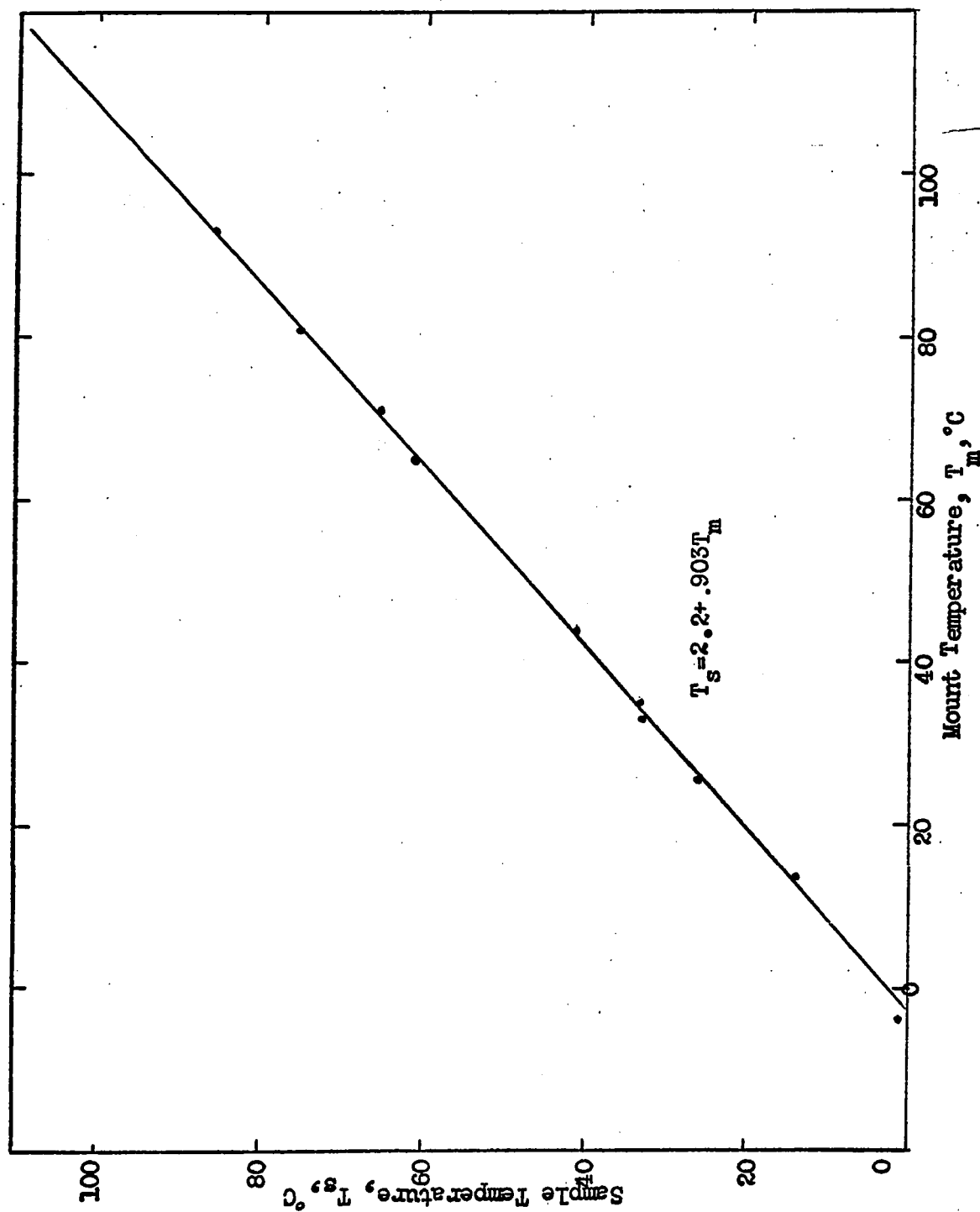
Fig. 4.12 – Sample Temperature versus Mount Temperature.

equation of this correction curve was determined and since a computer
was used for calculations the temperature correction was applied to the
raw input data as part of the computer program.

Once equilibrium was reached, the actual microwave measurement could
begin. With the waveguide switch closed the short circuit position was
adjusted to obtain the standing wave minimum closest to the physical
short circuit position. The detector would show a deep null at that
point. The corresponding reading on the dial indicator was recorded as
say, X_0 after which the short circuit was moved away from the pickup
probe till the second minimum in the standing wave pattern was detected.
The second indicator reading was recorded as X_2. Opening the waveguide
switch, the attenuator and phase shifter were adjusted to obtain a deep
null on the detector and the attenuation and phase shift values recorded.
The position of the sample and short circuit was then changed to a point
midway between the values of X_2 and X_0 and the measurement repeated.
Half the difference between X_2 and X_0 corresponded to the distance ℓ as
described in the theory. After a measurement, the sample was again
moved right up against the mica window and the temperature control set
to a new temperature. To run a complete test from -10 to $100^{\circ}C$ took
about 8 hours allowing for a larger initial stabilization time since the
samples originally were at about $25^{\circ}C$. By using three sample mounts
three tests could be run in almost the same amount of time, since the
actual measurement time was short compared to the 30 minute stabilizing
period.

MEASUREMENT ERRORS

A. Short circuit positioning

For a waveguide short circuit plunger, the electrical short circuit position is often somewhat different from the physical short circuit position. In the case of the resonant box-type short, used in the experiments described, the electrical short circuit position was found to lie about .9 mm ahead of the physical short circuit. However, because of the technique used in the measurement, this discrepancy was of no real concern in that the actual standing wave minima were located. Moreover, even for position errors of 1 mm ($\approx$ .040") the error in the values of the calculated dielectric constant was less than 1%. Since the dial indicators could be read to .001", the errors due to the uncertainty in the short circuit position were neglected.

B. Sample clearance

When the waveguide is not completely filled with a dielectric material, the measured value of dielectric constant will be less than the true value. If the sample height is less than the narrow waveguide dimension, b, the true value of the complex dielectric constant is given by

$$\varepsilon'_{true} = \left(\varepsilon'_{meas} - 1\right)\left(b/b-c\right) + 1$$

$$\varepsilon''_{true} = \varepsilon''_{meas} \cdot b/(b-c) \qquad (4.14)$$

where c is the clearance.

The effect of clearance between the sample and the narrow waveguide walls is negligible for reasonably small clearances.

The clearance error was corrected for in the calculations by use of equation (4.14).

C. Temperature variation

The sample temperature could be held to within $\pm\frac{1}{2}^{o}C$. And the resultant error in the dielectric constant was found to be less than 1%.

D. Moisture content variation

Variation in sample moisture content between the low and high temperature end of the measurement range was inevitable. No humidity control inside the sample mount could be provided and hence at the higher sample temperatures some of the moisture was driven from the sample. The moisture partly condensed on the mica window, partly filled the air space in the mount with vapor, and partly escaped through the back of the short circuit. The condensation problem was almost eliminated by providing a heat source on the other side of the mica window, thus reversing the temperature gradient. Only at temperatures above $70^{o}C$ did the moisture loss introduce significant errors which were estimated to lie between ±1 and ±5%.

E. Mismatch errors

In the experiment standing wave ratios were minimized throughout and worst SWR was less than 1.20. However, mismatch errors in the unknown arm of the bridge tend to cancel

since the ratio of electric fields is measured in the sample
and the reflection coefficients during a measurement remain
constant. Therefore this source of error was found to be
negligible.

In Appendix A an analysis is given for the calculation of errors
in the dielectric constant due to experimental variations in the magnitude
and phase of the detected signals. Variations are caused by fluctuations
in temperature and moisture content of the samples and by uncertainties in
the phase shifter, attenuator and dial indicators.

Resultant worst-case errors are summarized in Table 4.1. These errors
were based on a value of $\varepsilon'=2$ and $\varepsilon''=2$. Most of the experimental data
gave larger values of ε' and smaller values of ε'' which would decrease the %
errors considerably.

Table 4.1 – Summary of experimental errors

Amplitude and phase	Amplitude and phase error using: $\Delta A = \pm.05\,db,$ $\Delta\theta = \pm2°$	length measurement error $\Delta\ell = \pm.025\,cm$	temperature variation error $\Delta T = \pm.5\,°C$	moisture content variation error up to 70 °C	Total measurement error
$\Delta\varepsilon'$	$< \pm.1\%$	$< \pm1\%$	$< \pm1\%$	$< \pm2\%$	$< \pm5\%$
$\Delta\varepsilon''$	$< \pm1\%$	$< \pm1.5\%$	$< \pm1\%$	$< \pm1\%$	$< \pm5\%$
$\Delta\tan\delta$	$< \pm2\%$	$< \pm3\%$	$< \pm1\%$	$< \pm1\%$	$< \pm7\%$

During the course of this work a new Swept Frequency Dielectric Measure-
ment Technique was developed by Tinga and Edwards[37]. This technique
proved to be fast and reasonably accurate. However, samples measured by
this technique had to be a few wavelengths long. Since the samples had
already been cut to a shorter length and conditioned, the Swept Frequency
Method could not be used efficiently for all the measurements, but it was

used to check some of the results on Douglas Fir previously measured by

the bridge method. This procedure confirmed the results obtained by the

bridge technique to within ±5%.

    All experimental results obtained by the procedures described here are

presented in graphical form in chapter 5.

CHAPTER 5

CALCULATIONS AND RESULTS FOR TEMPERATURE DEPENDENCE

Following the procedure outlined in chapter 4 the dielectric properties of Douglas Fir were measured, and the data processed on a digital computer. Various plots of the important variables are presented as functions of temperature, moisture content and frequency. Theoretical results are compared with experimental data, and the physical meaning of the relaxation process is discussed more fully.

A. Experimental Results

1. Dielectric Constant Versus Temperature

In figures 5.1 through 5.9 the variation of the complex dielectric constant with temperature is given. All measurements were taken at a frequency of 2450 MHz, which was chosen for the simple reason that it is the centre frequency of a band designated for industrial, medical and scientific uses. It so happens that at this particular frequency, over the temperature range shown the dielectric loss curves for wood, exhibit distinct maxima. Referring back to the theory of chapter 3 this type of behavior is predicted to occur quite generally. However, since some of these data were obtained before chapter 3 was developed it was at first not obvious that these maxima would occur at this frequency in the rather narrow temperature range of 0-100°C. For this reason many of the tests were repeated and the results shown to be consistent with the previous ones. The results are very revealing about the

Fig. 5.1 — Dielectric Constant of Douglas Fir as a Function of Temperature at Various Moisture Contents Measured at 2450 MHz with E-field in the Longitudinal Grain Direction.

Fig. 5.2 – Dielectric loss of Douglas Fir as a Function of Temperature at Various Moisture Contents Measured at 2450 MHz with E-field in the Longitudinal Grain Direction.

Fig. 5.3 - Loss tangent of Douglas Fir as a function of
temperature at various moisture contents measured at
2450 MHz. with E-field in the longitudinal grain
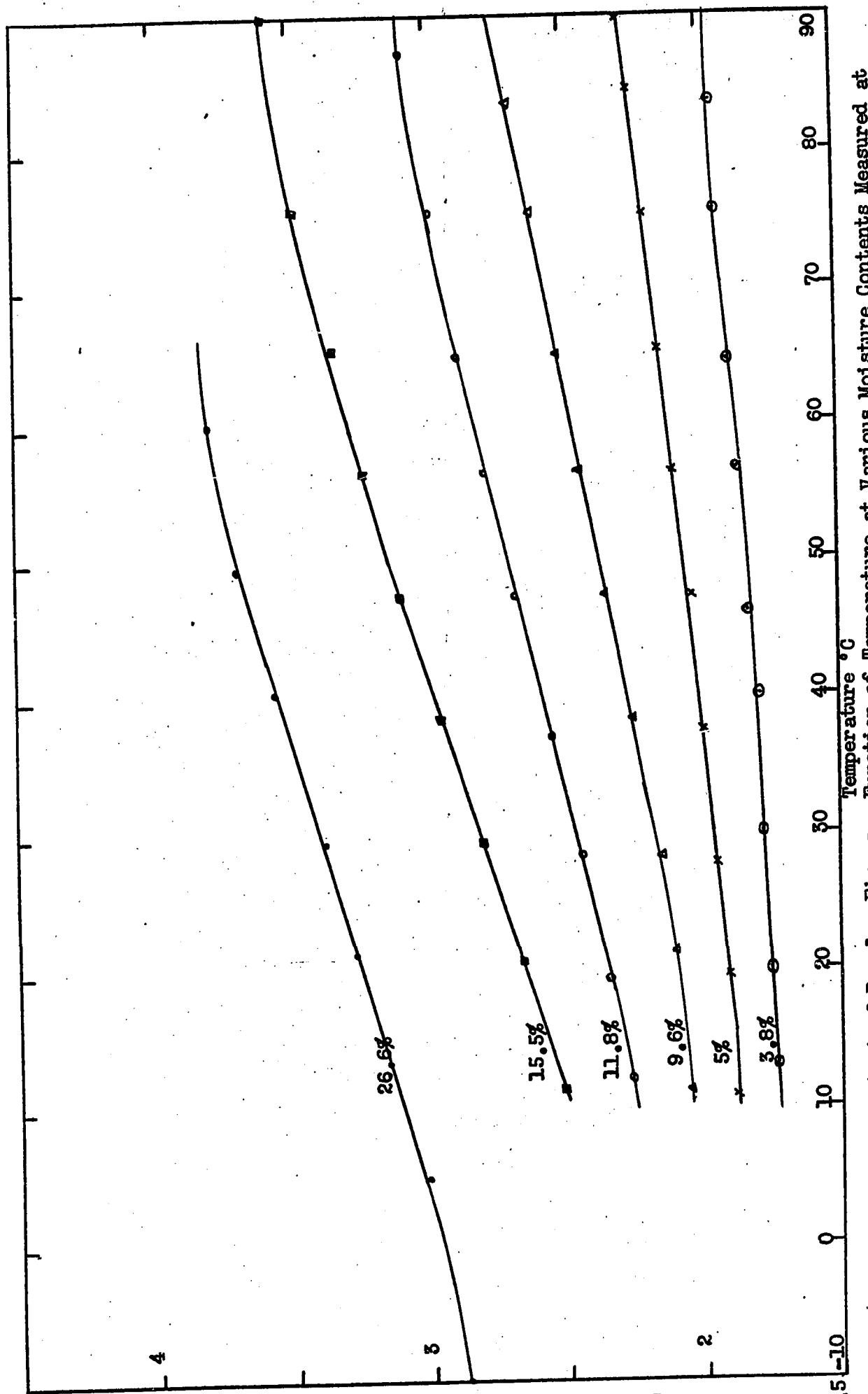
Fig. 5.4 — Dielectric Constant of Douglas Fir as a Function of Temperature at Various Moisture Contents Measured at 2450 MHz with E-field in the Tangential Grain Direction.
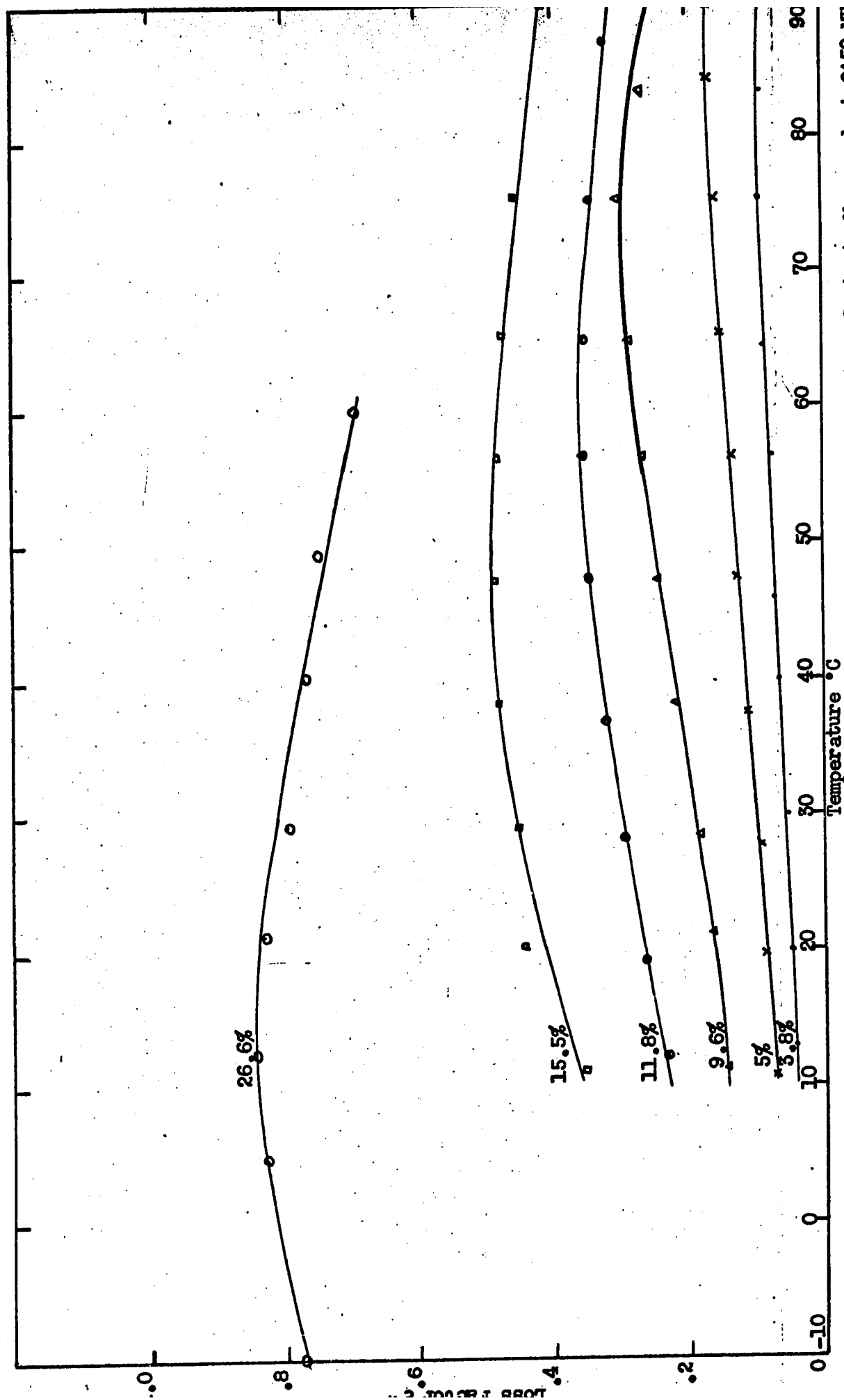
Fig. 5.5 — Dielectric Loss of Douglas Fir as a Function of Temperature at Various Moisture Contents Measured at 2450 MHz with E-field in the Tangential Grain Direction.
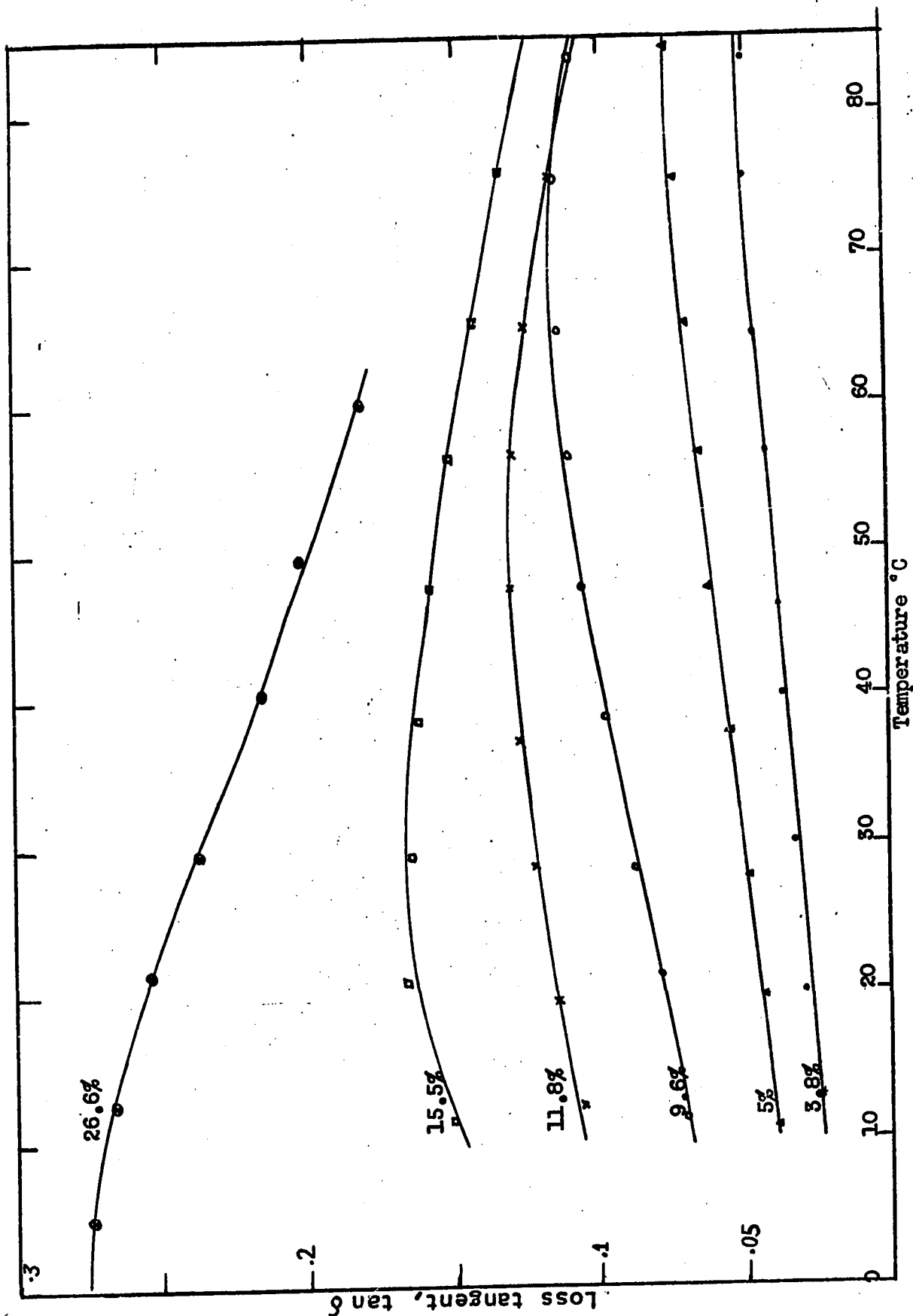
Fig 5.6 - Loss tangent of Douglas Fir asa function of temperature at various moisture contents measured at 2450 MHz. with E-field in the tangential grain direction.
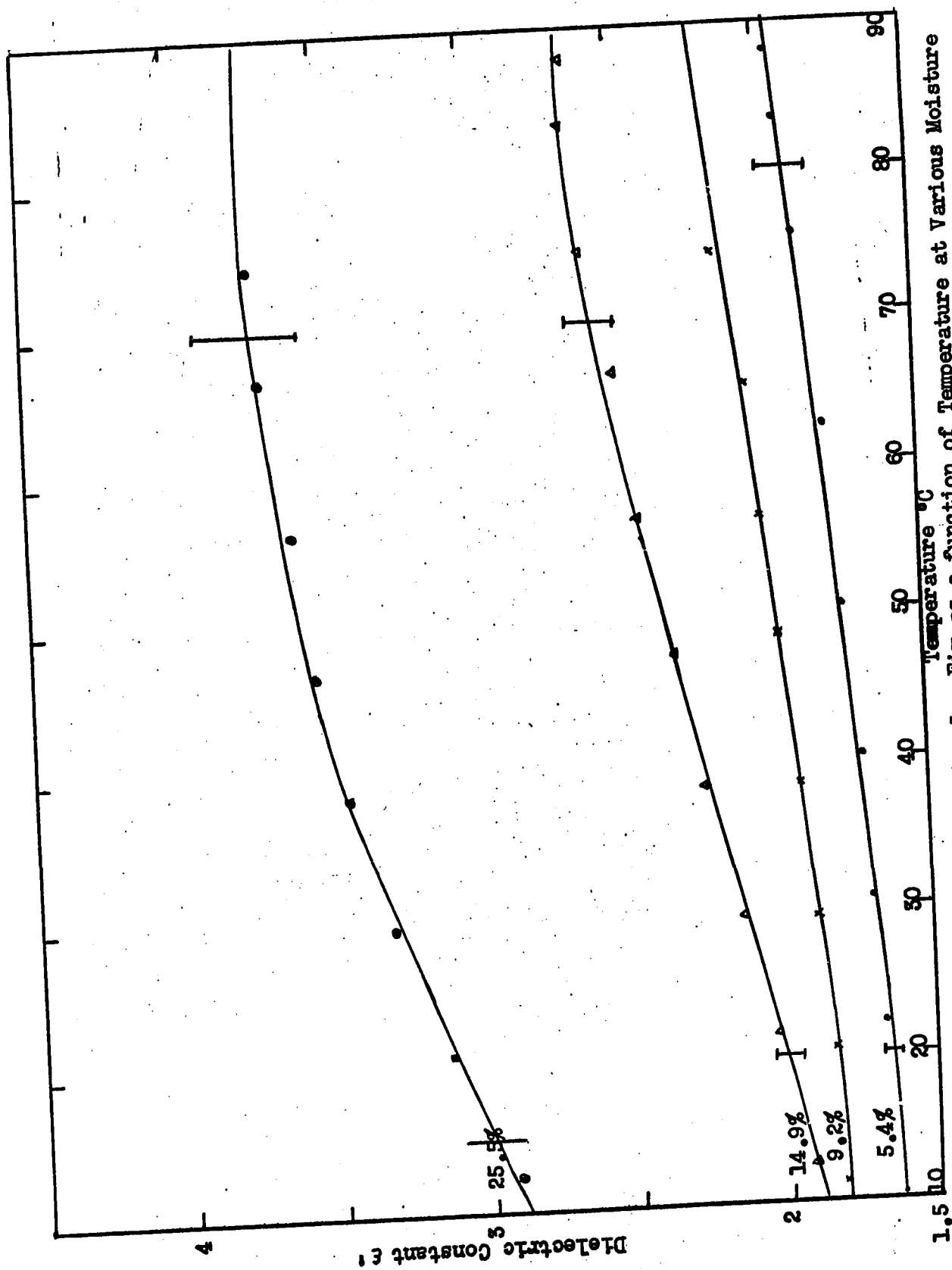
Fig. 5.7 - Dielectric Constant of Douglas Fir as a function of Temperature at Various Moisture Contents Measured at 2450 MHz with E-field in the Radial Grain Direction.
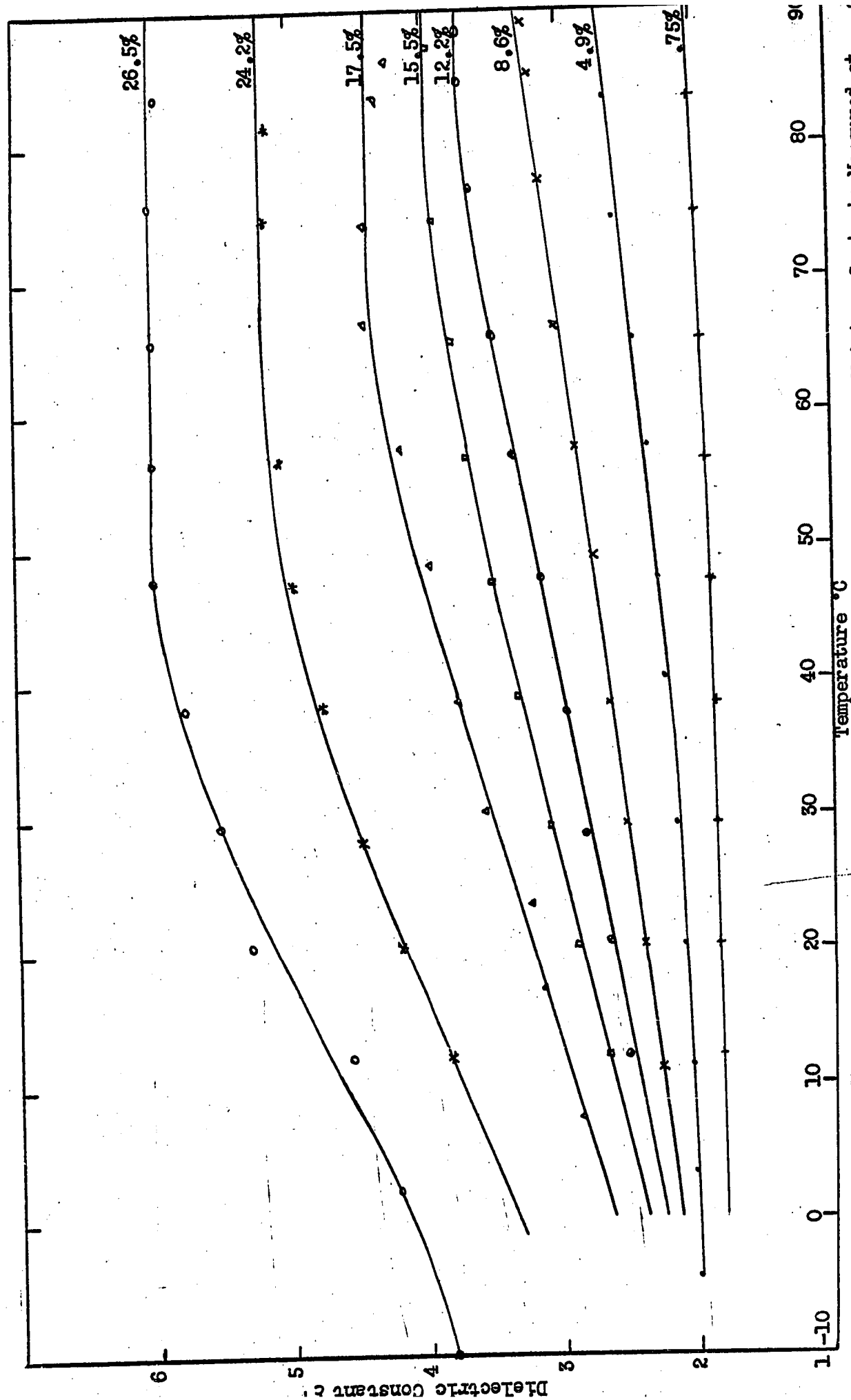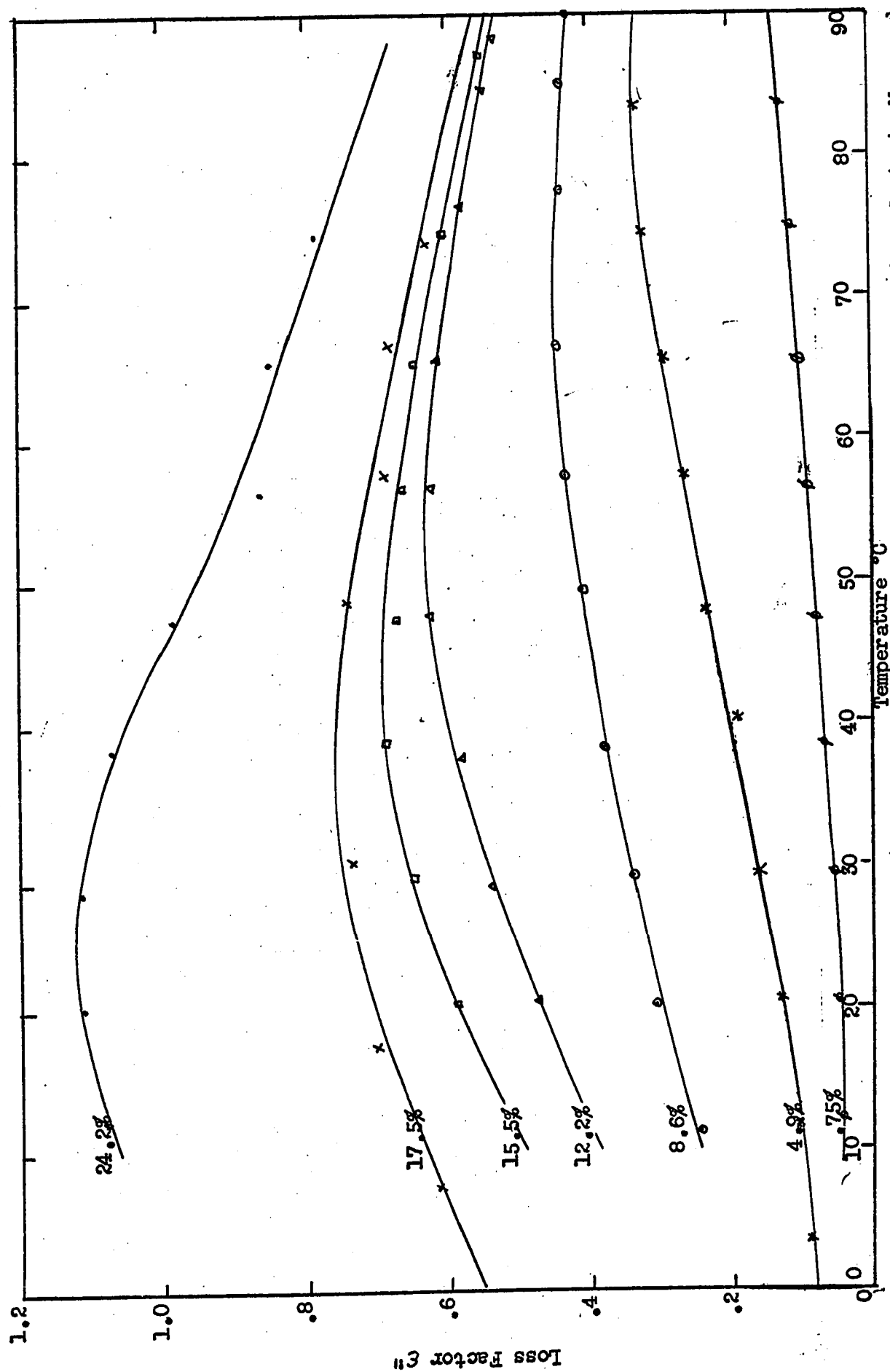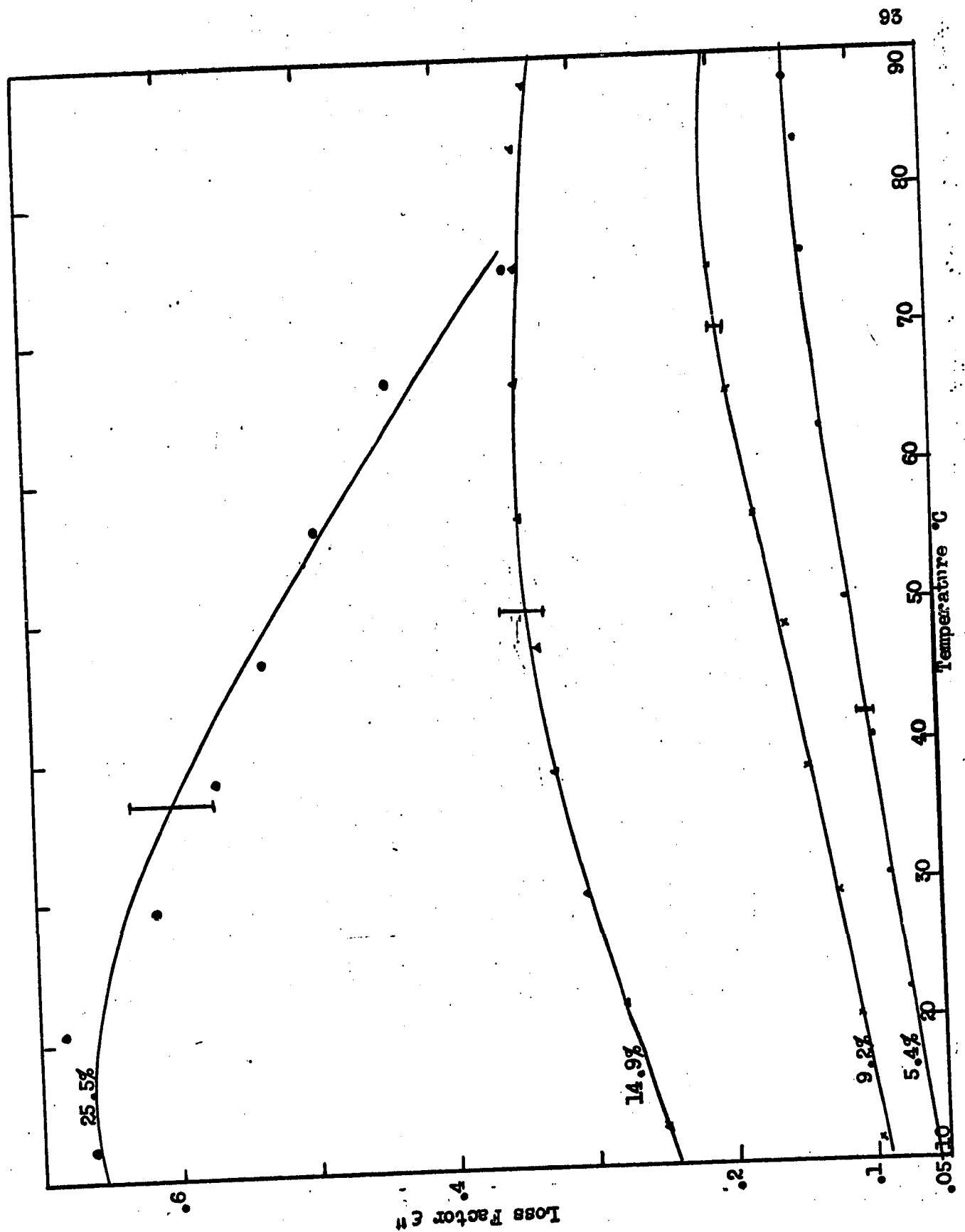
Fig. 5.8- Dielectric loss of Douglas Fir as a function of temperature at various moisture contents measured at 2450 MHz. with E-field in the radial grain direction.
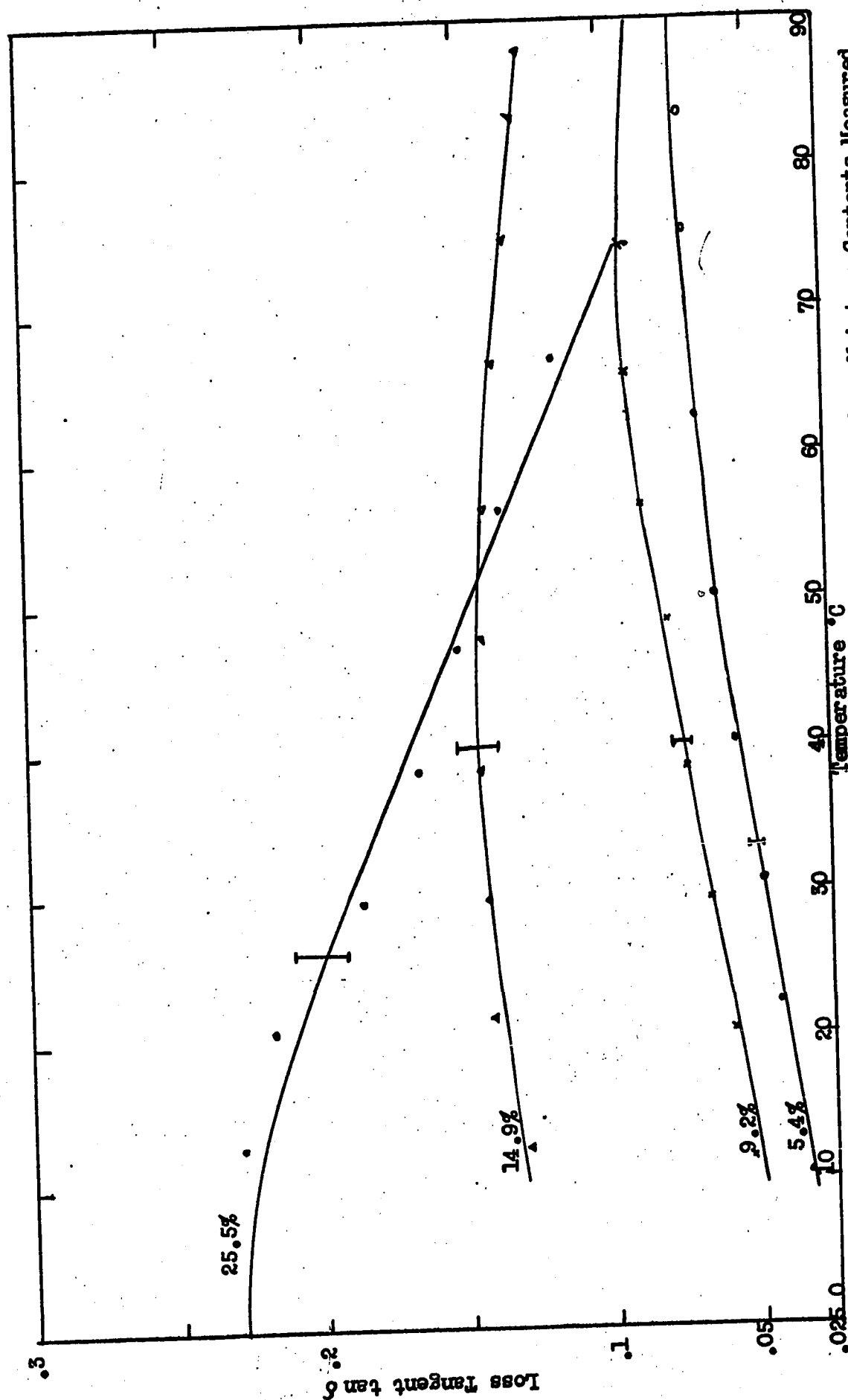
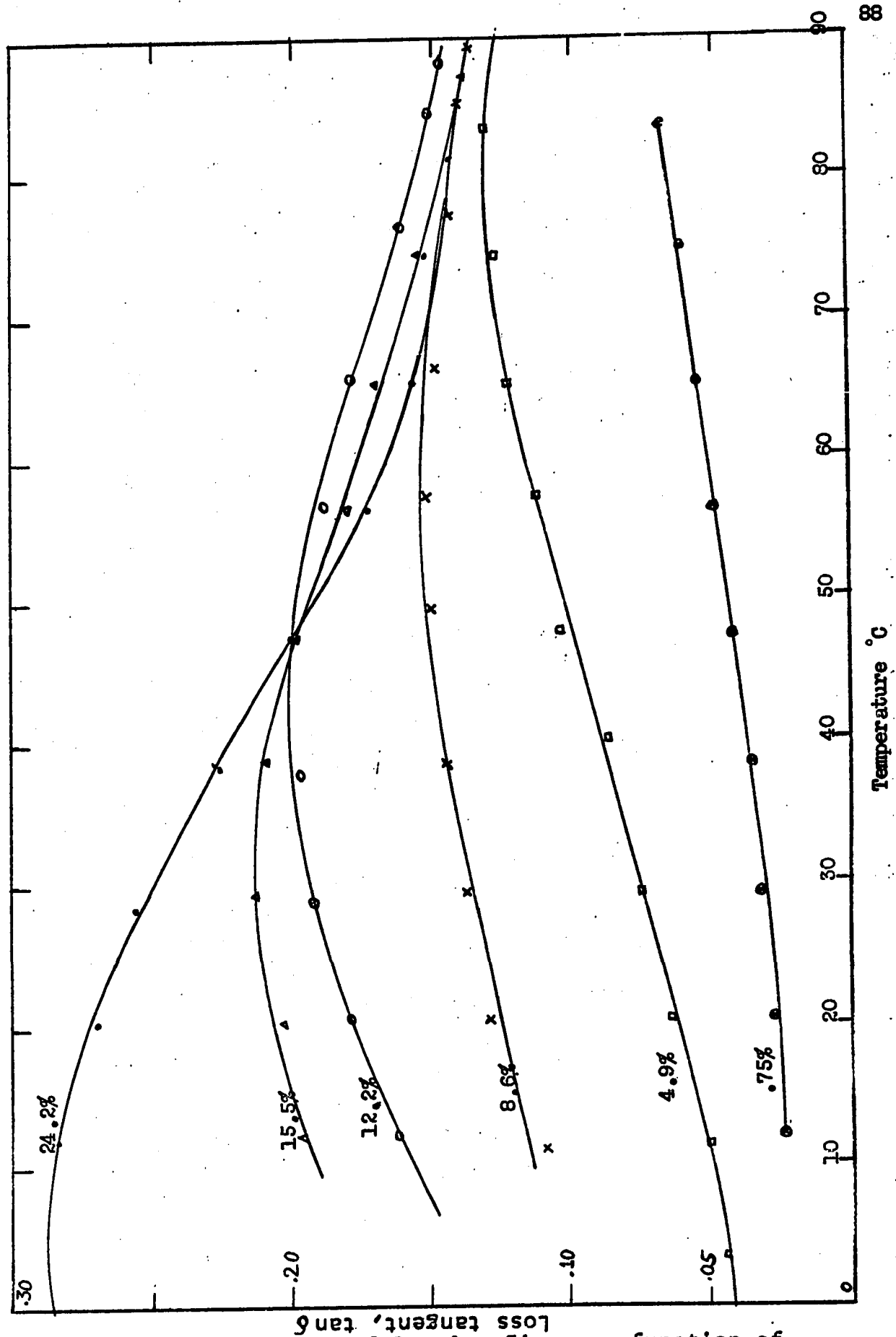Fig. 5.9 – Loss Tangent of Douglas Fir as a Function of Temperature at Various Moisture Contents Measured at 2450 MHz with E-field in the Radial Grain Direction.

94

nature of wood as a dielectric. Maximum loss temperatures, T_m, are plotted for Douglas Fir in figure 5.10 for the longitudinal grain direction. From the graph it is apparent that the maximum loss temperatures of $\mathcal{E}''$ and $\tan\delta$ are quite different. Theoretically, for low dispersion dielectrics ($\mathcal{E}_0 - \mathcal{E}_\infty$ small), the maxima for $\mathcal{E}''$ and $\tan\delta$ should occur at nearly the same temperature and frequency. As dispersion and loss increase, the two curves diverge, as is evident from figure 5.10. A similar plot of T_m versus moisture content is given for Western Hemlock in figure 5.11*.

3. Only small variations in density were found in the samples used for the tests and corrections for these variations were small and hence neglected. However, the correction for the real part of the dielectric constant is linearly proportional to density and further data on such corrections may be found in the literature[50].

2. Calculations of Activation Energies

In order to produce theoretical data for these materials it is necessary to calculate the activation energy required in the polarization process. Invoking the theory of chapter 3, the activation energies are calculated by the use of equation (3.32) which, when rewritten becomes

$$Q = RT \, Ln\left(1/\omega\tau_0\right) \tag{5.1}$$

τ_0 is assumed to have the same value for all wood species and is taken to be 1×10^{-18} sec (derived from Pinewood data in chapter 3). To evaluate Q, the values for T_m, τ_0, ω and R are put in equation (5.1). Figure 5.12 shows the calculated activation

----

* A. J. Curtis[53] gives a plot of T_m versus percentage composition for polyvinylchloride-tricresylphosphate. The functional relationship there is found to be similar to that of wood.
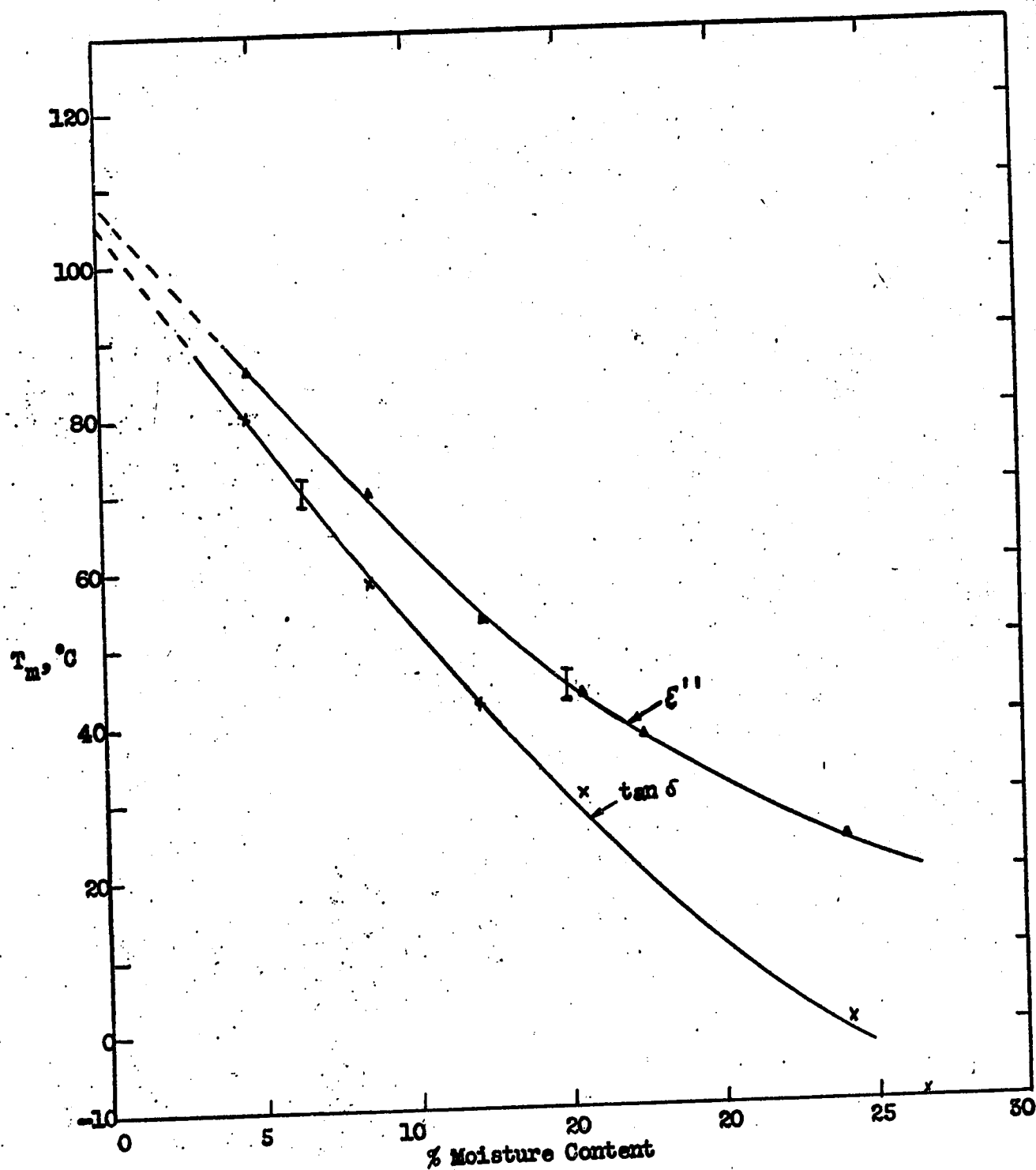
Fig. 5.10 — Maximum Dielectric loss temperature as a function of moisture content for Douglas Fir measured at 2450 MHz with E-field in the longitudinal grain direction.
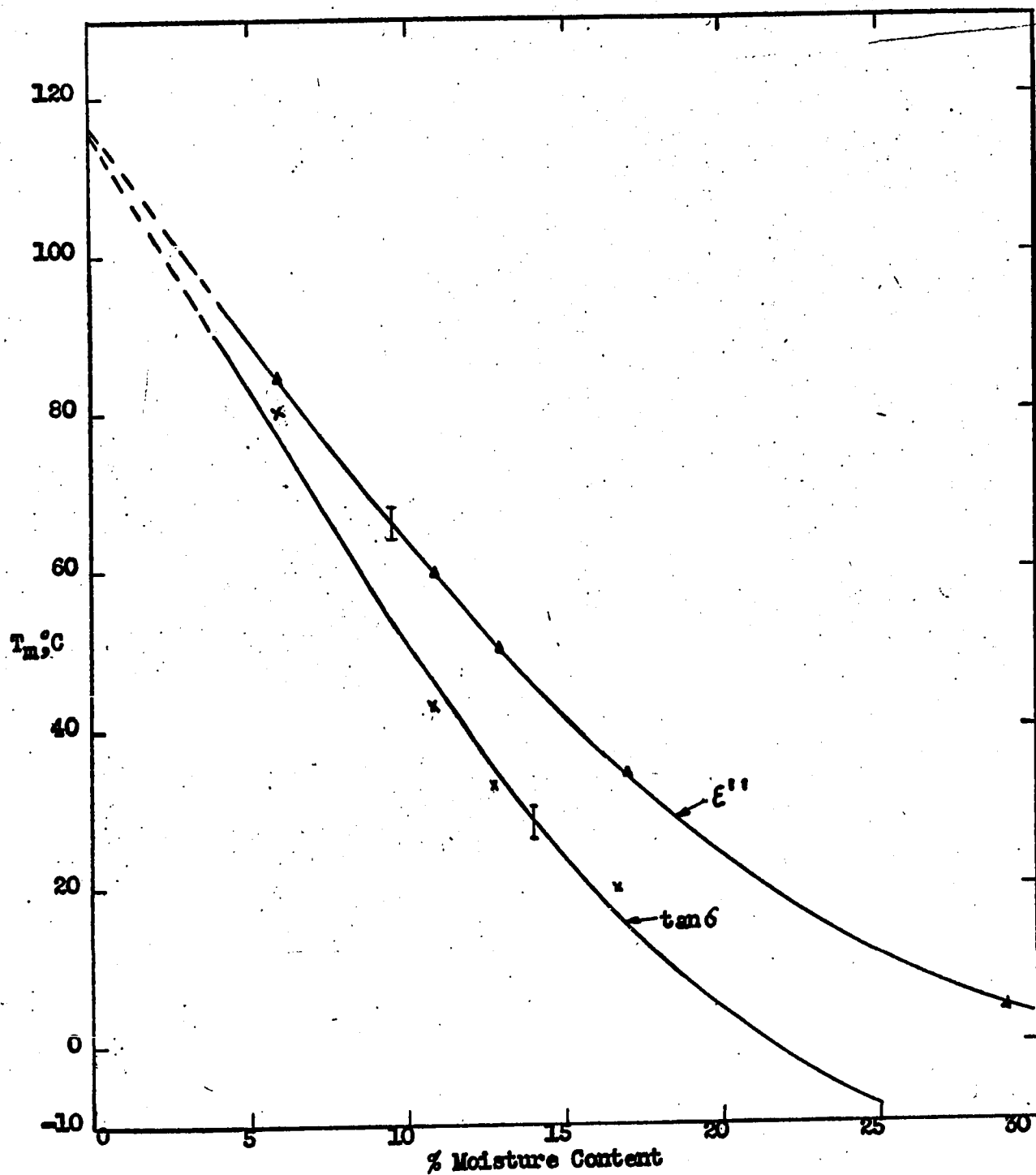
Fig. 5.11 — Maximum dielectric loss temperature as a function of moisture content for Western Hemlock measured at 2450 MHz with E-field in the longitudinal grain direction.

energy of polarization as a function of moisture content for Douglas Fir, Western Hemlock and, for comparison, the curve for Pinewood is given as well.

It is well known that wood is structurally an anisotropic substance which results in an anisotropic behavior of its mechanical and electrical properties. It turns out that the dielectric constant for wood measured with the electric field along the grain (longitudinal) is considerably higher than that measured in the radial and tangential directions. From the data obtained this can be interpreted as partially due to a variation of activation energy of polarization with grain direction. Figure 5.12 shows the activation energy for Douglas Fir in the tangential direction to be somewhat higher than that for the longitudinal grain direction. The difference in slope of the curves in figure 5.12 for the different wood species is likely related to the crystallinity of the material*. Western Hemlock and Pine both are less crystalline than Douglas Fir which is also reflected in their density and hardness.

3. Bound Water Concepts

The initial activation energy involved in the polarization process of wood at 0% moisture content is found to lie between 13.5

---

* An increase in crystallinity decreases the maximum loss and shifts the loss maximum to higher temperatures[53]. Decreased crystallinity, hence decreased hydrogen bonding, results in an increased dielectric constant. It is found that a linear relationship exists between dielectric constant and the crystallinity index for various cellulose materials[54, 55, 56].
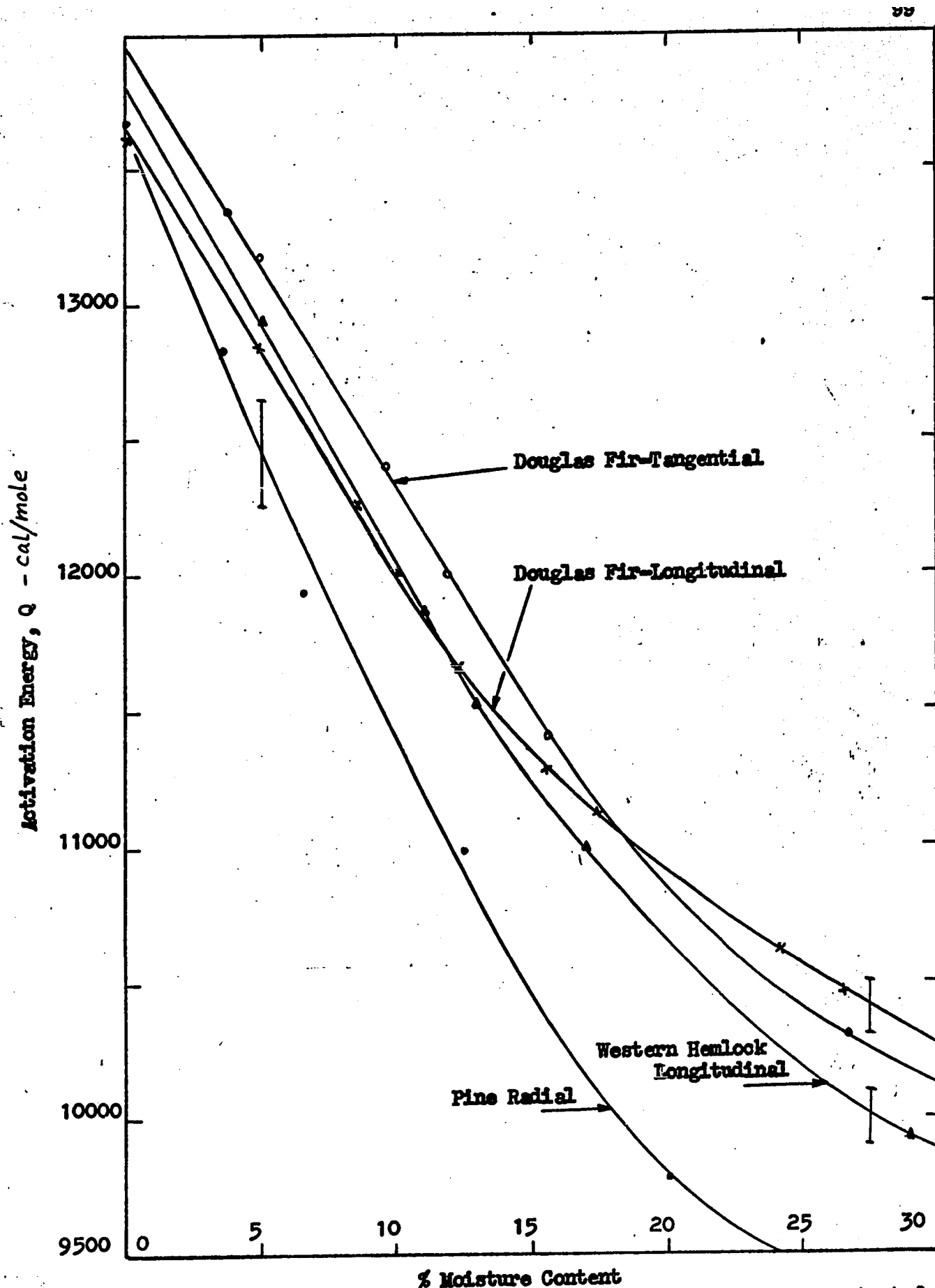
Fig. 5.12 — Activation energy of polarization versus moisture content for
Douglas Fir, Western Hemlock and Pine with E-field in the
longitudinal, tangential and radial grain directions.

to 14 Kcal/mole. This reveals the type of bonding taking place between the cellulose and water molecules. Hasted[51] and others [54] have done extensive tests on the dielectric properties of ice and water. It is found that for ice the activation energy of polarization is 13.5 Kcal/mole and for water the value drops to 4.5 Kcal/mole. Assuming the bond bending and breaking theory, advanced in the literature[59], holds, three or four hydrogen bonds occur in ice and for water only one single hydrogen bond is present between molecules. Hence, to break a hydrogen bond completely requires about 4.5 Kcal/mole, whereas breaking and immediately reforming of a bond is estimated to require about 3 Kcal/mole. Moreover, bond bending may occur in which case the required energy lies somewhere between 0 and 3 Kcal/mole. In light of these facts, it is reasonable to assume that the initial water molecules absorbed on wood are held in a fashion very similar to that of pure ice. As the moisture content in the wood increases the water molecules are bound less tightly than before because it becomes possible for the molecules to make water to water bonds as well, which requires a lower energy. This should happen, for example, after the initial monomolecular layer of water is filled up, which occurs at approximately 6% moisture content[17].

Bound water phenomena in wood have been discussed by Voss[57] from measurements at 3 cm wavelengths and by others[7, 17, 26, 58]. However, actual energies associated in the dielectric polarization process in wood were never given explicitly. From the data and the analysis presented here it is now possible for the first time

to see explicitly the relationship between intrinsic material parameters and the macroscopic dielectric properties of a bound-water system. An extremely important observation can be made about the so called free water in a substance. It has often been assumed that water absorbed beyond a certain moisture content, for example, the fiber saturation point in wood, behaves not as bound water, but as ordinary liquid water. However, Hasted[51] presents ample data to show the relaxation process of liquid water requires an activation energy of only 4.5 Kcal/mole, whereas the data on wood indicate that at fiber saturation (26-30% M.C.), the activation energy of polarization is still as high as 10 Kcal/mole (see figure (5.12.). Hence, unless a sharp break occurs in the relationship between activation energy and moisture content*, it is concluded that bound water effects extend beyond the fiber saturation point of wood. Other experimental evidence which supports such a behavior is found in a paper on wool-water systems[26].

Detailed arguments as to the bonding mechanism between water, organic and inorganic molecules can be found in the literature[59]. The discussion given there allows for the rather high activation energies found for wood-water systems. Based on the experimental data given in this thesis it can be assumed that the relaxation of water in high moisture content wood still involves 2 or 3 bonded water molecules, and hence does not have dielectric properties equal to that of pure liquid water.

---

* All experimental evidence points to a smooth transition of functional relationships at the fiber saturation point[28]. Similar arguments were presented in a quite different context by C. Skaar[49].

4. Dielectric Constant Versus Moisture Content

Data from the dielectric constant versus temperature curves can be used to obtain plots for the variation of dielectric constant with moisture content using temperature as the parameter. This is done for Douglas Fir, longitudinal grain, in figures 5.13, 5.14, and 5.15. The real part of the dielectric constant increases monotonically with moisture content up to at least the fiber saturation point and increases with temperature as well. Dielectric loss on the other hand shows a more complex behavior which is due mainly to the temperature dependence of the relaxation times. Thus at the higher temperatures the loss factor tends to level off with increasing moisture content. Only a few curves are given in figure 5.14 for the sake of clarity. The data compare favorably with some data obtained by James and Hamill[34]. Their results were obtained at "room temperature" interpreted here as 23°C.

From the experimental data on Douglas Fir and Western Hemlock it is possible to find the relationship between the values of the dielectric constant at the maximum loss temperatures and moisture content. The data are presented in Figure 5.16, which indicate a linear dependence between the parameters. These curves will be used to calculate the constants needed for some theoretical curves presented in the next section.

B. Theoretical Results

With the aid of the experimental data presented in the previous section, the equations developed in chapter 3 can be solved yielding the theoretical
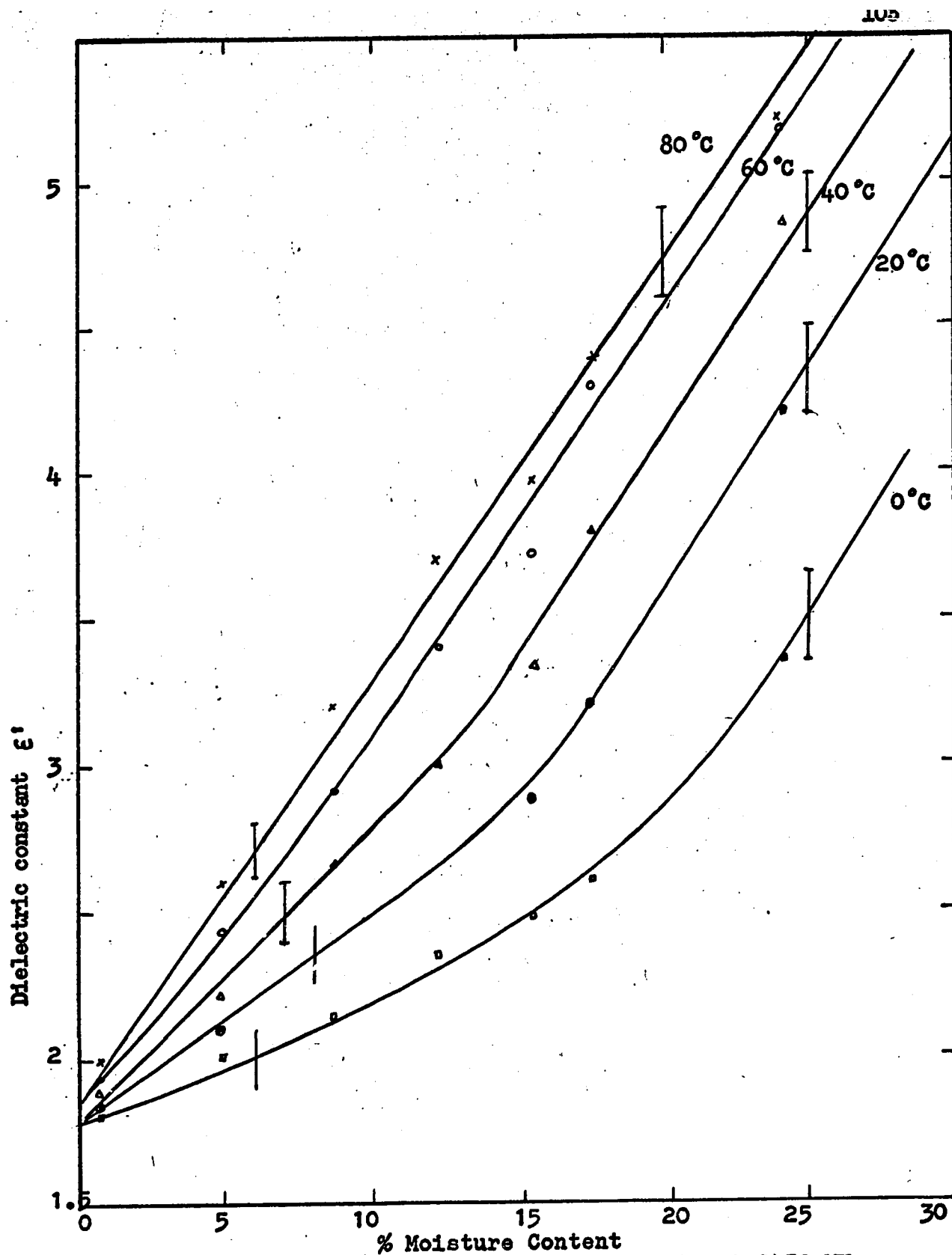
Fig. 5.13 — Dielectric constant of Douglas Fir at 2450 MHz as a function of moisture content with temperature as the parameter and E-field in the longitudinal grain direction.
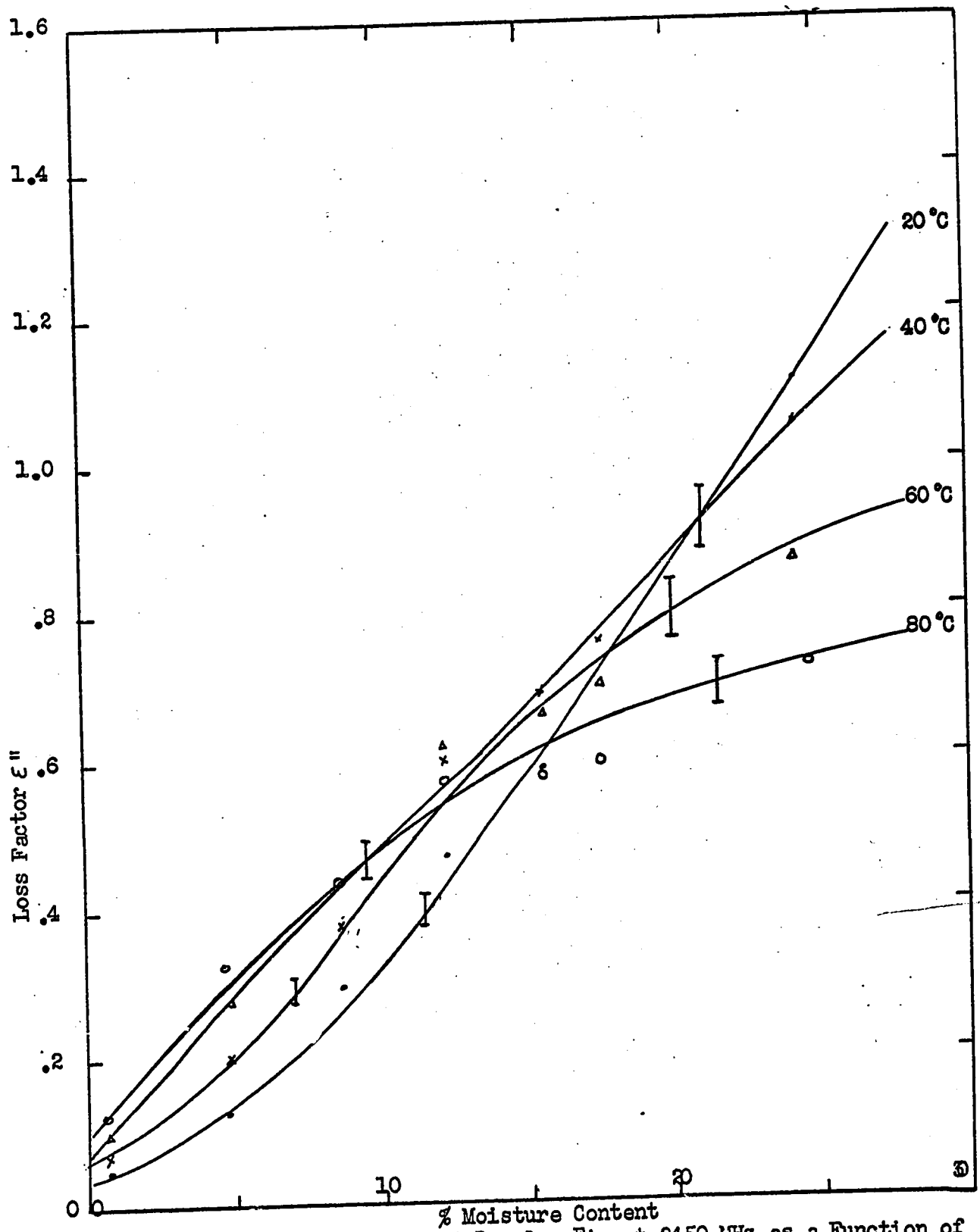
Fig. 5.14 — Dielectric Loss of Douglas Fir at 2450 MHz as a Function of
Moisture Content with Temperature as the Parameter with
E-field in the Longitudinal Grain Direction.
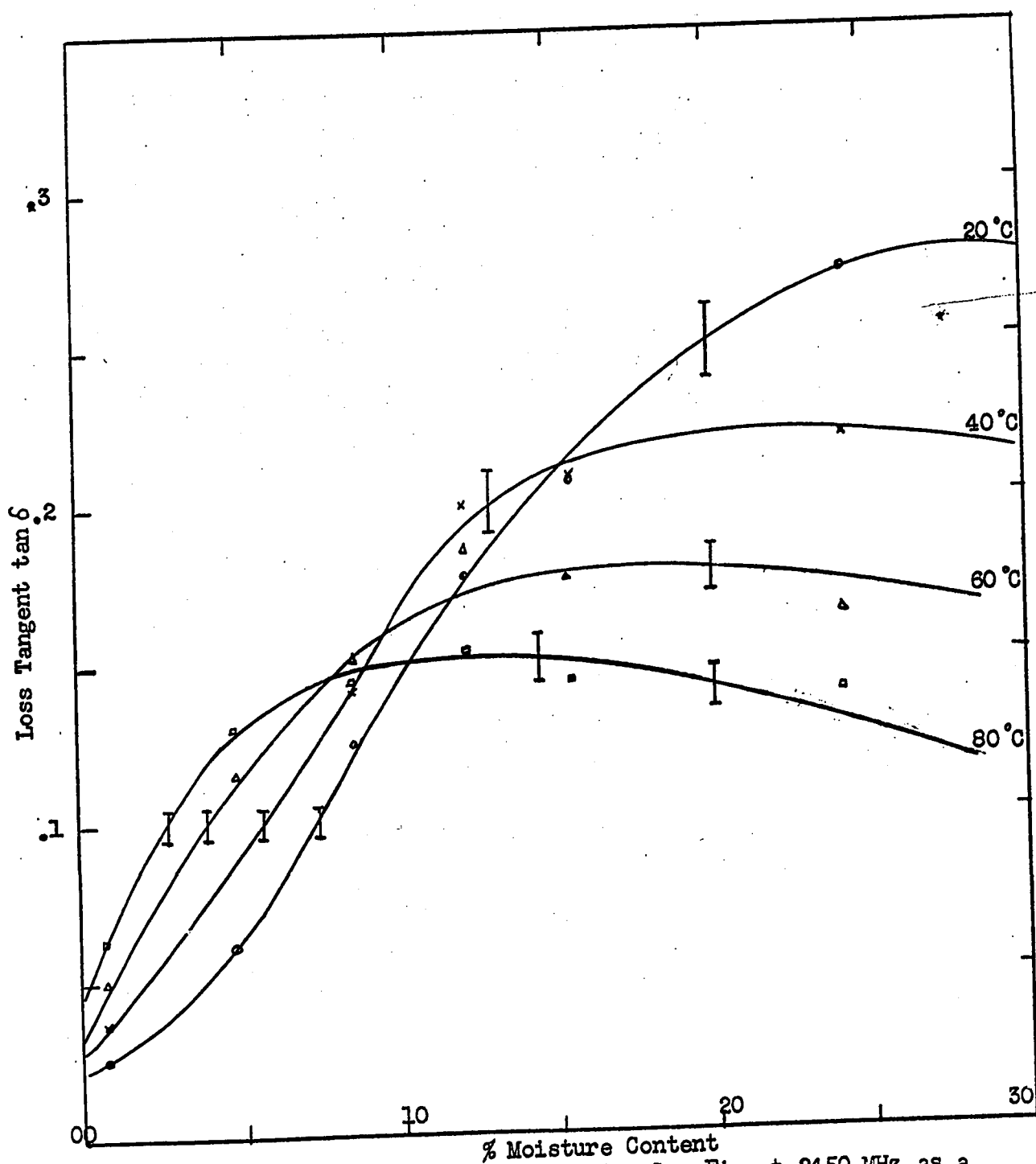
Fig. 5.15 – Dielectric Loss Tangent of Douglas Fir at 2450 MHz as a Function of Moisture Content with Temperature as the Parameter with E-field in the Longitudinal Grain Direction.
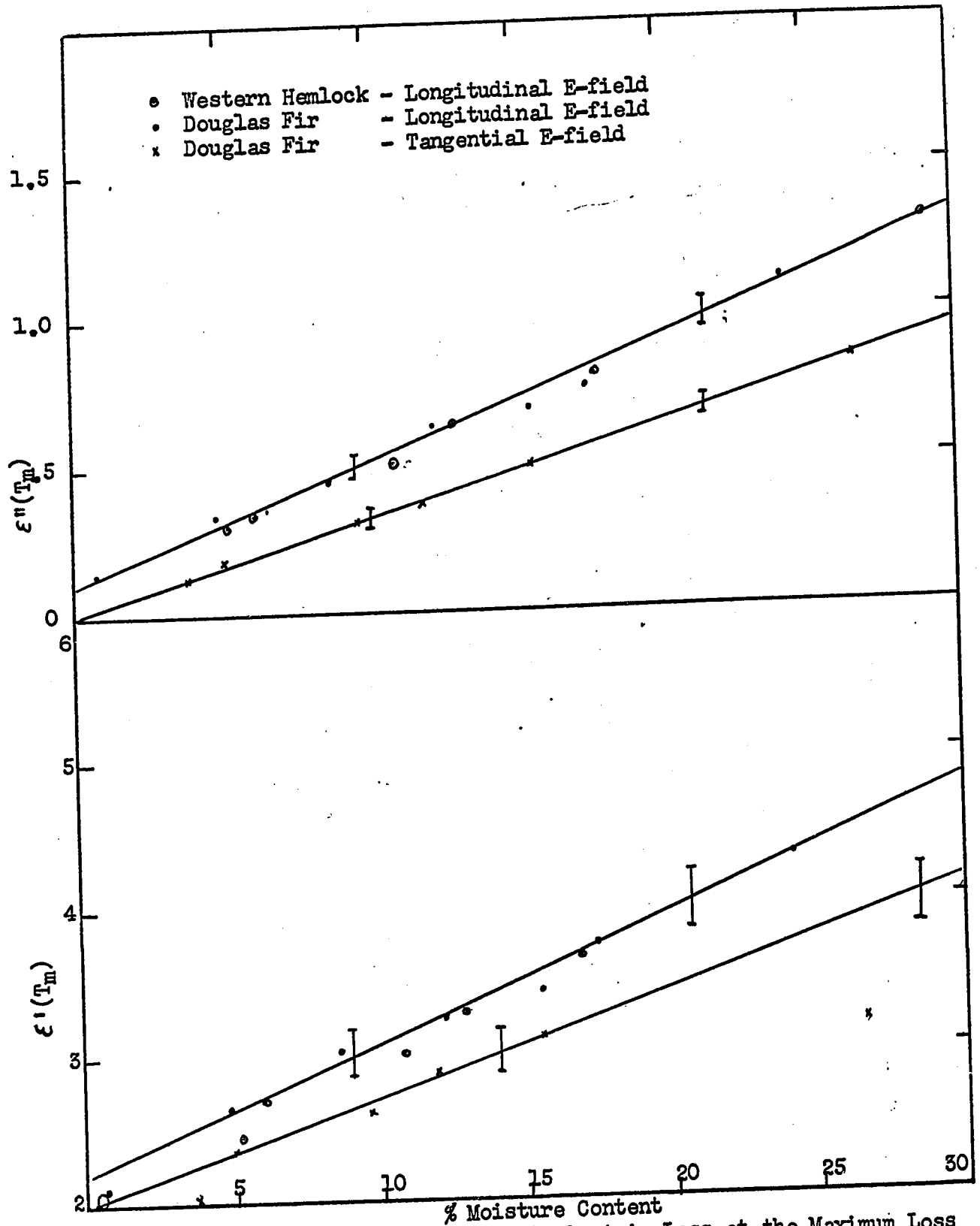
Fig. 5.16 — Dielectric Constant and Dielectric Loss at the Maximum Loss Temperatures as a Function of Moisture Content for Douglas Fir and Western Hemlock Measured at 2450 MHz with E-field in the Longitudinal and Tangential Grain Directions.

behavior of the dielectric constant for wood.

Equations (3.25) and (3.27) were solved numerically on a digital computer for various moisture contents. This required values of Q, and b. The values used were $\tau_0 = 10^{-18}$ sec , Q as found from figure 5.12 and b was given some trial value. The low and high frequency dielectric constants were obtained by integration of equations (3.33) and (3.36). The resulting solution was compared with the experimental curves for $\varepsilon(T)$ and b was incremented until a fit of better than ±10% between the theoretical and experimental dielectric loss was achieved. This procedure was carried out automatically for a range of 0-100 C. Repeating the calculations for each moisture content, values of b were found for all the curves. It turns out that the value of b is approximately constant (b=.255) with moisture content. For comparison, the experimental and theoretical values of ε' and ε'' versus T for a moisture content of 17.5% are plotted in figures 5.17 and 5.18. At the higher temperature the experimental values for the real part of the dielectric constant are too low because of moisture loss during the measurement. Since ε' increases rapidly with moisture content and temperature, see figure 5.13, the effect is quite noticeable. However, percentage error is less than ±10%. Curves for the other moisture content values give similar results, but are omitted for the sake of clarity. Because the theoretical data lie so close to the experimental, any further calculations will be done on the theoretical data, since its functional relationships are known.

Families of curves for the theoretical complex dielectric constant of Douglas Fir as a function of temperature are presented in figures 5.19 and 5.20, with moisture content given as a parameter. These two figures
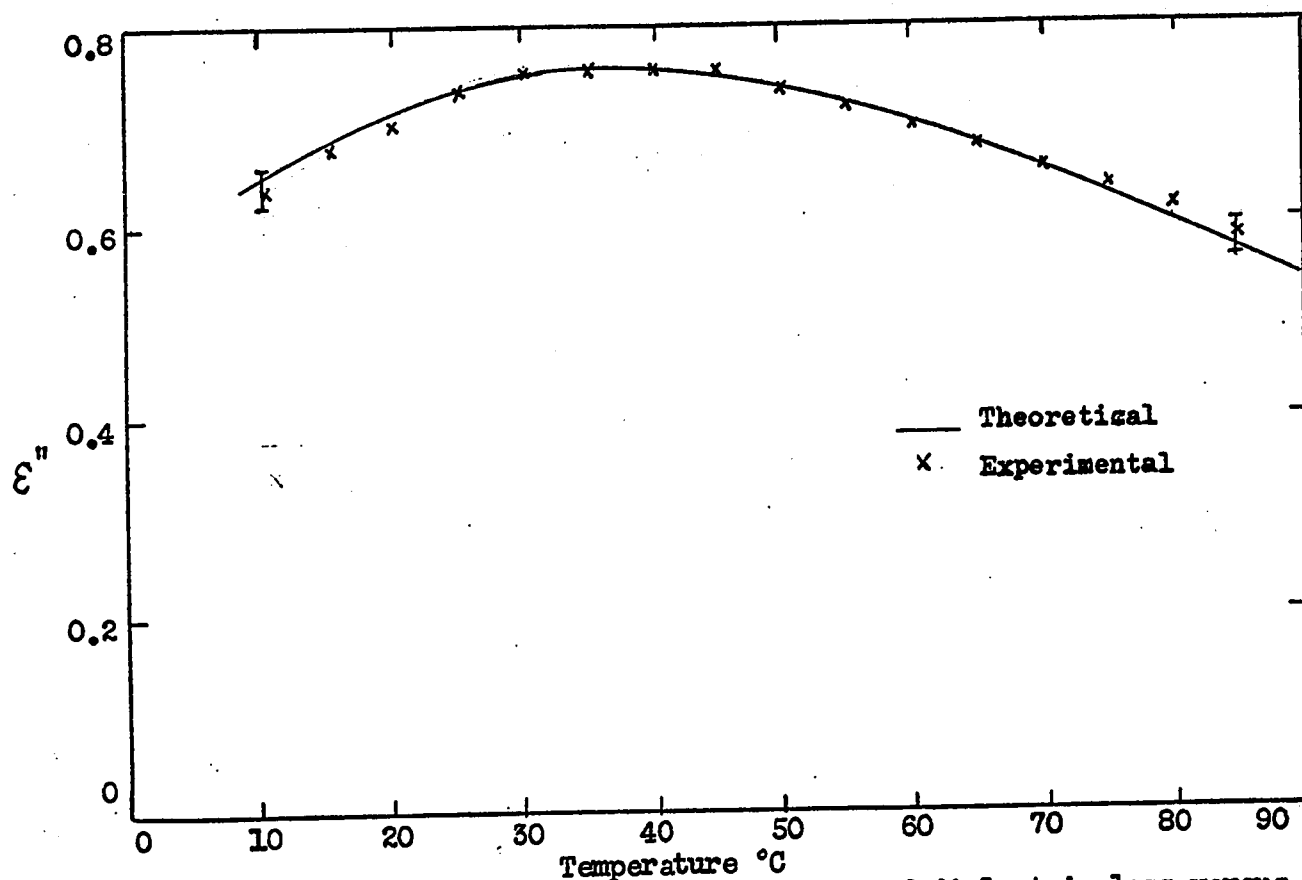
Fig. 5.17 — Theoretical and experimental plot of dielectric loss versus
temperature for 17.5% m.c. Douglas Fir with E-field in the
longitudinal grain direction; measured at 2450 MHz.
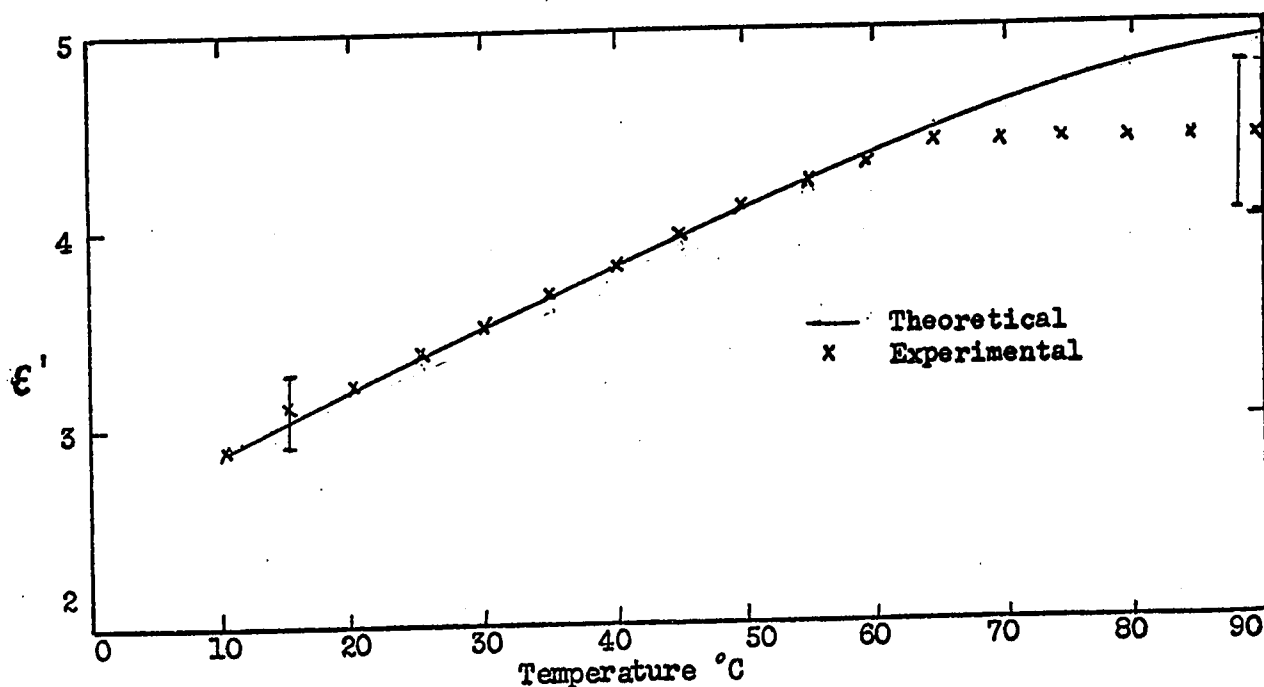
Fig. 5.18 — Theoretical and experimental plot of dielectric constant versus
temperature for 17.5% m.c. Douglas Fir with E-field in the
longitudinal grain direction; measured at 2450 MHz.
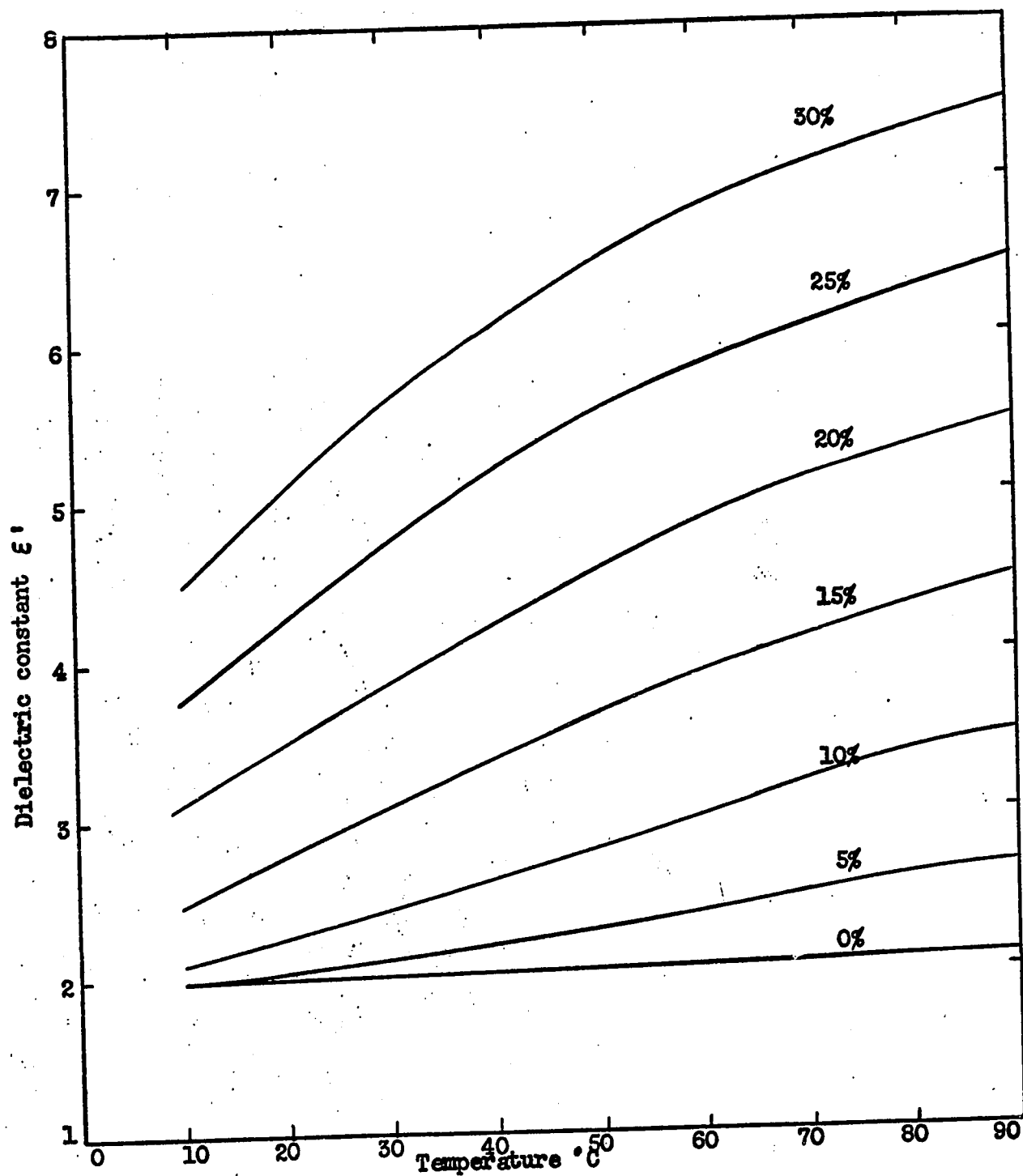
Fig. 5.19 — Theoretical dielectric constant versus temperature at various moisture contents for Douglas Fir at 2450 MHz with E-field in the longitudinal grain direction.
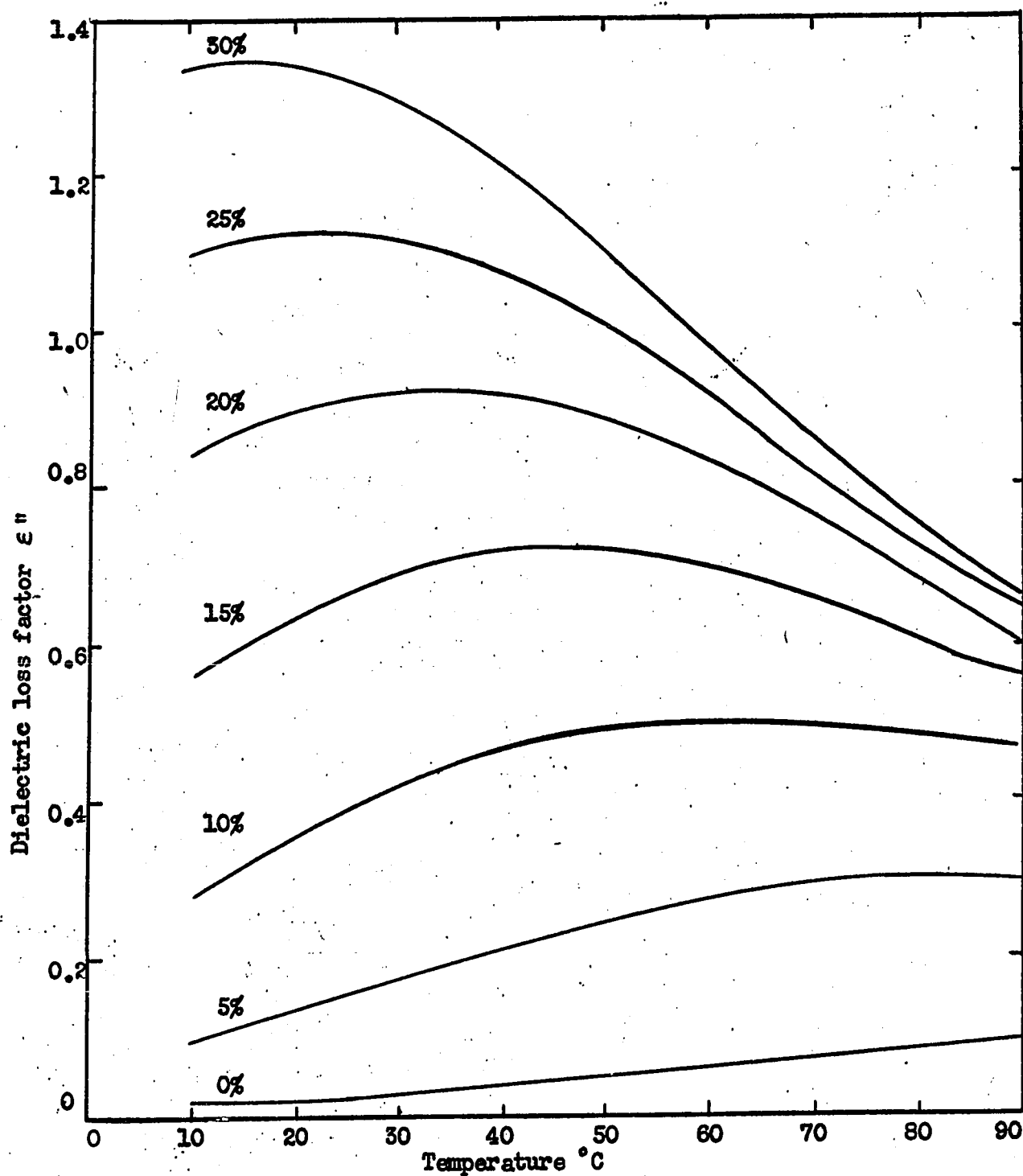
Fig. 5.20 – Theoretical dielectric loss versus temperature at various
          moisture contents for Douglas Fir at 2450 MHz with E-field
          in the longitudinal grain direction.

can be used as convenient reference charts for the dielectric constant of Douglas Fir. Calculations of the slope of the above two graphs yield the temperature coefficients of the real and imaginary parts of the dielectric constant*. Hence, curves of $d\mathcal{E}'/dT$ and $d\mathcal{E}''/dT$ versus moisture content are plotted in figures 5.21 and 5.22 with temperature as a parameter.

For completeness, the theoretical values of the dielectric constant versus moisture content are also calculated and presented in the form of figures 5.23, 5.24 and 5.25, with temperature as the parameter.

All of the above results are valid at the frequency of 2450 MHz. From the same experimental data however, the behavior of the dielectric constant at other frequencies can be determined. With the help of equation (3.26) it is possible to predict the relaxation times of wood at various moisture contents, thus

$$\tau = \tau_0 e^{Q/RT} \tag{3.26}$$

Table 5.1 - Activation energy and relaxation time for Douglas Fir versus moisture content.

Moisture Content,%	Activation Energy, Q cal/mole	Relaxation Time in sec. ($\times 10^{11}$) at:					
		0°C	20°C	40°C	60°C	80°C	100°C
.1	13660	8640	1550	346	92.4	28.7	10.1
.5	13600	7730	1400	314	84.4	26.4	9.32
1	13500	6420	1180	267	72.6	22.9	8.14
2	13310	4530	849	197	54.5	17.4	6.3
5	12800	1770	354	86.7	25.2	8.42	3.17
8	12300	704	150	38.8	11.8	4.13	1.61
10	12000	405	89.5	24.0	7.52	2.69	1.08
15	11350	122	29.3	8.43	2.82	1.07	.448
20	10900	53.3	13.5	4.09	1.43	.561	.244
25	10550	28.0	7.41	2.33	.841	.341	.152
30	10270	16.7	4.58	1.48	.551	.229	.104

* In the process of microwave heating, the temperature coefficients are important since they determine the heating rate and temperature profile of the treated dielectric.
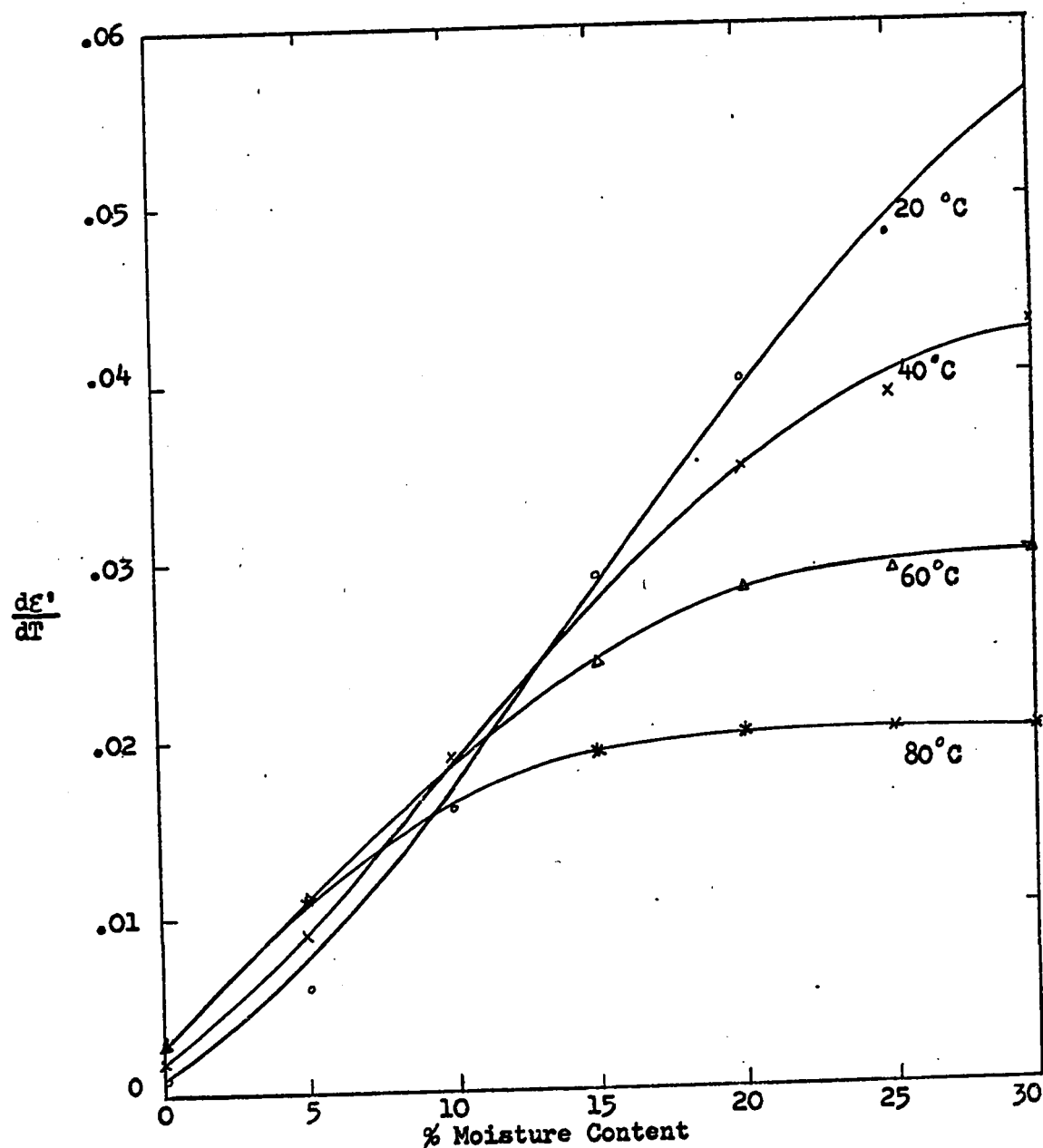
Fig. 5.21 - Temperature coefficient of the theoretical dielectric
constant versus moisture content at various temperatures
for Douglas Fir at 2450 MHz with E-field in longitudinal
grain direction.
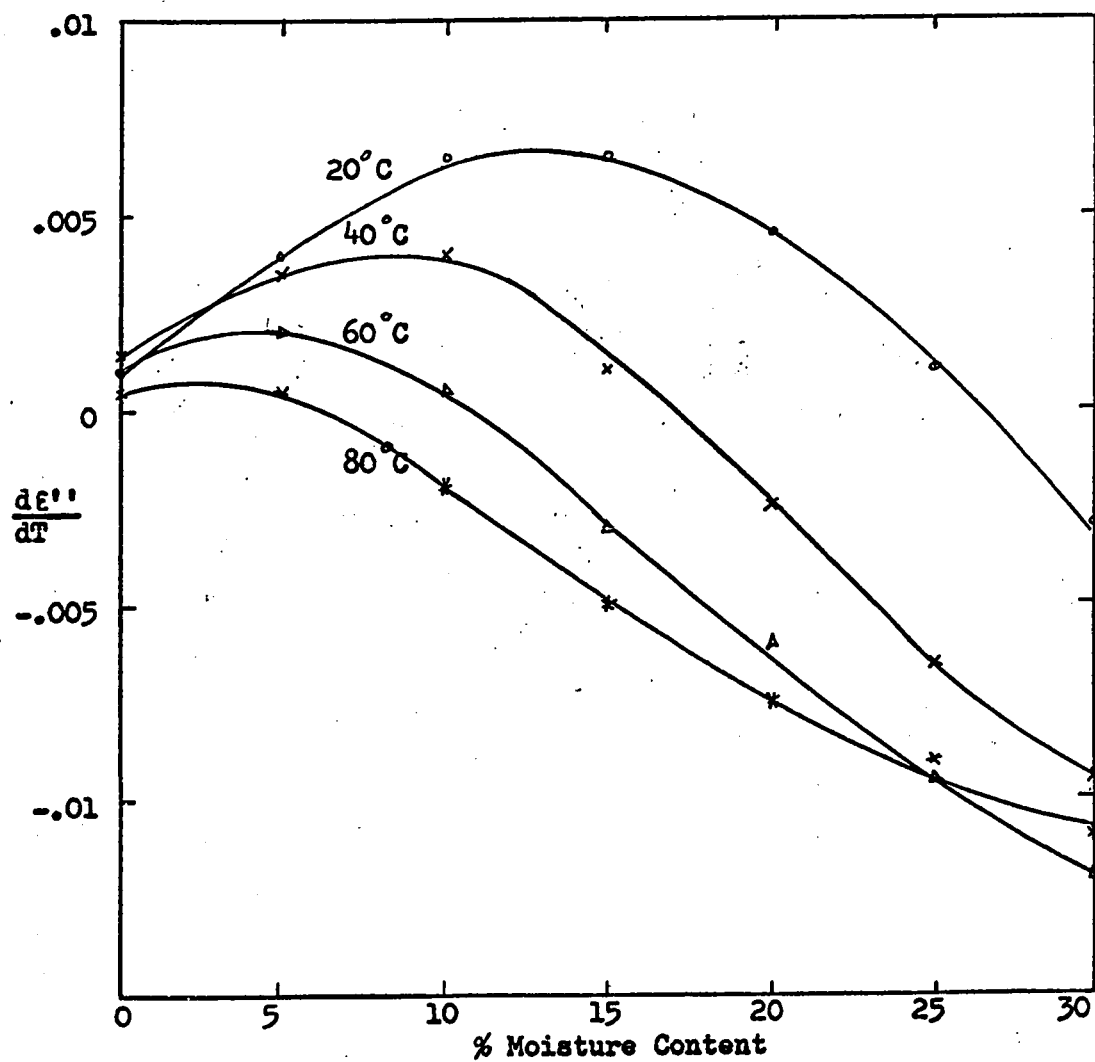
Fig. 5.22 – Temperature coefficient of the theoretical
dielectric loss versus moisture content at various
temperatures for Douglas Fir at 2450 MHz with E-field
in longitudinal grain direction.
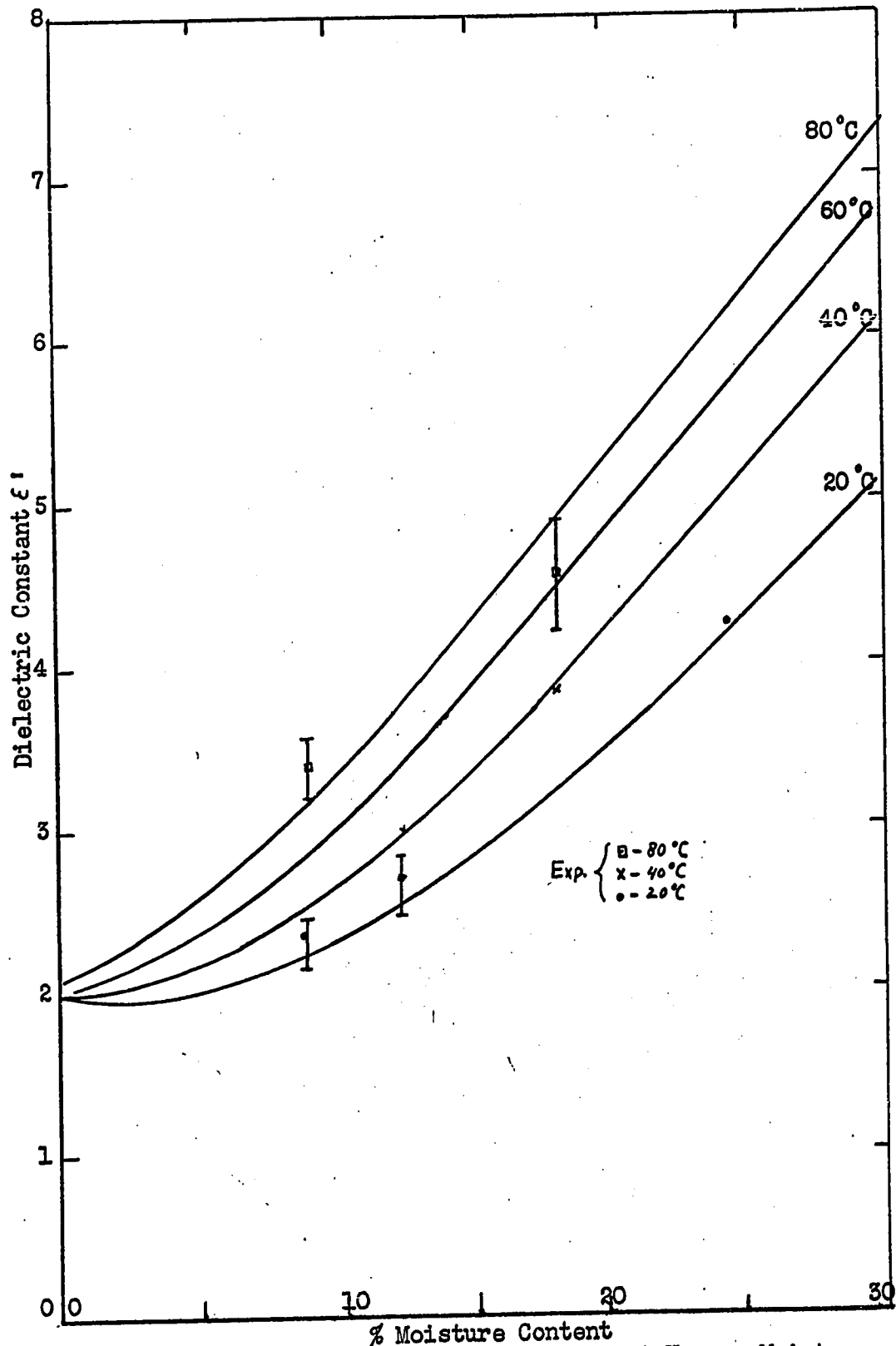
Fig. 5.23 — Theoretical Dielectric Constant Versus Moisture
Content at Different Temperatures at 2450 MHz for
Douglas Fir with E-field in the Longitudinal
Grain Direction.
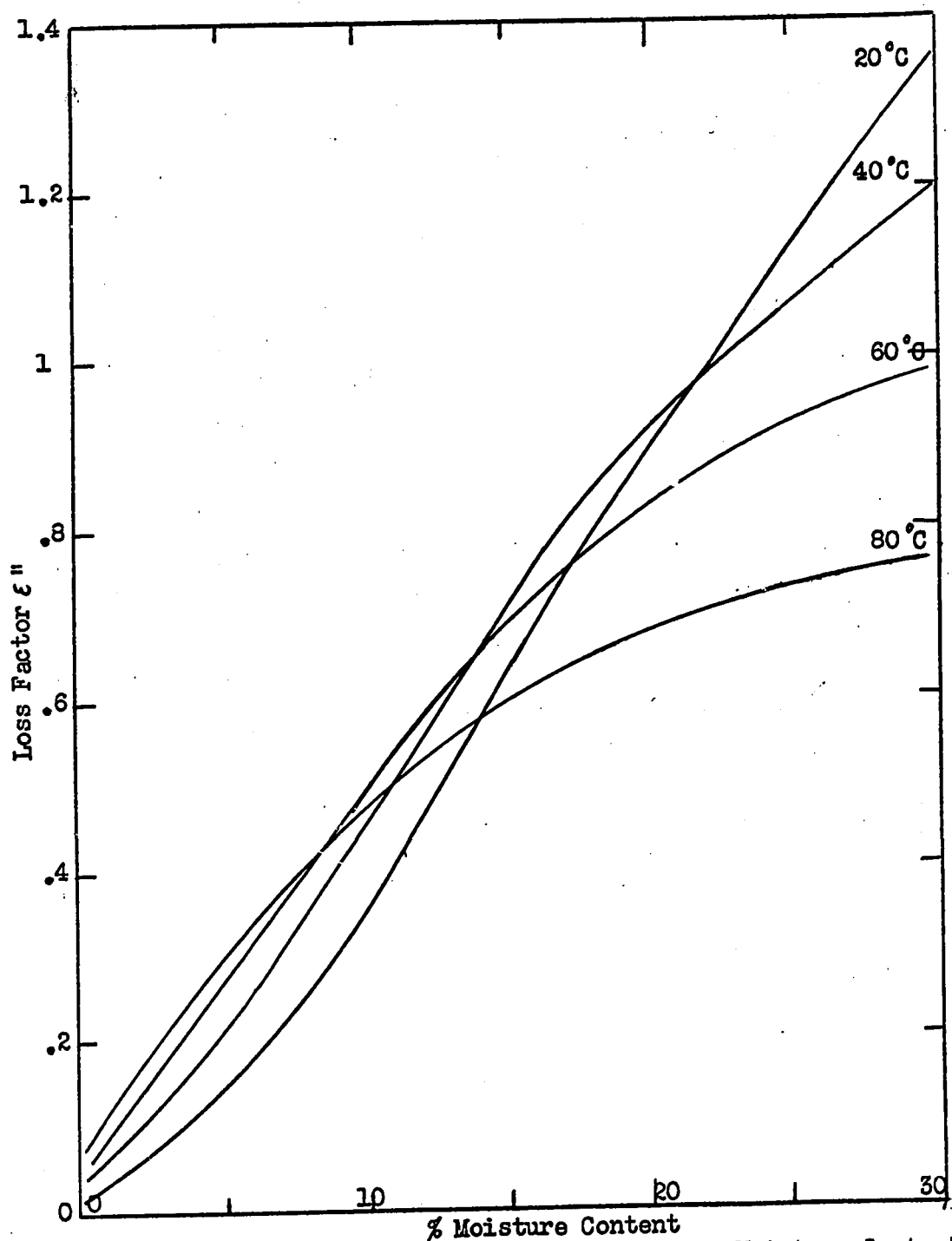
Fig. 5.24 – Theoretical Dielectric Loss Versus Moisture Content
at Different Temperatures at 2450 MHz for Douglas
Fir with E-field in the Longitudinal Grain Direction.
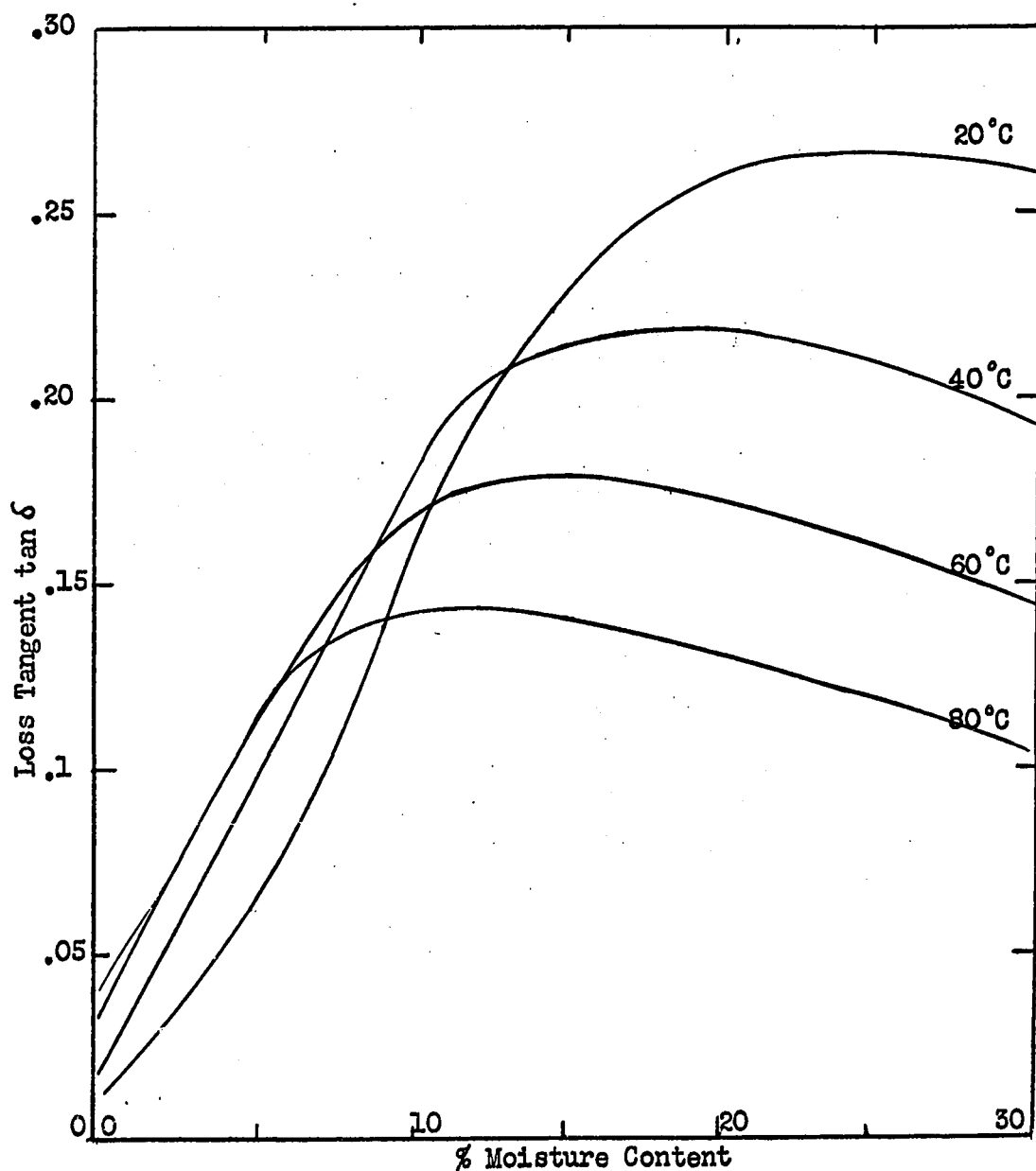
Fig. 5.25 — Theoretical Loss Tangent Versus Moisture Content
at Different Temperatures at 2450 MHz for Douglas
Fir with E-field in the Longitudinal Grain Direction.

Generally, care must be taken in the calculation of relaxation times from temperature varying data at a given frequency. Frohlich[66] states that $(\mathcal{E}_0 - \mathcal{E}_\infty)$ and $(\mathcal{E}' - \mathcal{E}_\infty)$ must be known as functions of temperature before τ can be calculated. Now, $d\mathcal{E}_\infty/dT$ is proportional to the linear expansion coefficient of the material, see, for example, chapter 3, which for various wood species is of the order of one part per million. As a result, the temperature dependence of the high frequency dielectric constant is negligible. Furthermore, data on Douglas Fir, for example, figure 5.1, indicate that the temperature dependence of $\mathcal{E}_0$, the low frequency or, conversely, the high temperature value of $\mathcal{E}'$, is also very small - $\mathcal{E}'$ becomes constant as T increases. It is concluded that values of τ may safely be calculated by the direct use of equation (3.26). When previously defining this equation, it was also stated that both τ_0 and Q were assumed to be temperature independent which according to the above paragraph has experimental justification.

Applying equation (3.26) for $\tau_0 = 10^{-18}$ sec and for values of Q found from figure 5.12, the relaxation times for Douglas Fir are evaluated and summarized in Table 5.1. Figure 5.26 is a graphical presentation of the relaxation time of Douglas Fir versus moisture content with temperature as the parameter. This log-log plot shows quite clearly that at about 6% moisture content the behavior of relaxation time with increasing moisture content changes to a nearly linear log-log plot, and at very high moisture contents (30-200%) the relaxation time approaches that of pure liquid water. The last part of the curves is shown by broken lines to indicate the probable asymptotic approach to the pure water relaxation times at the various temperatures[51]. This particular graph, figure 5.26, is very useful in
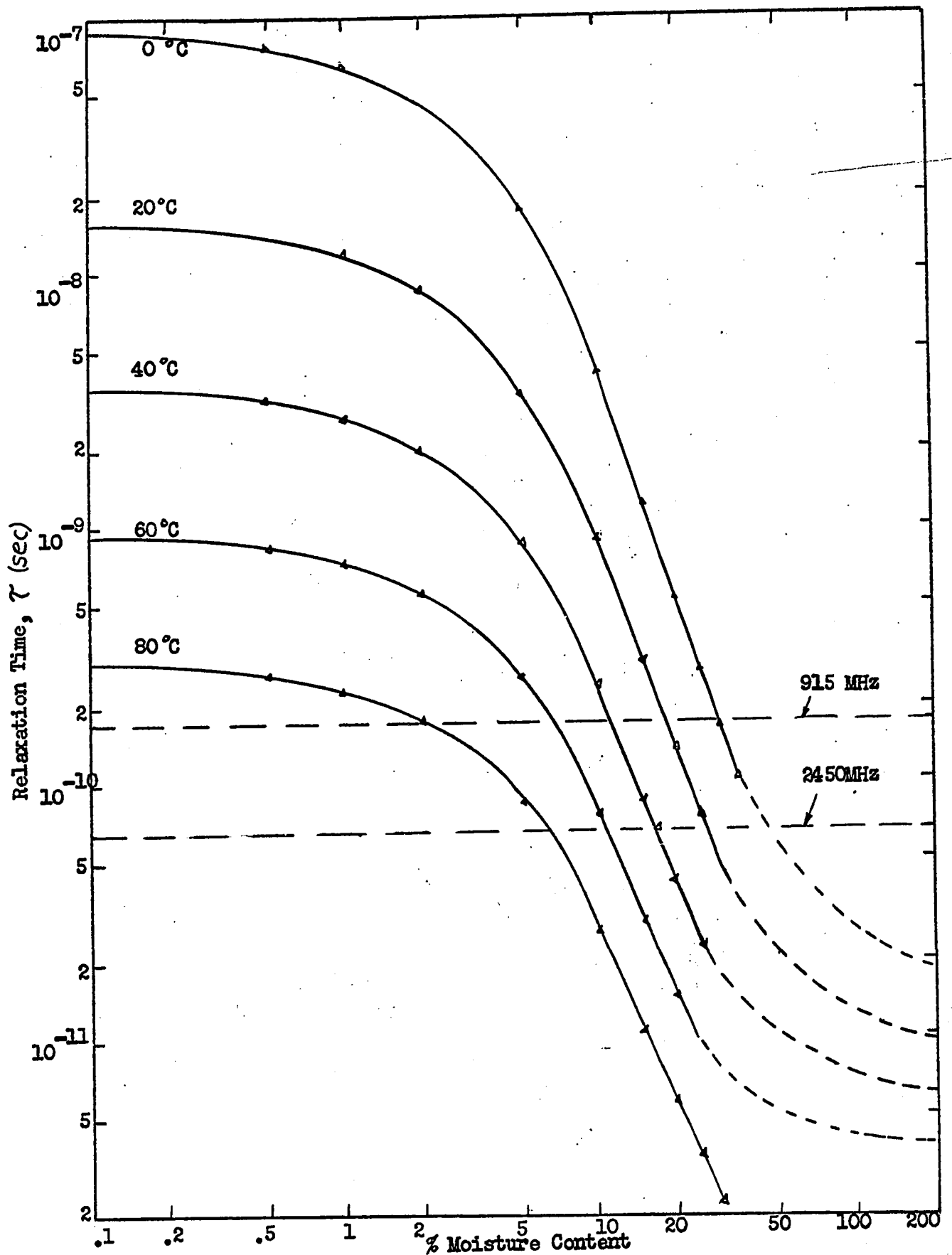
Fig. 5.26 — Relaxation time versus moisture content at different temperatures based on data from Douglas Fir with E-field in the longitudinal grain direction. Dotted portions indicate the probable asymptotic approach to the pure water relaxation times.
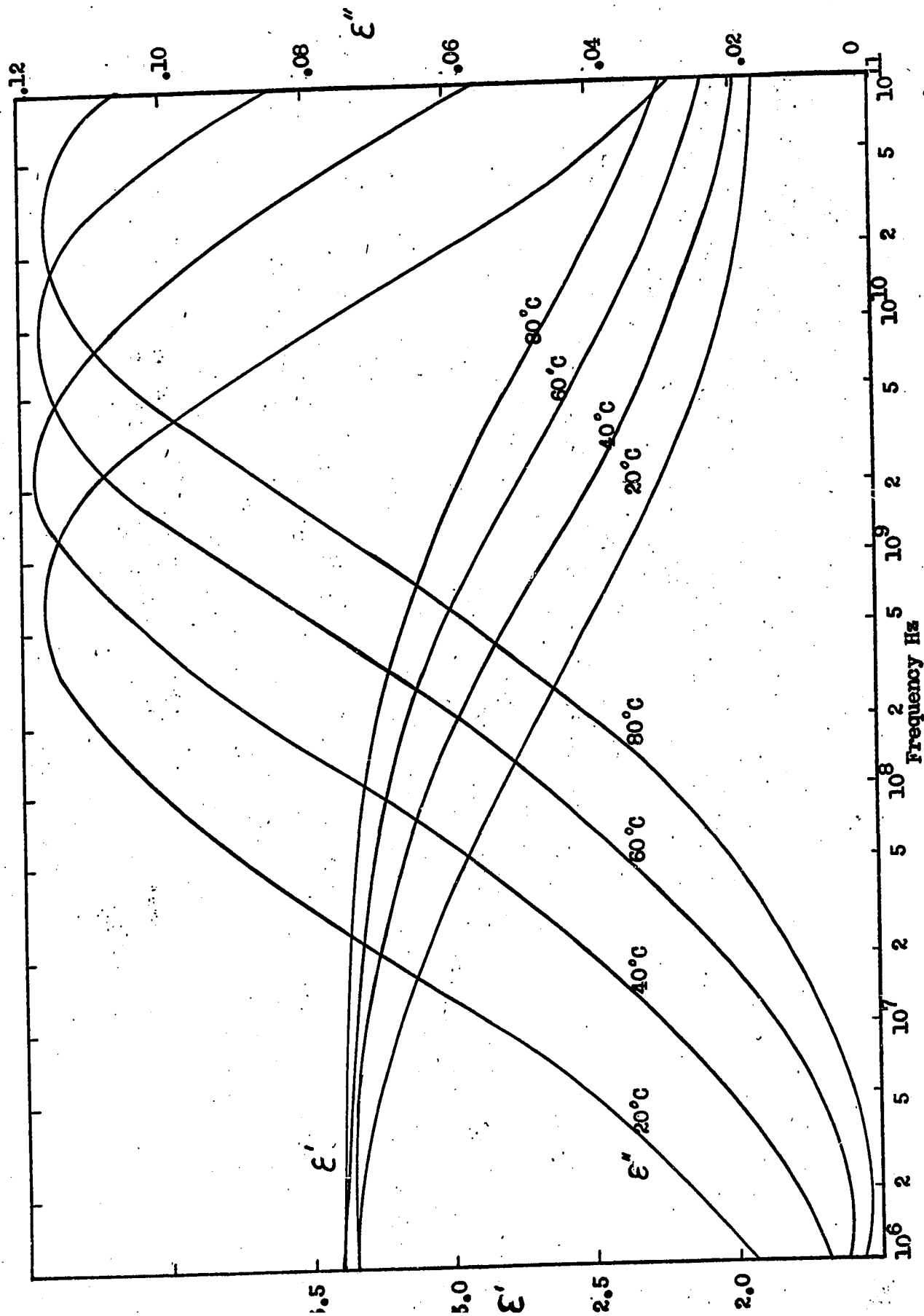
Fig. 5.27 — Theoretical dielectric constant and loss versus frequency at different temperatures and a moisture content of 5% for Douglas Fir with E-field in the longitudinal grain direction.
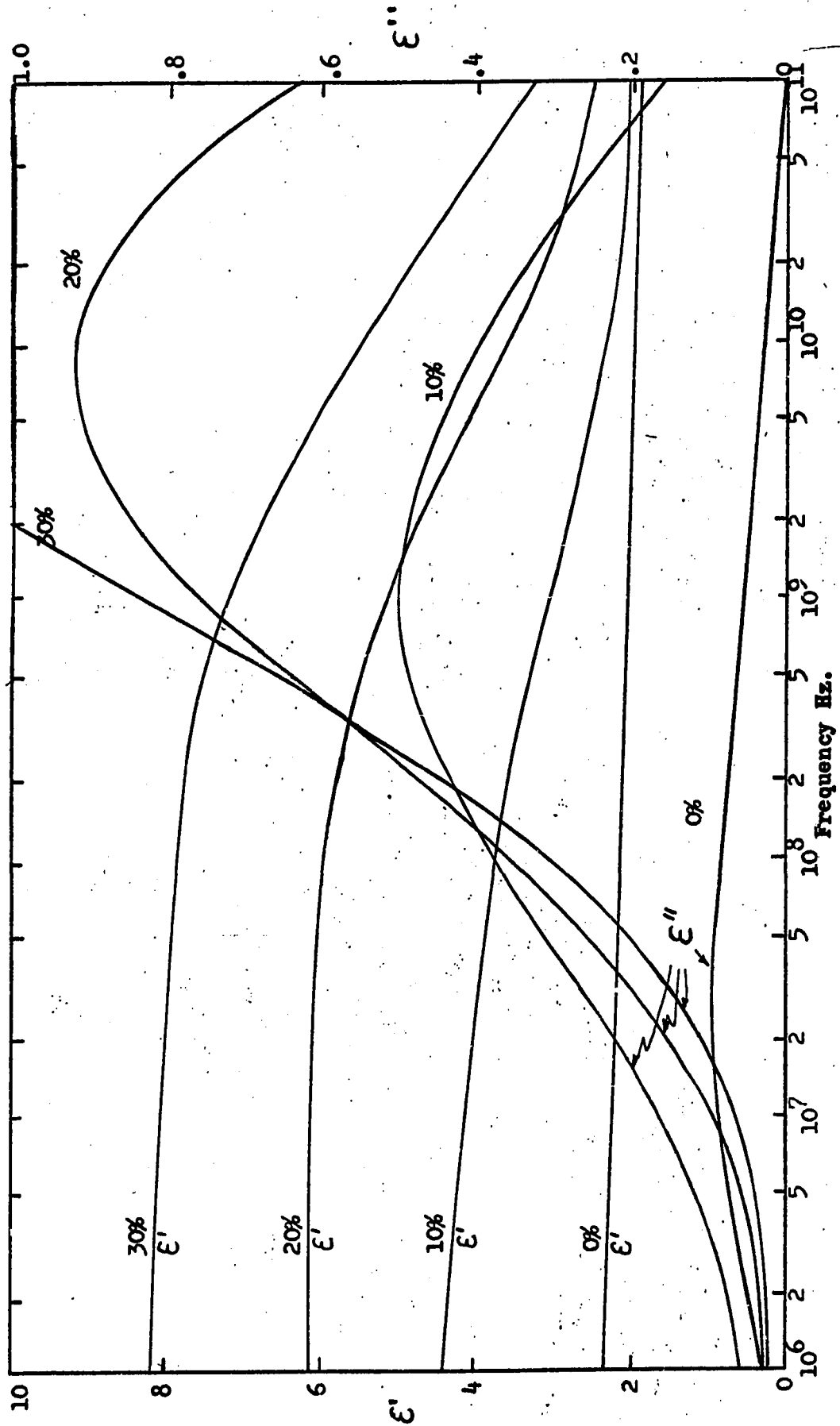
Fig. 5.28 - Theoretical dielectric constant and loss versus frequency at different moisture contents and a temperature of 20°C for Douglas Fir with E-field in the longitudinal grain direction.

determining the temperature behavior of wood at any given frequency and moisture content. For example, if it is desired to know the characteristics of Douglas Fir at 915 MHz the relaxation time corresponding to this frequency is $1/2\pi f = 1.74 \times 10^{-10}$ sec. Drawing a line for $\tau = 1.74 \times 10^{-10}$ parallel to the moisture content axis it is immediately apparent at which temperatures and moisture contents the maxima in the dielectric loss curves occur. In the example cited a 20% M. C. Douglas Fir will exhibit a loss maximum at about $18^\circ C$. Use of this figure clearly shows that to shift the loss maxima to a higher temperature for a fixed moisture content the applied frequency must increase. To obtain positive temperature coefficients on the dielectric constant of Douglas Fir from 0 to 30% moisture content a frequency of 8000 MHz or higher needs to be applied.

Having found values for the relaxation time, the frequency response of the dielectric can now be obtained by using equations (3.25) and (3.27) for various values of frequency, moisture content and temperature*. The resulting frequency varying data are presented in figures 5.27 and 5.28 based on the activation energy of polarization for longitudinal Douglas Fir.

Figure 5.27 shows the dielectric constant as a function of frequency at different temperatures for longitudinal Douglas Fir at a moisture content of 5%. In figure 5.28 the dependence of the dielectric constant on frequency at $20^\circ C$ for various moisture contents is shown. Qualitatively these results agree very well with data on Pinewood published by Trapp et al[7]. Their data were measured with the electric field in the radial grain direction, whereas the data on Douglas Fir were measured in the

* These results as all the others were obtained by the use of a digital computer.

longitudinal grain direction. Hence the magnitudes of the dielectric constant for the longitudinal Douglas Fir are higher than the radial Pine-wood. At the low frequency end, conductivity effects and charged double layers[27] tend to increase the dielectric constant considerably. Since these effects were not accounted for in the treatment given here the values for dielectric constant below 100 MHz are too low. Nevertheless the agreement between the theoretical curves in figures 5.26 and 5.27 and experimental frequency data as found in the literature[7] confirms the basic assumptions underlying the theory given in this thesis. Furthermore, one can make reasonable predictions of the dielectric properties at other frequencies in the range between 100 MHz and 20 GHz.

By the use of equations (3.35) and (3.39) the theoretical values of the low and high frequency dielectric constant can be calculated using the empirical values for $\varepsilon(T_m)$ as given in figure 5.16. The resultant dependence of ε_s and ε_∞ on moisture content is given by figure 5.29.

In assessing which parameters are basic to obtain the dielectric constant for wood it follows from this chapter that only the activation energy Q as a function of moisture content, and the variation of the low and high frequency dielectric constants must be known accurately. From the experimental data on Douglas Fir the following empirical relations for activation energy of polarization was determined by a least squares fit process.

(5.2)

$$Q = 2.716 M^2 - 194.7M + 13690$$

where M is the % moisture content of Douglas Fir. Equation (5.2) fitted the data to better than 1/2%.
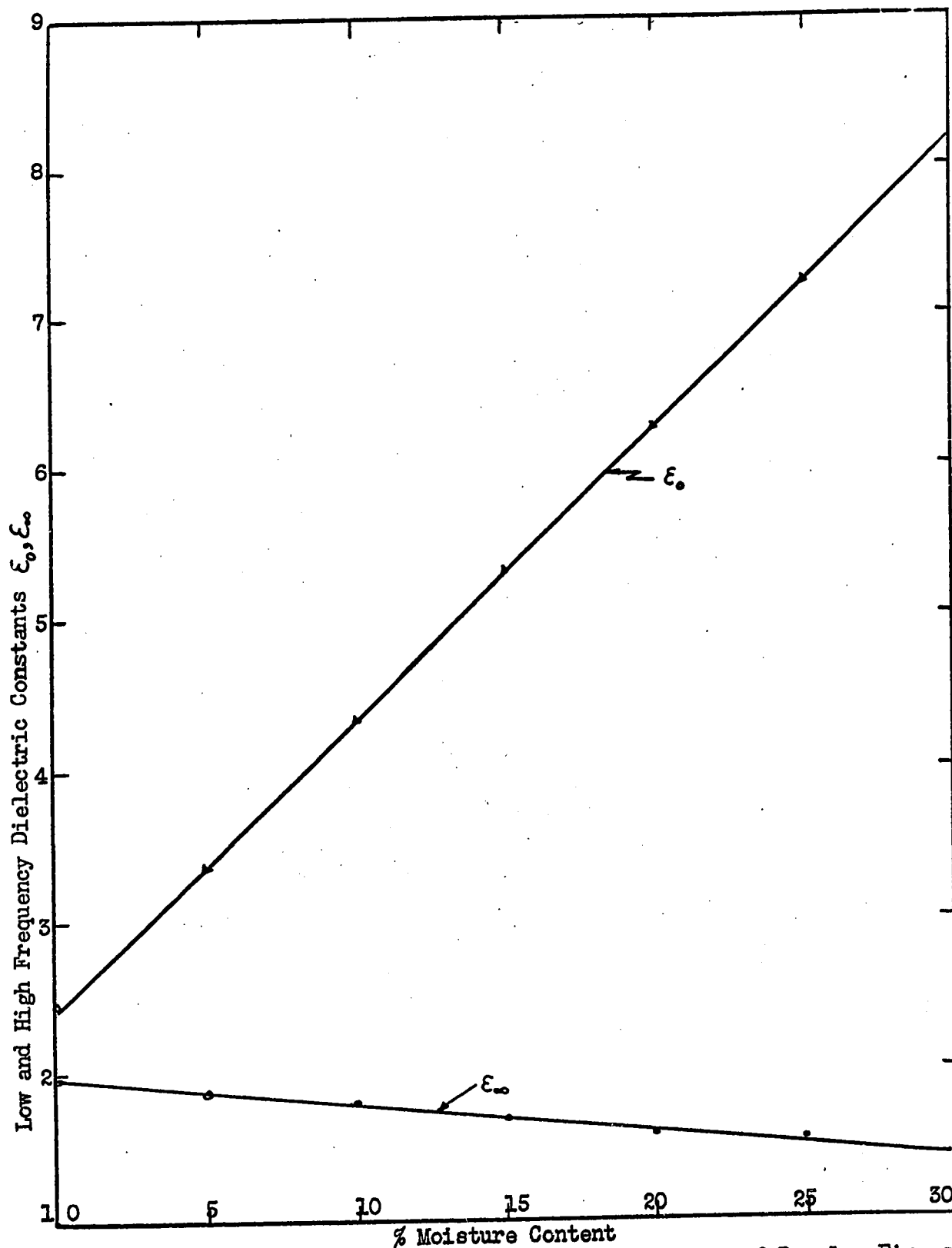
Fig. 5.29 — Low and High Frequency Dielectric Constant of Douglas Fir as a Function of Moisture Content with E-field in the Longitudinal Grain Direction.

Similarly for the low and high frequency dielectric constant the empirical relations were found to be

$$\varepsilon_0 = .1933 M + 2.4 \tag{5.3}$$

$$\varepsilon_\infty = -.0183 M + 1.95 \tag{5.4}$$

Equations (5.2), (5.3), and (5.4) are valid between 0 and 30% moisture content.

Conclusion

Combination of equations (3.25), (3.27), (5.2), (5.3) and (5.4) gives a complete description of the dielectric properties of Douglas Fir over a wide frequency and temperature range and at any moisture content between 0 and 30%. This defined system of equations though tedious and difficult to solve by hand was easily solved on a digital computer using APL, a direct access interpreter type language, requiring only seconds of computer time and 10 to 20 kilobytes of core storage.

The mathematical description of a wood system has the great advantage of improving predictability of a microwave wood heating system's performance under operating conditions where frequency, temperature and moisture content may all change continually.

CHAPTER 6

APPLICATION OF MIXTURE THEORY

In this chapter the dielectric mixture relations developed in chapter 2 will be applied to a cellulose-air-water mixture such as Douglas Fir. Values of the complex dielectric constant will be calculated as a function of moisture content and frequency and the results compared with experimental data.

WOOD AS A MIXTURE

Wood is a complex material, chemically and structurally[17]. Softwoods are structurally much simpler than hardwoods and the present work is mainly concerned with the natural multiphase mixtures occurring in Douglas Fir and Western Hemlock. For purposes of analysis a simplified diagrammatic sketch of a softwood sample is shown in Fig. 6.1
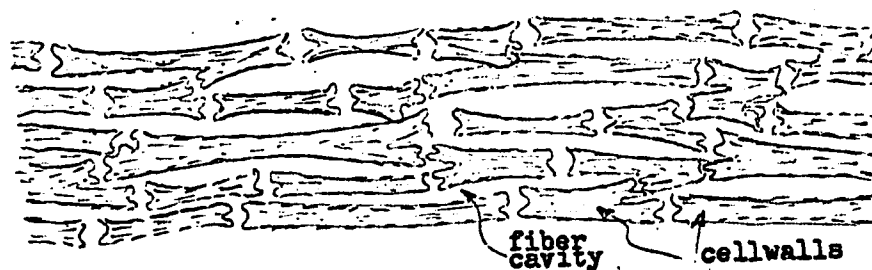
Fig. 6.1 - Diagrammatic sketch of softwood sample

The fiber cavities can be considered to be ellipsoidal in shape to a good approximation. These capillary cavities are air filled up to the fiber saturation point after which water condenses inside the cavities starting

with the smallest capillary diameter. Below fiber saturation the water is adsorbed by the cell walls and bonds to the cellulose fibers in layers of one to seven molecules thick. The number of bonded layers increases with increasing moisture content. Stamm* indicates that the water is adsorbed on the surface of the crystallites which are cylindrical in shape and in
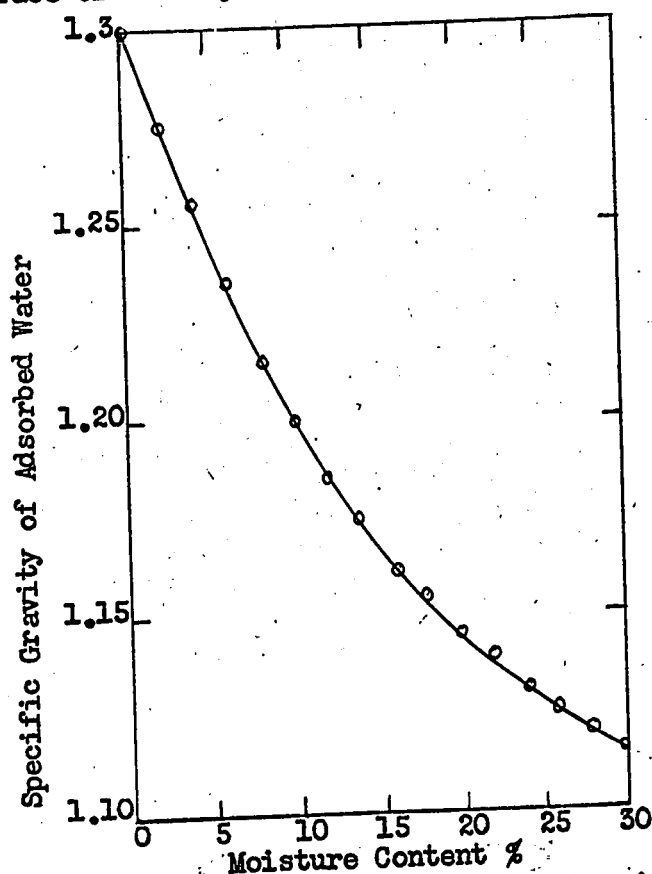
Fig. 6.2 — Specific gravity of adsorbed water in wood vs. moisture content.

the amorphous regions between the crystallites. The water is most likely adsorbed as little spheres ranging in curvature from .2 x 10^{-7} cm to 20 x 10^{-7} cm. Stamm shows a curve of radius of curvature of the adsorbed water vs. the fractional water volume in the cell wall. These values are calculated from Kelvin's capillary equation** and sorption isotherms for the wood[17].

* Stamm — ref. 17, p. 48
** Stamm — p. 390

Table 6.1 - Air and Water Volumes at Different Moisture Contents
and Specific Gravities

% Moisture Content	% Water Volume	% Air Volume	Specific Gravity
0	0	62.7	.475
5	2.14	61.4	
10	4.32	60.1	
15	6.52	58.7	
20	8.69	57.3	
25	10.8	56.0	
30	12.8	54.7	
0	0	64.9	.45
5	2.01	63.7	
10	4.07	62.4	
15	6.15	61.0	
20	8.21	59.7	
25	10.2	58.3	
30	12.1	57.1	
0	0	67.1	.425
5	1.89	65.9	
10	3.83	64.6	
15	5.79	63.3	
20	7.74	62.0	
25	9.63	60.7	
30	11.4	59.5	
0	0	69.3	.4
5	1.76	68.1	
10	3.58	66.9	
15	5.43	65.6	
20	7.26	64.3	
25	9.05	63.0	
30	10.8	61.8	
0	0	71.4	.375
5	1.64	70.3	
10	3.34	69.1	
15	5.07	67.9	
20	6.79	66.6	
25	8.48	65.4	
30	10.1	64.2	
0	0	73.5	.35
5	1.53	72.5	
10	3.11	71.3	
15	4.72	70.1	
20	6.33	68.9	
25	7.9	67.7	
30	9.41	66.6	
0	0	77.6	.3
5	1.29	76.7	
10	2.64	75.6	
15	4.01	74.6	
20	5.4	73.5	
25	6.76	72.4	
30	8.06	71.4	

It is also known that adsorbed water in wood is compressed to a considerable extent. The specific gravity of this bound water ranges from 1.3 at 0 moisture content to 1.115 at the fiber saturation point. MacLean[22] gives a curve of the specific gravity of adsorbed water vs. moisture content. A least squares fit to the data given by MacLean results in a quadratic function given by, (see Fig. 6.2),

$$\rho_w = 1.297 - 1.104(MC) + 1.0966(MC)^2 \qquad (6.1)$$

where ρ_w is the density of the adsorbed water and MC is the percentage moisture content. RMS deviation from the given data was less than .4%. MacLean[22] and Stamm[17] also give formulas for the determination of the void volume and the specific gravity of wood as functions of moisture content. These relations are repeated here for convenience. The fractional void volume of wood can be calculated from equation (6.2)

$$V_a = 1 - S\left(\frac{1}{1.46} + \frac{MC}{100\rho_w} + \frac{M_a}{100}\right) \qquad (6.2)$$

where M_a is the moisture content above fiber saturation, ρ_w is the density of the water, S is the specific gravity of the wood at a given moisture content, based on S_g, the specific gravity of wood when green. The equation for S is

$$S = S_g/\left[1 - .009 S_g (30 - MC)\right] \qquad (6.3)$$

Finally the fractional volume of water is given as

$$V_w = \frac{MC \times S}{100\, \rho_w} \qquad (6.4)$$

In the adsorption range of wood, roughly 0-30% M.C., the cell walls swell as a result of the water taken up. The total void volume, however, remains relatively constant, see table 6.1, and the fiber cavities are filled with air only.

Sizes of capillaries and crystallites can be found in the literature[17].

From X-ray diffraction studies the crystalline units in the cellulose, referred to as crystallites, have an estimated length of 800 A°, or 8×10^{-6} cm, and an average cross section of about 50 by 100 A°. An amorphous sheath, believed to exist around each crystallite*, has an estimated wall thickness of about 25 A°. The average fiber length for both Douglas Fir and Western Hemlock is 3.15 mm.** Fibers tend to be rectangular in cross section and the average fiber and fiber cavity width is about 33.3×10^{-4} cm and 26.2×10^{-4} cm respectively, giving a fiber wall thickness of about 7.1×10^{-4} cm†. The cell walls have a void volume less than 2%. These are the important dimensions necessary to predict the dielectric properties of the wood mixture from its component structure.

On basis of the foregoing discussion it is reasonable to assume that the cell walls can be treated as a homogeneous solid solution of cell wall material and small spheres or ellipsoids of adsorbed water, case I. Equally, one can postulate that the crystallites, impermeable to water, are surrounded by an almost continuous cylindrical or ellipsoidal sheath of adsorbed water, case II. Both of these configurations will be treated in the following analysis.

At moisture contents above the fiber saturation point, condensed water in the capillary structure will have to be accounted for. There is evidence†† that condensation occurs in pit membranes on the cell walls at relative vapor

---

*   Stamm – p.30
** Stamm – p.405
†   Stamm – p.388
†† Stamm – p.144

pressures as low as 0.9 ($\approx$ 20% M.C.). Initial condensation of water in the pit membranes probably consists of small spherical droplets. Above 30% the water condensed in fiber cavities will assume an ellipsoidal shape and the shape of the air inclusions in the cavities will change from ellipsoidal to circular as more water condenses in the capillaries. Unfortunately, it is difficult to predict how much air is held as spherical inclusions and how much is held in ellipsoidal inclusions.

Case I.

A. MIXTURE DESCRIPTION

It is assumed that the soft wood cell wall material is a mixture of randomly oriented small spherical water inclusions dispersed in a continuous medium consisting of the basic wood substance. Within this host medium, there are ordered ellipsoidal air cavities. Using the relations given in chapter 2, it is possible to set down one equation describing the mixture dielectric constant of the 3-phase mixture in terms of its component dielectric constants up to the fiber saturation point of softwoods. The ordered nature of the air cavities will introduce anisotropy into the mixture as a whole. Eventhough the basic cellulose structure has considerable anisotropy itself, the cell wall structure is such that the cellulose fibers must be considered as randomly oriented and not as ordered units. Hence, the anisotropy of the mixture due to the cellulose fibers is assumed negligible.[5]

The total air volume below fiber saturation is greater than 50% of the mixture volume for specific gravities of .4 or less. However, the interaction effects between the large number of air cavities are offset by the electrostatic shielding effect of the high dielectric constant of

the cell-wall mixture.

B. DIELECTRIC PROPERTIES OF THE MIXTURE COMPONENTS.

Wood cell substance consists basically of cellulose and Lignin, along with very small quantities of extractives. Careful measurements were made by Trapp and Pungs[6] on the dielectric properties of cellulose and Lignin, as well as on the air-free cell substance. They gave the dielectric constant of these three materials as a function of frequency. The low and high frequency dielectric constant as well as the relaxation time of the cell substance are estimated from their data as 6.6, 2, and 2×10^7 sec respectively at $20°C$. Similarly, for water the low and high frequency dielectric constants are given by Hasted[51] as 80.36, 5.5, with a relaxation time of $.923 \times 10^{11}$ sec at $20°C$.

However, when water is molecularly bound to the host material, as is the case for wood below fiber saturation, the dielectric properties of the water can be considerably different from the pure liquid water values. Haggis, Hasted, and Buchanan[59] showed this quite clearly for water in solutions. Windle and Shaw[26] actually calculated a value for the dielectric constant of localized and mobile* water in wool-water systems from their experimental data. The latter authors assume two states of adsorbed water whereas experimental evidence presented in this thesis, see for example Fig. 5.26, and arguments given by McLaren and Rowen[65] in their review paper on water sorption shows that mobile

---

* Localized water refers to that water which is attached directly to polar groups in the host material giving rise to high activation energies of polarization. Mobile water refers to that water which is indirectly attached to the mixture through other molecules, hence, having lower activation energies of polarization.

water likely has dielectric properties varying continuously between the properties of localized water and liquid water.

The dielectric constants of bound water are not adequately known nor readily calculated. By combining the experimental data on Douglas Fir as given in chapter 5 and the mixture relations developed in chapter 2, it is possible to determine semi-empirical estimates for the dielectric constant of adsorbed water as a function of moisture content.

C. ACTUAL MIXTURE RELATIONS USED FOR CASE I.

Under the assumptions of section A a 3-phase mixture relation is to be found for ordered ellipsoidal air cavities and random spheres of water dispersed in a homogeneous cell wall material as shown in Fig. 6.3. The internal field for the water spheres can be found from equation (2.66) averaged over all orientations using $n=\frac{1}{3}$ with $\varepsilon_1 = \varepsilon_w^*$, $\varepsilon_2 = \varepsilon_w$ gives

$$(6.5)$$

$$T_w = \frac{E_w}{E_{av}} = 3\varepsilon_w^* / 2\varepsilon_w^* + \varepsilon_w$$

where ε_w is the dielectric constant of the adsorbed water and ε_w^* is the effective dielectric constant of the material surrounding the water inclusions. For the air inclusions equation (2.66) is used again with $\varepsilon_1 = \varepsilon_a^*$, $\varepsilon_2 = \varepsilon_a$ which yields

$$T_a = \varepsilon_a^* \left[\varepsilon_a^* + n_a(\varepsilon_a - \varepsilon_a^*) \right]^{-1} \qquad (6.6)$$

where ε_a is the dielectric constant of air, ε_a^* is the effective dielectric constant of the material surrounding the air inclusions.

Substitution of equations (6.5) and (6.6) into (2.22), using $\varepsilon_h = \varepsilon_c$ gives the 3-phase mixture relation

$$\mathcal{E}_m - \mathcal{E}_c = \frac{V_a(\mathcal{E}_a - \mathcal{E}_c)\mathcal{E}_a^*}{\mathcal{E}_a^* + n_a(\mathcal{E}_a - \mathcal{E}_a^*)} + 3V_w \frac{(\mathcal{E}_w - \mathcal{E}_c)\mathcal{E}_w^*}{2\mathcal{E}_w^* + \mathcal{E}_w} \qquad (6.7)$$

where $\mathcal{E}_m$ is the mixture dielectric constant, $\mathcal{E}_c$ is the dielectric constant of the dry cell wall material, V_a and V_w are the fractional volume filling factors of the air and water respectively.
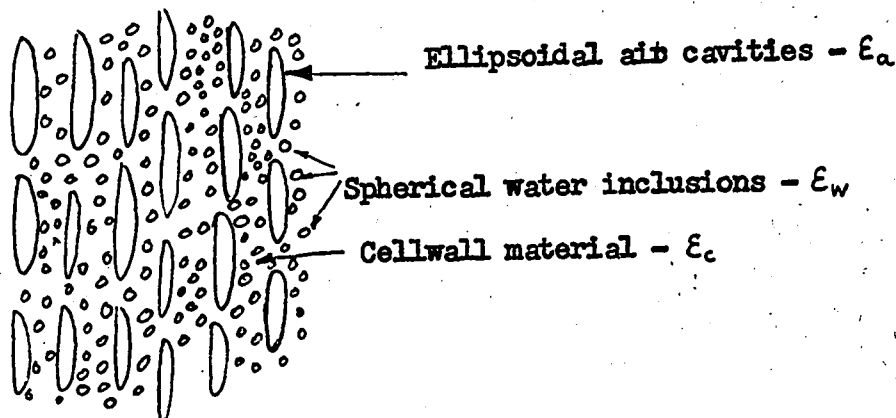
Fig. 6.3 - Cellulose-air-water mixture.

The maximum and minimum values that $\mathcal{E}_w^*$ and $\mathcal{E}_a^*$ can have lie between the maximum and minimum values of $\mathcal{E}_m$ and $\mathcal{E}_c$. In the following results it has been assumed that $\mathcal{E}_w^* = \mathcal{E}_a^* = \mathcal{E}_m$ since the lower limit given by $\mathcal{E}_c$ gives dielectric constants far below the experimental values. From the fiber cavity dimensions for softwoods it is found that in the direction of the major axis of the air inclusions $n=0$ and in the other two directions $n=\frac{1}{2}$. The standard formula for depolarization coefficients was used to obtain these values (see equation (2.50) and also reference 2). Assuming a specific gravity of .400, V_a and V_w can be found from Table 6.1. The dielectric constant of the cellwall material is taken from Trapp and Pungs' data as $\mathcal{E}_c = 3.5 - j.012$ at 2450 MHz. Different values for $\mathcal{E}_w$ are used in the following results to indicate the fact that the adsorbed water behaves different than pure liquid water. Plots of the dielectric

constant and dielectric loss versus moisture content at 20°C are given in figures 6.4 and 6.5 under the assumption of spherical water inclusions. Experimental data, taken from figures 5.13 and 5.14 are given for comparison and are tabulated for convenience in Table 6.2.

TABLE 6.2 - Experimental values of the dielectric constant of long-itudinal Douglas Fir at 20 C and 2450 MHz (s.g. = .4).

Moisture Content, %	ε'	ε''
0	1.78	.04
5	2.14	.14
10	2.5	.325
15	2.9	.58
20	3.6	.86
25	4.35	1.16
30	5.15	1.46

The parameter in figures 6.4 and 6.5 is the dielectric constant of the included water. Using the value for pure liquid water[23] gives a complex dielectric constant which falls far below the experimental data. Similarly the value for mobile water calculated by Windle and Shaw[26], namely $\varepsilon_w = 60-j\ 12.5$ gives values much lower than the experimental. Even values of the dielectric constant of adsorbed water as determined semi-empirically in the following section give values which are low. The only remaining cause for the discrepancy is that the assumed model for the mixture is wrong. Since the air inclusions are known to be ellipsoidal in shape from microscope studies, the assumed shape of the water inclusions must be the cause of the disagreement. It can further be stated that the shape of the water inclusions must be such as to give rise to a very small reaction or depolarization field to cause the required increase in dielectric constant, for example, ellipsoids or ellipsoidal shells.
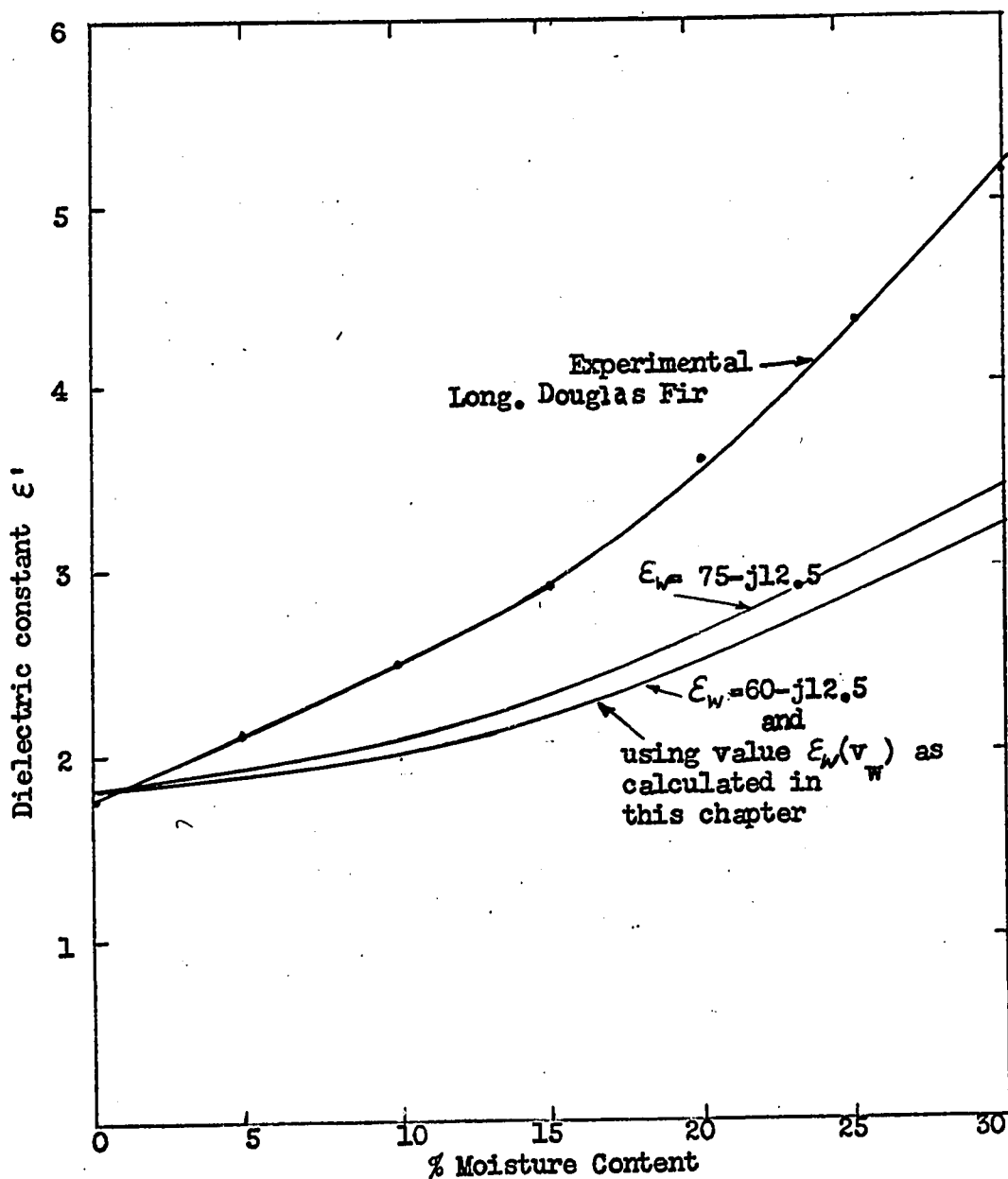
Fig. 6.4 - Theoretical dielectric constant of a softwood
mixture versus moisture content with the dielectric
constant of included water as a parameter; E-field
in the longitudinal grain direction at 2450 MHz for
a s.g. of .4; spherical water inclusions.
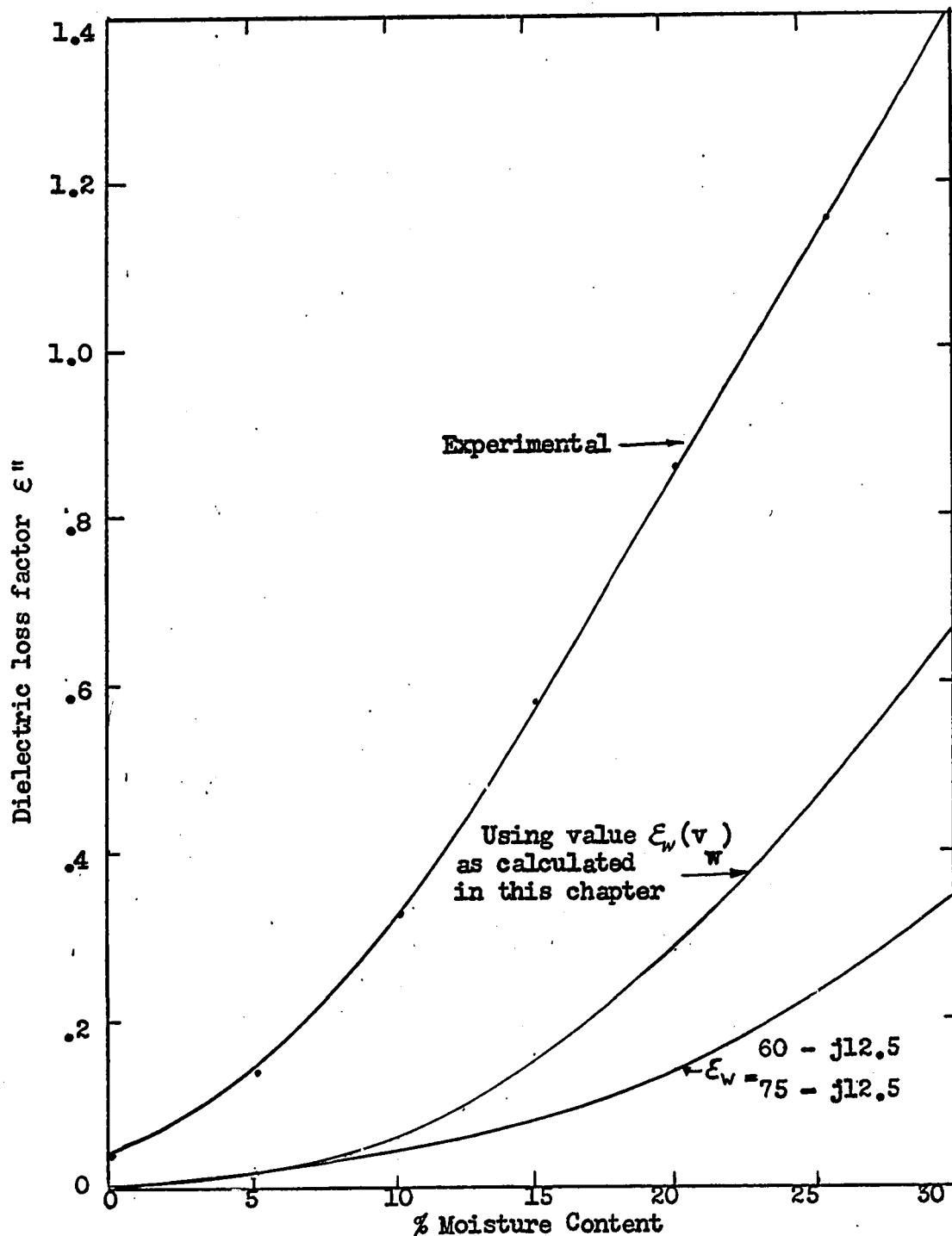
Fig. 6.5 - Theoretical dielectric loss of a softwood mixture
versus moisture content with the dielectric constant
of adsorbed water as a parameter; E-field in the
longitudinal grain direction at 2450 MHz for a
s.g. of .4; spherical water inclusions.

Case II.

A. MIXTURE DESCRIPTION

In this case it is assumed that the included water occurs in the form of ellipsoidal shells and the mixture further contains ordered air cavities as in Case I. The arguments regarding anisotropy, localized and mobile water for Case I apply equally well here and will not be repeated. The mixture model used here is depicted in figure 6.6.
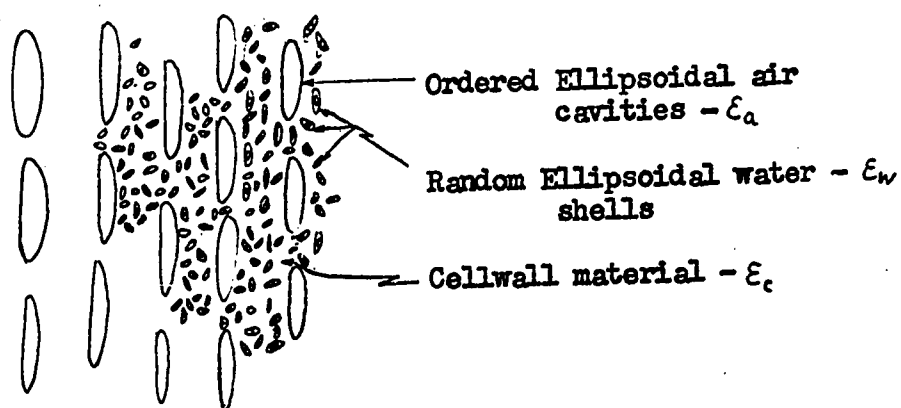
Fig. 6.6 - Cellulose-air-water mixture; Case II.

B. MIXTURE RELATIONS USED IN CASE II.

In a manner very similar to that given under Case I, the appropriate internal fields are given by equations (2.65) and (2.66) for the water and air inclusions respectively. Substitution of these internal field expressions for $\overline{T}_i$ in equation (2.22) then gives the final equation for this 3-phase mixture.

$$\varepsilon_m - \varepsilon_h = \frac{v_a (\varepsilon_a - \varepsilon_h) \varepsilon_a^*}{\varepsilon_a^* + n_a(\varepsilon_a - \varepsilon_a^*)} +$$

$$+ \frac{v_w(\varepsilon_w - \varepsilon_h)}{3} \sum_{i=1}^{3} \frac{\varepsilon_i \left[\varepsilon_2 + \frac{\varepsilon_3 - \varepsilon_2}{2} \left(n_w^{i\prime} - n_w^i \frac{V'}{V} \right) \right]}{\left\{ \left[\varepsilon_2 + (\varepsilon_2 - \varepsilon_3)(n_w^i \frac{V'}{V} - n_w^{i\prime}) \right] \left[\varepsilon_1 + n_w^i(\varepsilon_2 - \varepsilon_1) \right] - n_w^i \frac{V'}{V} \varepsilon_2(\varepsilon_2 - \varepsilon_3) \right\}} \quad (6.8)$$

where ε_a and ε_a^* are the dielectric constants of air and of the material surrounding the air inclusions, n_a is the depolarization coefficient for the air cavities which is $n_a = 0$ when the E-field is applied in the direction of the major axis. The second term concerns the random water inclusions. It is assumed that the material in region three, the inner ellipsoid is that of the dry cell wall $(\varepsilon_3 = \varepsilon_c)$, the material in region 1 is assumed to have a dielectric constant equal to that of the complete mixture, i.e., $\varepsilon_1 = \varepsilon_m$ and ε_2 is the dielectric constant of the adsorbed water $(\varepsilon_2 = \varepsilon_w)$. The host material has a dielectric constant equal to that of the dry cell wall $(\varepsilon_h = \varepsilon_c)$ and the depolarization coefficients n_w and n_w' are defined by equations (2.50) and (2.52) respectively. These coeficients can be calculated using the dimensions of the shell structure.

As indicated in the beginning of this chapter, little is known about the exact sizes of the amorphous and crystallite regions. n_w and n_w' are based on the approximate amorphous sheath dimensions given earlier in this chapter, namely, the axes a, b and c of the outer ellipsoid are approximately, 425, 50, 75 Å and for the inner ellipsoid a', b' and c' are 400, 25, and 50 Å[*] respectively.

These values were substituted into equation (6.8) which was then solved numerically for two different values of the dielectric constant of the adsorbed water. The results are presented in figure 6.7. Experimental values for the dielectric constant of

[*] It turns out that the depolarization coefficients along the major axis are nearly equal to zero and along the two minor axes are approximately equal to $\frac{1}{2}$.
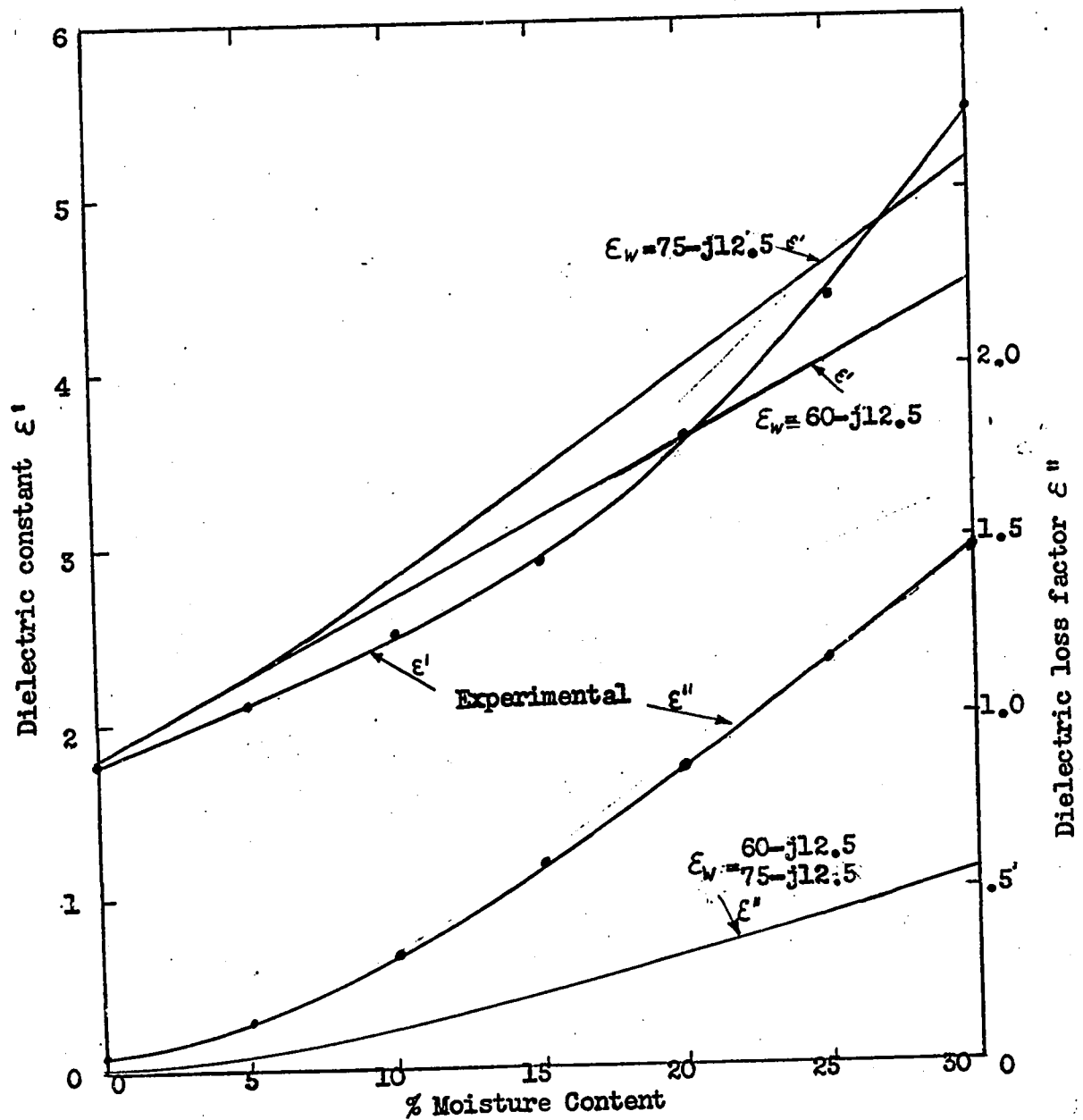
Fig. 6.7 — Complex dielectric constant of a cellulose-air-water mixture versus moisture content, assuming ellipsoidal shell water inclusions with experimental data for longitudinal Douglas Fir given for comparison; $f = 2450$ MHz, s.g.$=.400$, T$=20°C$.

longitudinal Douglas Fir are given for comparison. It is observed that the calculated dielectric loss is too low and the real part of the dielectric constant is too high at low moisture contents compared to the experimental data.

One probable reason for the disagreement with the mixture models given so far is that the assumed dielectric constant of the adsorbed water is incorrect. To resolve this question an estimate of the bound water dielectric constant was obtained by the following procedure. The wood is assumed to consist of a homogeneous host material of dielectric constant ε_{m_1} in which ellipsoidal air cavities are included.[*] Since the depolarization coefficient for the air cavities is nearly equal to zero along the major axis, it is found that equation (2.66) substituted into (2.22) simplifies to

$$\varepsilon_m = \varepsilon_{m_1} + V_a(\varepsilon_a - \varepsilon_{m_1})$$

Hence, the dielectric constant of the 'cellulose-water' host material is given by

(6.9)

$$\varepsilon_{m_1} = \frac{\varepsilon_m - V_a \varepsilon_a}{1 - V_a}$$

A plot of equation (6.9) is given in fig. 6.8. The dielectric constant ε_{m_1} thus obtained is the value for a mixture of water inclusions in the basic cell wall material. The value of ε_c the cell wall material is about 3.5 −j.012 and the dielectric constant of the adsorbed water, can be assumed to be considerably greater than the value

_____

[*] Since the water inclusions are orders of magnitude smaller than the air cavities below fiber saturation, this assumption is valid.
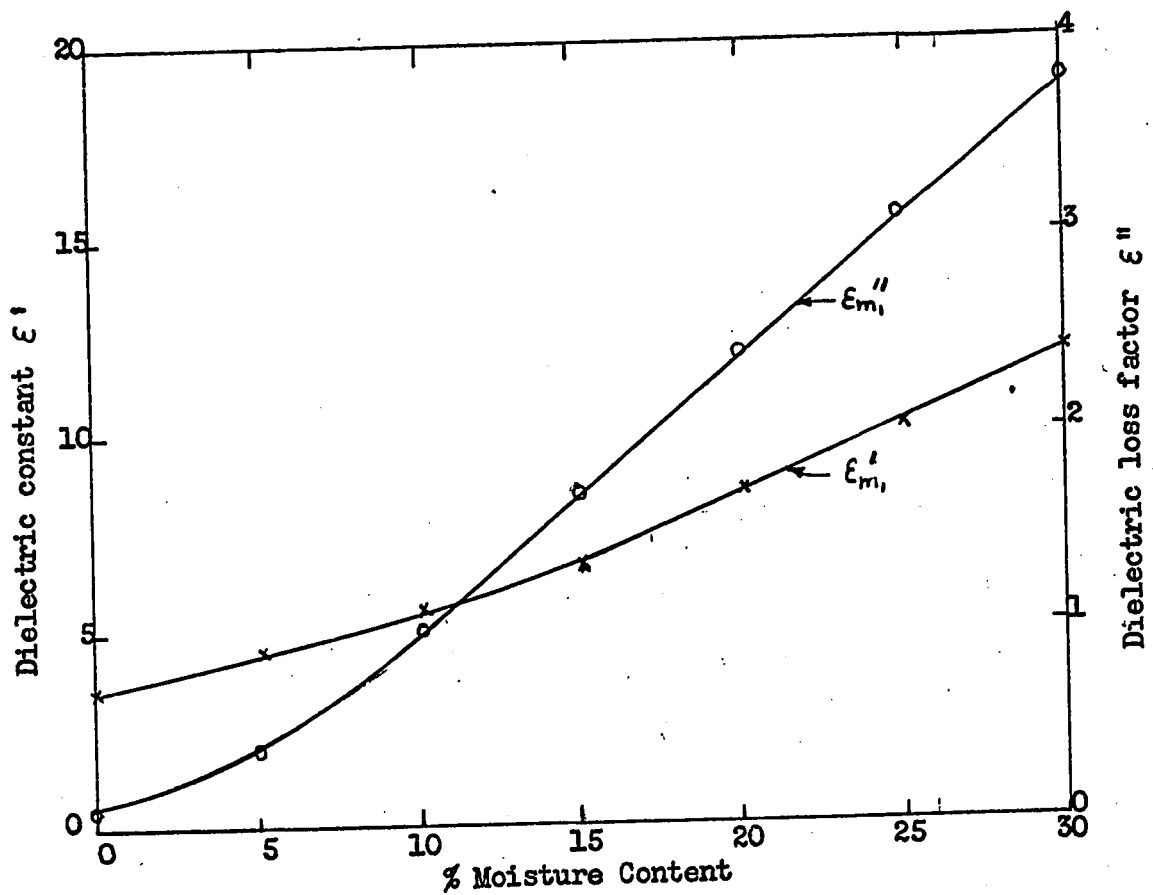
Fig. 6.8 — Dielectric constant of the cell wall water mixture with no air inclusions, versus moisture content, calculated from equation (6.9) using the experimental dielectric constant of Douglas Fir from Table 6.2; $f = 2450$ MHz, s.g.$= .400$, $T=20°C$.

of ε_c. The final results will show this assumption to be valid, hence, $\varepsilon_c \ll \varepsilon_w$. To simplify the calculation, the water is assumed to be in the form of thin ellipsoidal shells so that $n_w = n_w'$ and $V = V'$ [*]. Under these conditions, equation (6.8), remembering $V_a = 0$, and ε_m is now ε_{m_1}, simplifies and when solved for the dielectric constant of the adsorbed water gives

$$\varepsilon_w \simeq \frac{\varepsilon_{m_1} - \varepsilon_c (1-V_w)}{V_w} \qquad (6.10)$$

where ε_{m_1} is given by equation (6.9).

The numerical results for this approximation to the bound water dielectric constant are presented graphically in figure 6.9. It is clear that the adsorbed water behaves differently than pure water. Windle and Shaw's value for ε_w, 60-j 12.5 at 3 GHz seems to agree reasonably with the values calculated here. However, the dielectric loss of the adsorbed water as given here is a lot higher than theirs. If now the values of ε_w from figure 6.9 are used in equation (6.8) to calculate the total mixture dielectric constant, assuming the amorphous sheath model again, it is found that agreement between the experimental and theoretical values is very good, indicating that the approximations made in deriving equation 6.10 were reasonable. Figure 6.10 shows the resultant theoretical and experimental curves as a function of moisture content.

The calculation is repeated with $n_a = \frac{1}{2}$ and the result plotted in

---

[*] This may seem to be a crude approximation, but it is shown to give reasonable results and the errors due to the approximation can be shown to be about 25%.
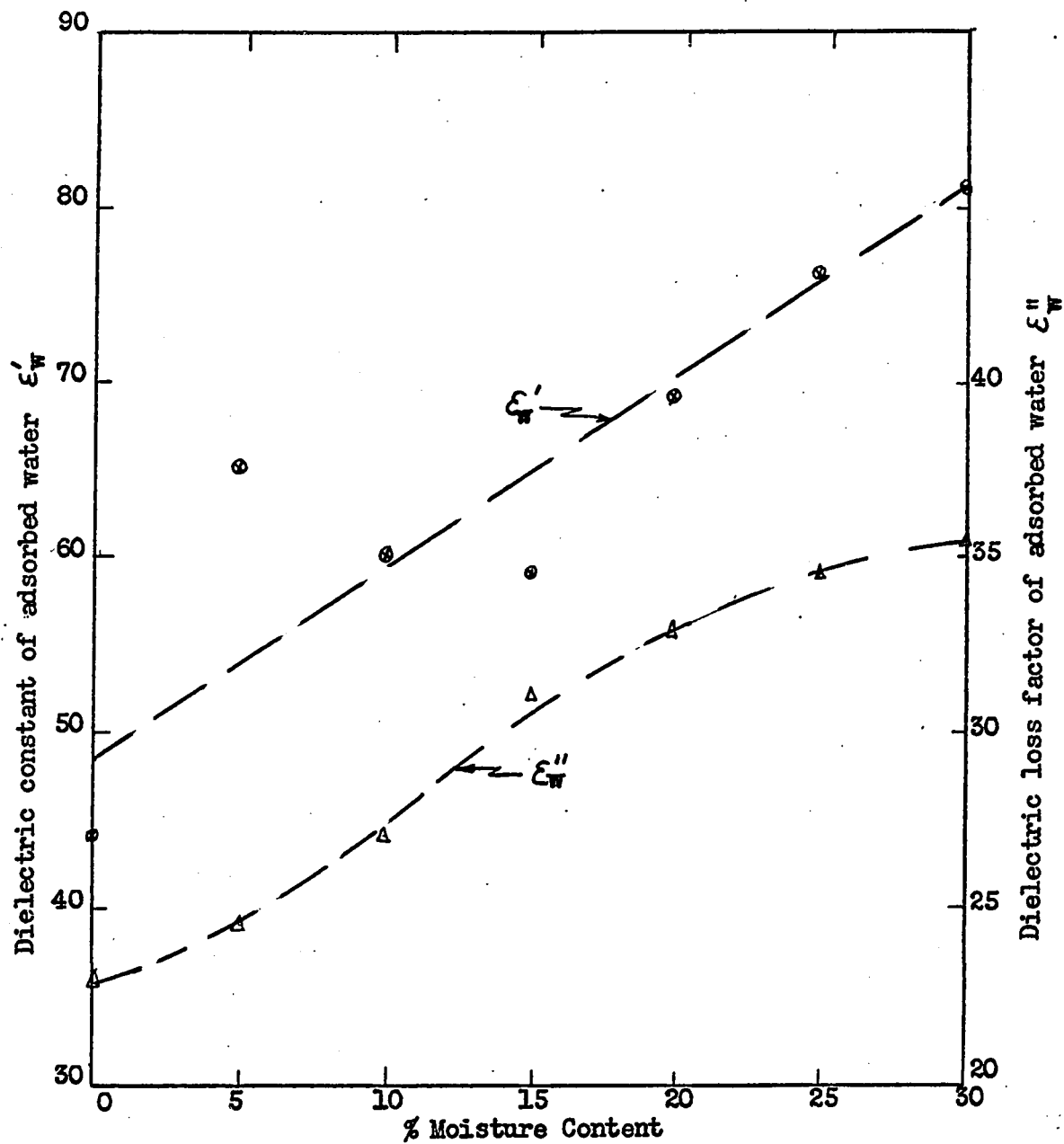
Fig. 6.9 — Approximate value for the dielectric constant of
adsorbed water versus moisture content based on
equation (6.10) assuming random thin shell inclu-
sions; f = 2450 MHz, T=20°C.
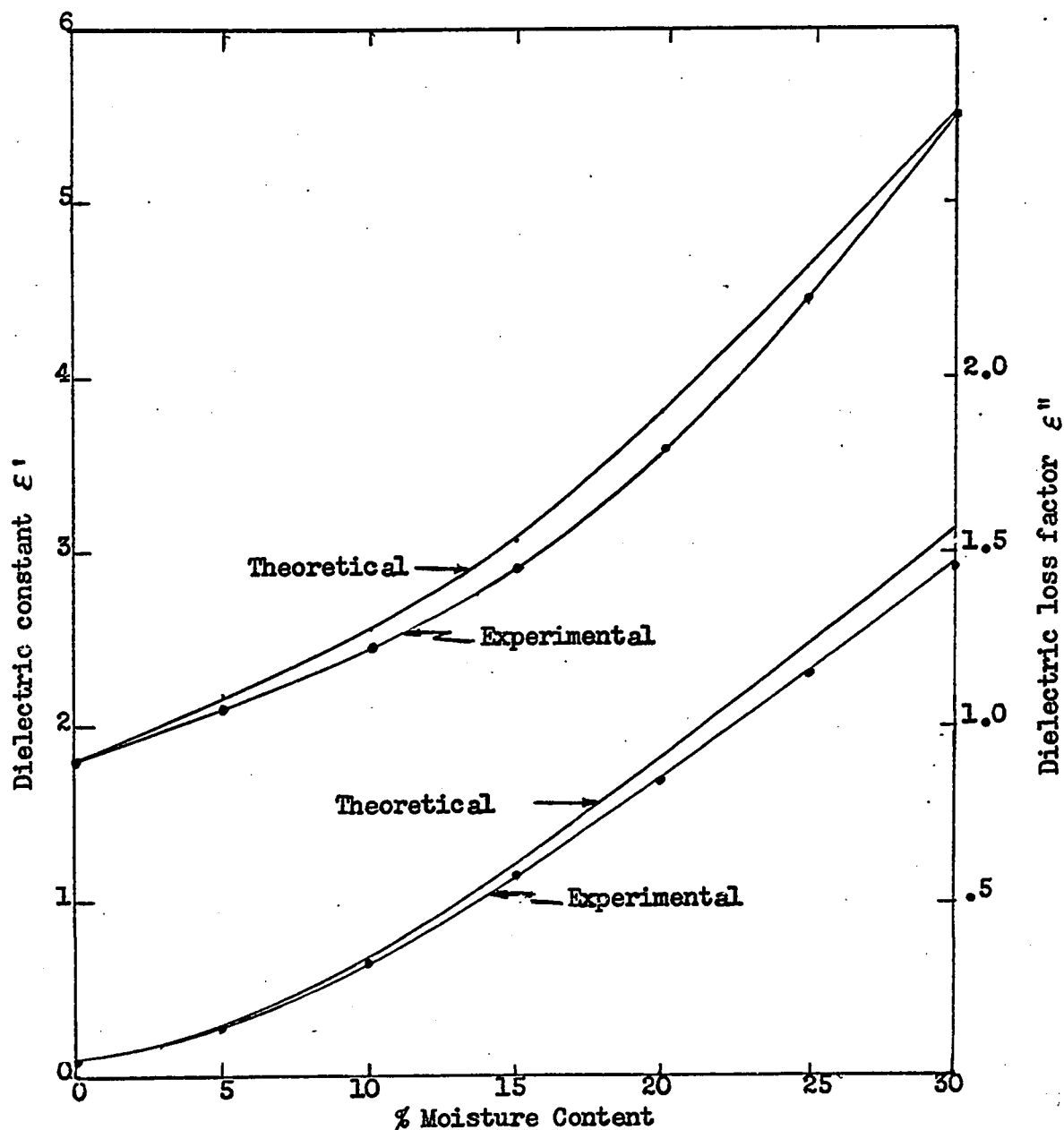
Fig. 6.10 — Theoretical and experimental plot of the dielectric
constant of Douglas Fir versus moisture content
with the E-field in the longitudinal grain direc-
tion using semi-empirical values for the adsorbed
water dielectric constant; Mixture model: ellip-
soidal water shells and ellipsoidal air cavities;
f= 2450 MHz, T=20°C., s.g.=.400.
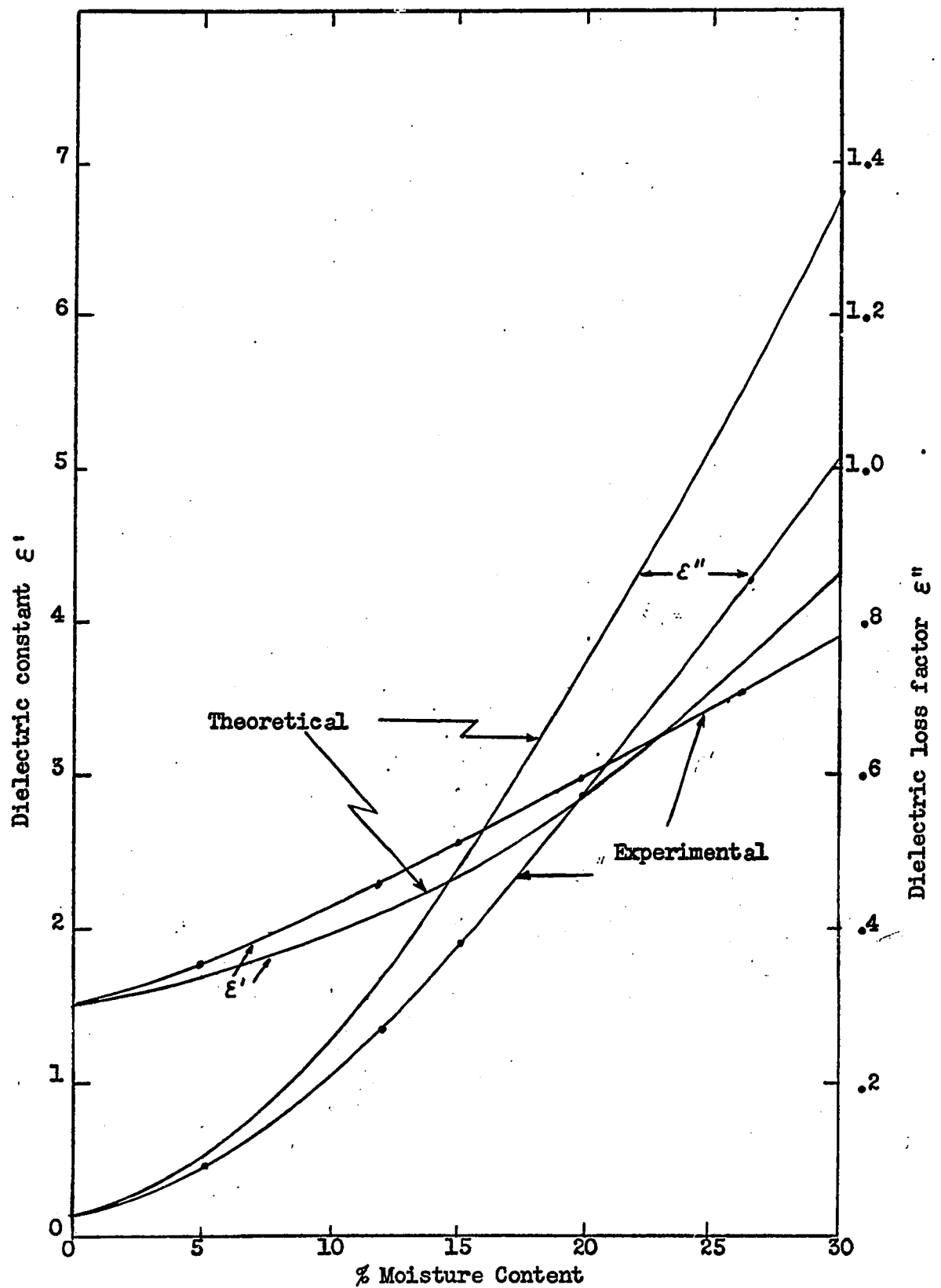
Fig. 6.11 — Theoretical and experimental dielectric constant
of Douglas Fir versus moisture content with E-field
in the tangential grain direction; f = 2450 MHz,
s.g.=.400, T=20°C.

figure 6.11. This plot thus gives the dielectric constant in the radial or tangential direction since the depolarization coefficients were assumed equal along the two minor axes. For comparison the experimental values for tangential Douglas Fir, given in chapter 5, are superimposed and the agreement is fair. Therefore, the assumption that the anisotropy of wood is mainly due to the ordered nature of the air cavities is shown to be reasonable also.

Finally the static and high frequency dielectric constants can be calculated by substituting the corresponding low and high frequency component dielectric constants (found under case I section B in this chapter) into equation (6.8). Figure 6.12 shows that here also reasonable agreement between theoretical and experimental values is found.

It can thus be concluded that the cellulose-air-water mixture as found in wood is adequately described by the amorphous sheath approximation. Since the sheath's dimensions are only approximately known the results could be improved by a better understanding and description of the actual crystalline - amorphous structure of the cell-wall material. The estimate of the bound water dielectric constant found here should be a useful tool in the analysis of other structures containing adsorbed water. More detailed description of the geometry is essential for further improvement in the values given here.

Thus, the complicated wood mixture analyzed in this thesis can
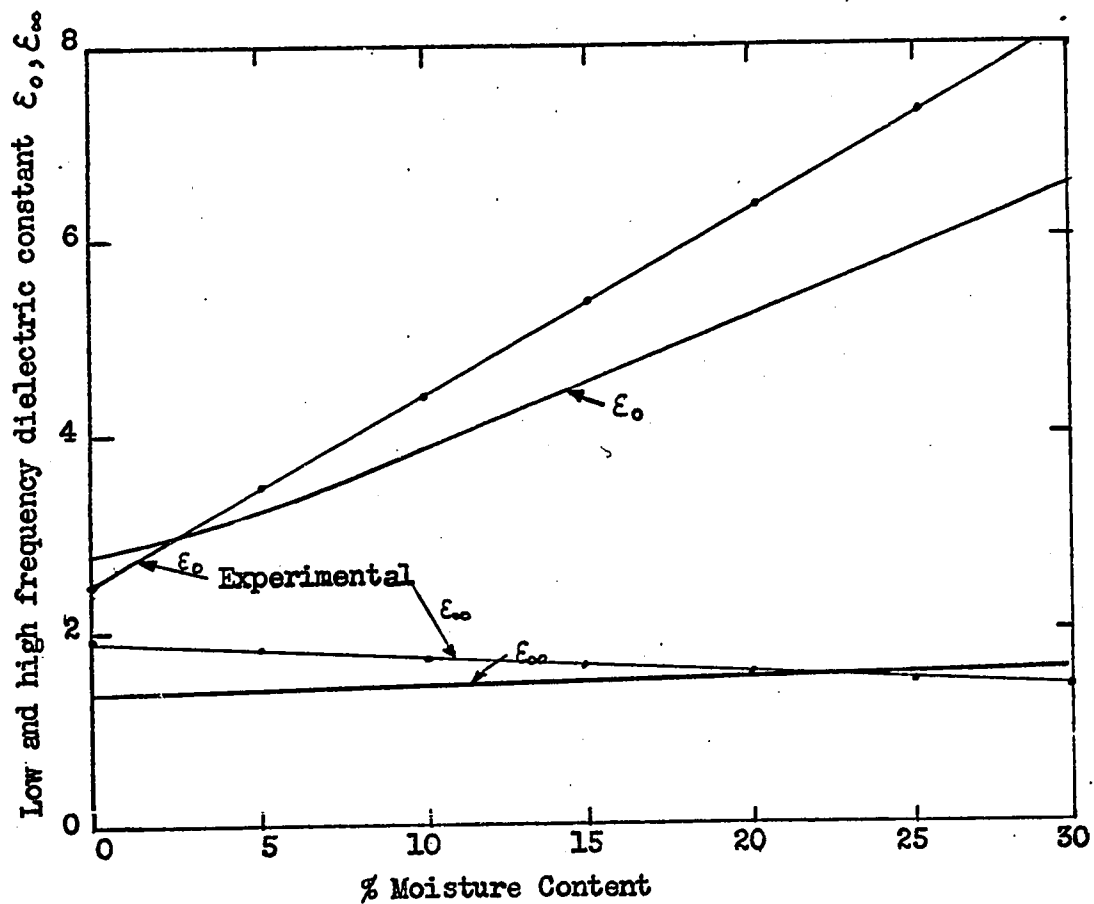
Fig. 6.12 — Theoretical and experimental low and high frequency
dielectric constants versus moisture content for
Douglas Fir with E-field in the longitudinal grain
direction; f = 2450 MHz, s.g.=.400, T=20°C.

adequately be described by the new mixture relation using the shell inclusions and the semi-empirical values of the bound water dielectric constant as calculated in this chapter. Previous mixture relations were unable to describe the wood mixture satisfactorily as a function of moisture content.

CHAPTER 7

CONCLUSION

A multiphase dielectric mixture theory is presented which allows analysis of ellipsoidal shell inclusions. The mixture equations developed by others for ellipsoidal and spherical inclusions are shown to be a subset of the more general solution presented in this thesis. Examples of shell-type inclusions can be found in natural materials such as brick and wood. The latter case is analyzed by means of the mixture theory given here and the results indicate that the model chosen for the mixture is reasonable. Dielectric properties for adsorbed water are determined semi-empirically from experimental Douglas Fir data which indicate that adsorbed water behaves very differently than pure liquid water. The numerical values given here for the bound water dielectric constant are only crude estimates since the results depend very heavily on the mixture model chosen for wood. This model is not necessarily exact because relatively little is known about the way water is held in the cell walls.

Behavior of mixed dielectrics as a function of temperature and moisture content is analyzed under the assumption that distributions of relaxation times exist for many multiphase mixtures. Experimental data on Douglas Fir and Western Hemlock confirm the theory to better than ± 10%. As a result it is possible to describe the dielectric properties of wood as a function of moisture content, temperature and frequency knowing only the activation energy of polarization and

the static and high frequency dielectric constant of the material as a function of moisture content. If easier methods of measurement could be found to determine these three parameters, it would greatly facilitate the acquisition of dielectric data yet needed for many materials.

It is evident from the experimental method chosen for this work and the material under test that acquiring enough data to adequately describe the dielectric properties is a laborious and time consuming process. Nevertheless, the data obtained in this manner allow a good description of a rather wide class of cellulose containing materials. The basic accuracy of the measurement technique used is extremely good, but if all possible variations due to the material, control and readout devices used are taken into account the overall accuracy of the measurement deteriorates to $\pm$ 10%.

Methods described and data obtained in this work can be used to advantage in the description of microwave heating and drying processes. From the results on wood it is possible to select optimum operating frequencies and temperatures for such processes. Applying the results to control instrumentation design allows one to select a frequency which minimizes calibration problems, by which present instruments, for example, moisture meters are plagued. To adequately design processing systems and accompanying instrumentation requires a thorough knowledge of the materials to be treated.

This work has laid the basis for a better understanding of the

properties of adsorbed water and the way in which it occurs in cellulose materials. Electron microscope and X-ray diffraction studies coupled with more detailed dielectric measurements will likely resolve the remaining uncertainties in the model of cellulose-air-water mixtures given here. Complexity of the resulting mathematics is greatly offset by modern computing facilities which extend the research power of a scientist by orders of magnitude.

APPENDIX A

ERROR ANALYSIS

In this section, the basic equations determining the errors in the dielectric constant are worked out and some useful approximations are stated. The results are applied to the dielectric measurement techniques used in Chapter 4.

Let the dependent variable, E, and the independent variable, V, be related by

$$E = f(V) \qquad\qquad A(1)$$

E and V are any two variables and have no other significance. Let ΔE be the increment in E due to an incremental change, ΔV, in V. Then by definition of the derivative,

$$\operatorname*{Lim}_{\Delta V \to 0} \Delta E/\Delta V = dE/dV \qquad\qquad A(2)$$

When ΔV is very small

$$\Delta E \simeq (dE/dV)\,\Delta V \qquad\qquad A(3)$$

However, the exact expression for ΔE can be obtained by a Taylor series expansion of equation A(2)[36]. Thus

$$\Delta E = f(V + \Delta V) - f(V) \qquad\qquad A(4)$$

hence,

$$\Delta E = f'(V)\,\Delta V + f^2(V)(\Delta V)^2/2! +$$
$$+ f^3(V)(\Delta V)^3/3! + \cdots \qquad \text{A (5)}$$

Where $f'(V), f^2(V)$, etc., designate the first, second and higher order derivatives of f w.r.t. V. More generally, E can be a function of more than one variable, in other words, V can be a vector, V1, V2, ... Similarly, E itself can be a vector of dependent variables, E1, E2, ..., in which case the functional relationship can be written as,

$$E1 = f_1(V1, V2, \cdots)$$
$$E2 = f_2(V1, V2, \cdots) \qquad \text{A (6)}$$
$$\vdots$$

Writing the incremental changes in E due to incremental changes in V by using a Taylor series expansion for n independent variables, equation A(6) becomes,

$$\Delta E1 = f'_{1_{V1}}\Delta V1 + f'_{1_{V2}}\Delta V2 + \cdots + \left\{ f^2_{1_{V1V1}}(\Delta V1)^2 + f^2_{1_{V1V2}}\Delta V1\,\Delta V2 + \cdots \right\} + \cdots$$

$$\text{A (7)}$$

$$\Delta E2 = f'_{2_{V1}}\Delta V1 + f'_{2_{V2}}\Delta V2 + \cdots + \left\{ f^2_{2_{V1V1}}(\Delta V1)^2 + f^2_{2_{V1V2}}\Delta V1\,\Delta V2 + \cdots \right\} + \cdots$$
$$\vdots$$

Where

$$f'_{1_{V1}} = \partial f_1 / \partial V1$$

and so on.

If $\Delta V1, \Delta V2, \ldots$ are small, as is usually the case, higher order terms can be neglected and hence A(7) can be rewritten as,

$$\Delta E1 \simeq f'_{1_{V1}}\Delta V1 + f'_{1_{V2}}\Delta V2 + f'_{1_{V3}}\Delta V3 + \cdots$$

$$\text{A (8)}$$

$$\Delta E2 \simeq f'_{2_{V1}}\Delta V1 + f'_{2_{V2}}\Delta V2 + f'_{2_{V3}}\Delta V3 + \cdots$$
$$\vdots$$

Equation A(7), therefore, gives the total change in the dependent variables, E1, E2, as a function of the change in the independent variables, V1, V2,...

In practice, equation A(8) becomes a very good approximation, and usually consists of just a few terms, since many of the derivatives will be zero and the increments are usually small.

Consider now a particular measurement technique, for example, the bridge method used in chapter 4 for measuring dielectric constants. The dependent variables are the real and imaginary parts of the dielectric constant, ε' and ε'' respectively. For the case of guided, fundamental mode, electromagnetic propagation, the functional relationships are given by equations A(9) and A(10)

$$\varepsilon' = p + (\lambda_0/2\pi)^2(\beta^2 - \alpha^2) \qquad \text{A(9)}$$
$$\varepsilon'' = 2(\lambda_0/2\pi)^2 \alpha\beta \qquad \text{A(10)}$$

where α and β, the two independent variables, are the attenuation and phase constants of the material, λ_0 is the free-space wavelength, and p is the ratio squared of the cutoff to signal frequency. By application of equation A(7) it is found that,

$$\Delta\varepsilon' = (\partial\varepsilon'/\partial\beta)\Delta\beta + (\partial\varepsilon'/\partial\alpha)\Delta\alpha + \\ + \{(\partial^2\varepsilon'/\partial\beta^2)(\Delta\beta)^2 + (\partial^2\varepsilon'/\partial\alpha^2)(\Delta\alpha)^2\} \qquad \text{A(11)}$$
$$\Delta\varepsilon'' = (\partial\varepsilon''/\partial\beta)\Delta\beta + (\partial\varepsilon''/\partial\alpha)\Delta\alpha$$

since all other derivatives vanish. Evaluating the partials by using equations A(9) and A(10) and neglecting second order terms one obtains

$$\Delta\varepsilon' \simeq 2(\lambda/2\pi)^2(\beta\Delta\beta - \alpha\Delta\alpha) \qquad \text{A(12)}$$
$$\Delta\varepsilon'' \simeq 2(\lambda/2\pi)^2(\alpha\Delta\beta + \beta\Delta\alpha)$$

Thus, equation A(12) gives the error in dielectric constant directly in terms of the two variables α and β which in turn are to be determined experimentally.

Note that α and β are themselves functions of some signal amplitude, r, and phase angle, θ. For the bridge method under discussion here, these functional relationships are known and can be written as, see chapter 4,

$$\alpha = (1/2\ell)\cosh^{-1}\left\{(r^2/4)+\sqrt{(1-r^2/4)^2+r^2\sin^2\theta}\right\} \qquad A(13)$$

$$\beta = (1/2\ell)\cos^{-1}\left\{(r^2/4)-\sqrt{(1-r^2/4)^2+r^2\sin^2\theta}\right\} \qquad A(14)$$

where ℓ is the sample length, r is the amplitude ratio of the detected signal at two different positions, and θ is the phase angle between the two signals. By again using equation A(7) we can obtain the incremental change in α and β due to small changes in r and θ. Hence,

$$\Delta\beta = (\partial\beta/\partial r)\Delta r+(\partial\beta/\partial\theta)\Delta\theta +(1/2)\left\{(\partial^2\beta/\partial r^2)(\Delta r)^2+\right.$$
$$\left. +2(\partial^2\beta/\partial r\partial\theta)\Delta r\Delta\theta +(\partial^2\beta/\partial\theta^2)(\Delta\theta)^2\right\} \qquad A(15)$$

$$\Delta\alpha = (\partial\alpha/\partial r)\Delta r+(\partial\alpha/\partial\theta)\Delta\theta +(1/2)\left\{(\partial^2\alpha/\partial r^2)(\Delta r)^2+\right.$$
$$\left. +2(\partial^2\alpha/\partial r\partial\theta)\Delta r\Delta\theta +(\partial^2\alpha/\partial\theta^2)(\Delta\theta)^2\right\} \qquad A(16)$$

Again second and higher order terms can be neglected since Δr and $\Delta\theta$ are small if a reasonably good attenuator and phase shifter are used in the experiment.

Evaluating $\partial\alpha/\partial r$ from equation A(13) gives
$$\partial\alpha/\partial r = (1/2\ell)(\partial/\partial r)\cosh^{-1}\left\{(r^2/4)+\sqrt{(1-r^2/4)^2+r^2\sin^2\theta}\right\} \qquad A(17)$$

It can be shown, remembering that r is less than unity, that,

$$\qquad A(18)$$
$$\partial\alpha/\partial r \leq 1/\ell$$

and similarly,

$$\partial \beta / \partial r \leq -3/2\ell \qquad\qquad A(19)$$

$$\partial \alpha / \partial \theta \leq r/2\ell \qquad\qquad A(20)$$

$$\partial \beta / \partial \theta \leq -r/2\ell \qquad\qquad A(21)$$

Using these upper error limits in equations A(15) and A(16) yields

$$\Delta \beta \leq -(1/2\ell)(3\Delta r + \Delta \theta) \qquad\qquad A(22)$$

$$\Delta \alpha \leq (1/\ell)[\Delta r + (r/2)\Delta \theta]$$

If the experimental errors Δr and $\Delta \theta$ are known, then the error in ε' and ε'' can be computed by use of equation A(22) and A(13) for any value of α and β.

As an example, some typical values will be substituted in equation A(12). The resulting errors are indicative of the overall accuracy of this measurement technique.

The uncertainty in the attenuation measurement is ± .05db and the phase shift error is ± 2 degrees. Further for a loss tangent of 1, $r \leq .5$ for a half wavelength sample. For $\lambda = 12$cm, $\ell \leq 3cm$, $\beta \approx .5$, $\alpha \approx .4$. By definition, $r = Emin/Emax$, and $A = 20 \log_{10} r$. Thus, by equation A(3)

$$\Delta r = (r/8.686)\Delta A = \pm .0029$$
$$\Delta \theta = 2/360 = \pm .0056$$

Using equation A(22) the errors in β and α are

$$\Delta \beta \leq \pm .0024$$
$$\Delta \alpha \leq \pm .00143$$

Finally using equation A(12) the errors, due to variations in r and θ, at fixed temperature, moisture content, etc., are

$$\Delta \varepsilon' \leq \pm .022$$
$$\Delta \varepsilon'' \leq \pm .0123$$

For a dielectric constant of 2 and loss tangent of 1 the percentage errors in ε' and ε'' are less than ±1%. Similar calculations for a dielectric

constant of 2 and a loss tangent of .01 yields percentage errors in ε' and ε'' which are less than ± 0.1%.

For an error of .010" or .025 cm. in the measurement of ℓ the corresponding errors in ε' and ε'' are about ±1%. From experimental data the relationship between $\propto$ and temperature, T, was obtained and thus the errors in ε' and ε'' w.r.t. temperature were calculated. It was found that errors due to temperature variation were always less than ±1%.

BIBLIOGRAPHY

1. Korneenko, I. A., 'Mean Values of the Parameters in Inhomogeneous Media', Soviet Physics – Technical Physics, vol. 5, p.40, 1960.

2. Landau, L. D., Lifshitz, E. M., 'Electrodynamics of Continuous Media', Ch. 2, Pergamon Press, Addison Wesley Publishing Co. Inc., Reading, Mass., 1960.

3. Stratton, J. A., 'Electromagnetic Theory', Ch. 3, McGraw-Hill Book Co. Inc., 1941.

4. Batygin, V. V., Toptygin, I. N., 'Problems in Electrodynamics', Academic Press, New York, 1964.

5. Kroner, K., Pungs, L., 'Zur Dielektrischen Anisotropie des Naturholzes im grossen Frequenzbereich', Holzforschung vol. 10, no. 1, pp. 13-16, 1956. Also in: Abh.d.Br.Wiss. Ges. IV, 127 1952.

6. Trapp, W., Pungs, L., 'Bestimmung der Dielektrischen Werte Von Cellulose, Glukose, und der Zellsubstanz von Naturholz im Grossen Frequenzbereich', Holzforschung, vol. 10, no. 3, pp. 65-68, July 1956.

7. Trapp, W., Pungs, L., 'Einfluss von Temperatur und Feuchte auf das dielektrische Verhalten von Naturholz im grossen Frequenzbereich', Holzforschung, vol. 10, no. 5, pp. 144-150, 1956.

8. Taylor, L. S., 'Dielectric Properties of Mixtures', IEEE – TRANS. vol. AP-13, no. 6, pp. 943-947, Nov. 1965.

9. Taylor, L. S., 'Dielectrics Loaded with Anisotropic Materials', IEEE-TRANS. vol. AP-14, pp. 669-670, Sept. 1966.

10. Polder, D., Van Santen, J. H., 'The Effective Permeability of Mixtures and Solids', Physica XII, no. 5, pp. 257-271, Aug. 1946.

11, Kirkwood, J. G., 'On the Theory of Dielectric Polarization', Journal of Chemical Physics, vol. 4, pp. 592-601, Sept. 1936.

12. Onsager, L., 'Electric Moments of Molecules in Liquids', Journal of American Chemical Society, vol. 58, pp. 1486-1493, 1936.

13. Brown, W. F., Jr., 'Solid Mixture Permittivities', Journal of Chemical Physics, vol. 23, no. 8, pp. 1514-1517, Aug. 1955.

14. DeLoor, G. P., 'Electric Properties of Heterogeneous Mixtures', Thesis, Leiden, 1956.

15. Lewin, L., 'The Electrical Constants of a Material Loaded with Spherical Particles', Proceedings IEE, vol. 94, part 3, pp. 65-68, 1947.

16. Mikhailov, G. P., Lobanov, A. M., 'A Study of the Temperature Dependence of Dielectric Losses and Permeability of Polymers in the Centimeter Wavelength Range', Soviet Physics - Technical Physics, vol. 3, part 1, pp. 243-254, 1958.

17. Stamm, A. J., 'Wood and Cellulose Science', Ronald Press Co., New York, 1964.

18. Venkateswaran, A., 'Formulas for the Dielectric Constant and Dissipation Factor of Mixtures and their Application to the Cellulose System', Journal of Applied Polymer Science, vol. 9, pp. 1127-1138, 1965.

19. Van Vleck, J. H., 'On Dielectric Constants and Magnetic Susceptibilities in the New Quantum Mechanics', Phys. Review, vol. 29, pp. 727-744, May 1927.

20. Van Vleck, J. H., 'On Dielectric Constants and Magnetic Susceptibilities in the New Quantum Mechanics', Phys. Review, vol. 30, pp. 31-54, 1927.

21. Van Beek, L. K. H., 'Dielectric Behavior of Heterogeneous Systems', Progress in Dielectrics, vol. 7, pp. 69-114, Heywood and Company Ltd., London, 1967.

22. MacLean, L. D., 'Effect of Moisture Changes on the Shrinking, Swelling, Specific Gravity, Air or Void Space, Weight and Similar Properties of Woods', Report no. R1448, Aug. 1944, United States Dept. of Forest Service, Forest Products Lab. Madison 5, Wisconsin.

23. Von Hippel, A. R., 'Dielectric Materials and Applications', M. I. T. Press, 1954.

24. Tinga, W. R., Edwards, E. M., APL - 'A Computer Language for the Applications Engineer', Journal of Microwave Power, vol. 3(1), pp. 39-41, 1968.

25. Turner, L. B., 'Balanced Calorimeters for 3000 and 10,000Mc/S with Tapered Water Loads for Ho_1 Rectangular Pipes', Journal IEE, pp. 1467-1476, 1946.

26. Windle, J. J., Shaw, T. M., 'Dielectric Properties of Wool-Water Systems at 3000 and 9300 Megacycles', Journal of Chemical Physics, Vol. 22, no. 19, pp. 1752-1757, October 1954.

27. DeLoor, G. P., 'Dielectric Properties of Heterogeneous Mixtures Containing Water', Journal of Microwave Power, vol. 3, no. 2, pp. 67-73, 1968.

28. Busker, L. H., 'Measurement of Water Content above 30% by Microwave Absorption Methods', Tappi, vol. 51, no. 8, pp. 348-353, Aug. 1968.

29. Maxwell, J. C., 'A Treatise on Electricity and Magnetism', vol. 1 and 2, 3rd Edition 1891, Dover Publications Inc. 1954.

30. Böttcher, C. J. F., 'Theory of Electric Polarisation', Elsevier Publishing Co., New York, 1952.

31. Montgomery, C. G., 'Technique of Microwave Measurements', Rad. Lab. series vol. 11, ch. 10, McGraw-Hill Book Co. Inc., New York, 1947.

32. Harvey, A. F., 'Microwave Engineering', Academic Press, New York, 1963.

33. Buchanan, T. J., 'Balance Methods for the Measurement of Permittivity in the Microwave Region', IEE - Proc., pp. 61-66, 1952.

34. James, W. L., Hamill, D. W., 'Dielectric Properties of Douglas Fir Measured at Microwave Frequencies', Forest Products Journal, vol. XV, no. 2, pp. 51-56, Feb. 1965.

35. Marcuvitz, N., 'Waveguide Handbook', Rad. Lab. Series, vol. 10, McGraw-Hill, 1961.

36. Lowry, H. V., Hayden, H. A., 'Advanced Mathematics', part II, Longmans Green and Co., New York.

37. Tinga, W. R., Edwards, E. M., 'Swept Frequency Dielectric Measurement Technique', Journal of Microwave Power, vol. 3, no. 3, pp. 114-125, Sept. 1968.

38. Gevers, M., DuPré, F. K., 'Power Factor and Temperature Coefficient of Solid (amorphous) Dielectrics', Trans. Far. Soc., Vol. 43, pp. 47-55, 1947.

39. Gevers, M., 'The Relation between the Power Factor and the Temperature Coefficient of the Dielectric Constant of Solid Dielectrics', Philips Technical Reviews, in five parts, Report 15, pp. 197-224, Nov. 1945 (part I); Report 20, pp. 279-313, Dec. 1945 (part II and III); Report 25, pp. 361-379, March 1946 (part IV); Report 30, pp. 447-464, July 1946, (part V).

40. Garton, C. G., 'The Distribution of Relaxation Times in Dielectrics', Trans. Far. Soc., Vol. 43, pp. 56-60, 1947.

41. Garton, C. G., 'Discussion', Trans. Far. Soc., vol. 43, pp. 76-77, 1947.

42. Yager, W. A., 'The Distribution of Relaxation Times in Typical Dielectrics', Physics, vol. 7, pp. 434-450, Dec. 1936.

43. Kronig, R., J. Opt. Soc. America, vol. 12, p. 547, 1926.

44. Sutton, P. M., 'The Dielectric Properties of Glass', Progress in Dielectrics, vol. 2, pp. 145-146, John Wiley and Sons Inc., New York, 1960.

45. Smyth, C. P., 'Dielectric Behavior and Structure', McGraw-Hill Book Co. Inc., New York, 1955.

46. Scaife, B. K. P., 'Dispersion and Fluctuation in Dielectrics', Progress in Dielectrics, vol. 5, pp. 145-186, John Wiley and Sons Inc., New York, 1963.

47. Lin, R. T., 'A Study on the Electrical Conduction in Wood', Forest Products Journal, pp. 506-514, Nov. 1965.

48. Brown, J. H., Davidson, R. W., Skaar, C., 'Mechanism of Electrical Conduction in Wood', Forest Products Journal pp. 455-459, Oct. 1963.

49. Skaar, C., Simpson, W., 'Thermodynamics of Water Sorption by Wood', Forest Products Journal, vol. 18, no. 7, pp. 48-58.

50. Peterson, R. W., 'The Dielectric Properties of Wood', Forest Products Lab. of Canada, Technical Note no. 16, Ottawa Laboratory, 1960.

51. Hasted, J. B., 'The Dielectric Properties of Water', Progress in Dielectrics, vol. 3, pp. 101-150, Heywood and Company Ltd., London, 1961.

52. Meakins, R. J., 'Mechanisms of Dielectric Absorption in Solids', Progress in Dielectrics, vol. 3, pp. 151-202, Heywood and Company Ltd., London, 1961.

53. Curtis, A. J., 'Dielectric Properties of Polymeric Systems', Progress in Dielectrics, vol. 2, pp. 29-76, Heywood and Company Ltd. London, 1960.

54. Venkateswaran, A., VandenAkker, J. A., 'Effect of Ethylamine Treatment on the Dielectric Properties and Crystallinity of Cellulose', Journal Appl. Pol. Science, vol. 9, pp. 1149-1166, part I, 1965.

55. Venkateswaran, A., VandenAkker, J. A., 'Effect of Ethylamine Treatment on the Dielectric Properties and Crystallinity of Cellulose', Journal Appl. Pol. Science, vol. 9, pp. 1167-1192, part II, 1965.

56. Ventkateswaran, A., Riemen, W. P., 'Experiments on the Effect of Ethylamine Treatment on the Crystallinity of Cellulose', Journal Appl. Pol. Science, vol. 9, pp. 1139-1148, 1965.

57. Voss, W. A. G., 'Factors Affecting the Operation of High Power Microwave Heating Systems for Lumber Processing', IEEE, 7th Biennial Electric Heating Conference, Cleveland, Ohio, Sept. 1965.

58. Taylor, H. B., 'Microwave Moisture Measurement', AEI Engineering, vol. 5, no. 1, pp. 39-46, Jan/Feb., 1965.

59. Haggis, G. H., Hasted, J. B., Buchanan, T. J., 'The Dielectric Properties of Water in Solutions', Journal of Chem. Physics, vol. 10, no. 9, pp. 1452-1465, Sept. 1952.

60. Onsager, L., Journal American Chem. Soc., vol. 58, p. 1486, 1936.

61. Franck, V., 'On the Penetration of a Static Homogeneous Field in an

Anisotropic Medium into an Ellipsoidal Inclusion Consisting of another Anisotropic Medium', Symposium on Electromagnetic Theory and Antennas, June 1962, pp. 615-623, Oxford Perganon, London.

62. Hasted, J. B., Shah, M. A., 'Microwave Absorption by Water in Building Materials', Brit. J. Appl. Phys., vol. 15, pp. 825-836, 1964.

63. Pearce, C. A. R., Brit. J. Appl. Phys., Vol. 6, p. 358, 1955.

64. Skaar, C., 'The Dielectrical Properties of Wood at Several Radio Frequencies', Tech. Publ. New York, State College, For. no. 69,

65. McLaren, A. D., Rowen, J. W., 'Sorption of Water Vapor by Protiens and Polymers - A Review', J. Pol. Science, vol. 7, pp. 289-324, 1951.

66. Fhrohlich, H., Theory of Dielectrics, Oxford University Press, Ely House, London W.I., 1958, 2nd edition, Chapter 3.